This is to certify that the

dissertation entitled

STOCHASTIC RESPONSE OF DECK ARCH BRIDGES TO CORRELATED SUPPORT EXCITATIONS

presented by

BASHEER NMAIR SWEIDAN

has been accepted towards fulfillment
of the requirements for

Ph.D degree in Civil and Environmental Engineering

Major professor

Date May 8, 1990

STOCHASTIC RESPONSE OF DECK ARCH BRIDGES TO CORRELATED SUPPORT EXCITATIONS

By

Basheer Nmair Sweidan

A DISSERTATION

Submitted to
Michigan State University
in partial fulfillment of the requirements
for the degree of

DOCTOR OF PHILOSOPHY

Department of Civil and Environmental Engineering

1990

Sto

formed on m

California

Virginia.

A s

both cohere

support mo

ments was

types of

lated supp

and (3) c

coherency

model par

sidered.

Th

variation

plane res

ments of

velocity

bridges.

on the l

another.

the verti

tion. Th

ABSTRACT

STOCHASTIC RESPONSE OF DECK ARCH BRIDGES
TO CORRELATED SUPPORT EXCITATIONS

By

Basheer Nmair Sweidan

Stochastic analysis to correlated support excitations was performed on models of the 700 foot Cold Spring Canyon Bridge (CSCB) in California, and the 1700 foot New River Gorge Bridge (NRGB) in West Virginia.

A space-time earthquake ground motion model that accounts for both coherency decay and seismic wave propagation is used to specify the support motion. A random vibration approach combined with finite elements was used to develop expressions for the structural response. Three types of excitations were considered at the supports: (1) fully correlated support motion; (2) delayed excitation caused by wave propogation; and (3) correlated excitation accounting for both wave propogation and coherency decay. For each type of support motion, two seperate sets of model parameters representing stiff and soft site conditions were considered.

The results of the study indicate that the effect of the spatial variation of ground motion is very significant, especially on the in-plane responses of axial forces, bending moments and vertical displacements of the bridge. The ground motion parameters and seismic wave velocity is found to substantially influence the responses of the two bridges. The influence of different correlation models of ground motion on the lateral responses was irregular and differs from one member to another. The lateral displacements were not as greatly influenced as the vertical displacements by the type of correlation of support excitation. The response to the wave propogation effect and the more general

case (inclu

the most, a

Nor

an earthqua

the respons

case (including wave propogation and coherency decay) were within 20% at the most, and in general within 7% to 10% from each other.

Nonstationary response was also examined. It was found that for an earthquake having a duration of strong shaking of 5 seconds or more, the responses were close to those for stationary exctiation.

To my wife Carol

and my children Eric and Gina

for their love and encouragement

Wi

substanti

Without th

this study

I

Environm

Dr. Robe

serving o

ACKNOWLEDGEMENTS

With deep gratitude and thanks I would like to acknowledge the substantial contribution made to this study by Dr. Ronald Harichandran. Without the assistance, cooperation and the help of Dr. Harichandran this study would not have been possible.

I would also like to thank the Department of Civil and Environmental Engineering. Finally, I would also like to thank Dr. Robert K. Wen, Dr. Parvis Soroushian and Dr. Norman Hills for serving on the dissertation committee and for their helpful comments.

TABLE OF CONTENTS

4. ANALYSI

4.1

4.2

4.3

4

LIST OF TABLES

LIST OF FIGURES

Figure 4-1

Figure 4-1

Figure 4-2

Figure 4-3

Figure 4-

Figure 4-

Figure 4-

Figure 4

Figure 4

Figure 4

Figure 4

Figure 4

Figure 4-3

Figure 4-3

Figure 4-

Figure 4-

Figure 4-

Figure 4-

Figure 4-

Figure 4-

Figure 4-

The follow

A

[A]

A_{il}

A_x, A_y

b

[C]

$[C_{ij}]$

$Cov(u_{s_i}, t$

$Cov(s_i, f_j$

(D_G)

D_m

(D_m)

D_p

E

f

(f)

F_{ij}

LIST OF SYMBOLS

The following symbols are used in this dissertation:

A = cross section area, or a parameter of ground motion model;

$[A]$ = matrix related to pseudo-static support displacements;

A_{il} = entries of matrix [A];

A_x, A_y = shear area in x and y directions;

b = parameter of ground motion model;

$[C]$ = damping matrix;

$[C_{ij}]$ = partitions of matrix [C];

$Cov(u_{s_i}, u_{d_i})$ = covariance of pseudo-static and dynamic displacements;

$Cov(s_i, f_i)$ = covariance of pseudo-static and dynamic element end forces;

$\{D_G\}$ = vector of nodal displacements in the global coordinate system;

D_m = translation due to a moment M_z;

$\{D_m\}$ = vector of displacements in member coordinates;

D_p = translation due to a force p;

E = modulas of elasticity;

f = linear frequency (Hz);

$\{f\}$ = vector of element end forces;

F_{ij} = element end force corresponding to the i^{th} d.o.f. and the j^{th} eigenvector;

G

G_1, G_2

G_j

$h_j(t)$

$H_j(w)$

I_{xx}, I_{yy}

$[K]$

$[K_{ij}]$

L

L_{ex}, L_{ey}

L_{ew}

$[M]$

$[M_{ij}]$

P_x, P_y

R_P, R_m

$R_{u_{d_i}}(r)$

$R_{u_{F_i}}(r)$

$R_{u_{s_i}}(r)$

G = shear modulas;

G_1, G_2 = dimensionless shear constant with respect to x and y axes;

G_j = generalized modal excitation;

$h_j(t)$ = modal impulse response function;

$H_j(w)$ = modal frequency response function;

I_{xx}, I_{yy} = moment of inertia of cross section with respect to x and y axes;

$[K]$ = stiffness matrix of structure;

$[K_{ij}]$ = partitions of matrix [K];

L = element length;

L_{ex}, L_{ey} = "effective" length with respect to x and y axes;

L_{ew} = "effective" length with respect to warping;

$[M]$ = mass matrix;

$[M_{ij}]$ = partitions of matrix [M];

P_x, P_y = force in the direction of x and y axes;

R_p, R_m = rotation due to a force and a moment;

$R_{u_{d_i}}(\tau)$ = autocorrelation function of the dynamic component of free displacement;

$R_{u_{F_i}}(\tau)$ = autocorrelation function of the free displacement;

$R_{u_{s_i}}(\tau)$ = autocorrelation function of the pseudo-static component of free displacement;

$R_{u_{s_i} u_{d_i}}(\tau$

$R_{X_{Rf} Y_{Rm}}$

$R_{X_{Rf} \hat{Y}_{Rm}}$

$R_{\hat{X}_{Rf} \hat{Y}_{Rm}}(\tau$

S_0

$S_{u_{d_i}}(\omega)$

$S_{u_{s_i}}(\omega)$

$S_{u_{F_i}}(\omega)$

$S_{u_{d_i} u_{s_i}}($

$S_{\hat{X}_{Rf} \hat{Y}_{Rm}}($

$S_{X_{Rf} \hat{Y}_{Rm}}($

$S_{X_{Rf} Y_{Rm}}$

t

u_d

$R_{u_{s_i} u_{d_i}}(\tau)$ = cross correlation function of pseudo-static and dynamic displacements;

$R_{X_{R\ell} X_{Rm}}$ = cross correlation function of support displacements;

$R_{X_{R\ell} \ddot{X}_{Rm}}$ = cross correlation function of support displacement and acceleration;

$R_{\ddot{X}_{R\ell} \ddot{X}_{Rm}}(\tau)$ = cross correlation function of support acceleration;

S_o = intensity parameter;

$S_{u_{d_i}}(\omega)$ = spectral density function of dynamic displacement;

$S_{u_{s_i}}(\omega)$ = spectral density function of pseudo-static displacement;

$S_{u_{F_i}}(\omega)$ = spectral density function of free displacement;

$S_{u_{d_i} u_{s_i}}(\omega)$ = spectral density function of pseudo-static and dynamic displacements;

$S_{\ddot{X}_{R\ell} \ddot{X}_{Rm}}(\omega)$ = cross spectral density function of ground accelerations;

$S_{X_{R\ell} \ddot{X}_{Rm}}(\omega)$ = cross spectral density function of ground displacement and acceleration;

$S_{X_{R\ell} X_{Rm}}(\omega)$ = cross spectral density function of ground displacement;

t = time;

u_d = dynamic nodal displacement of free node;

u_s

u_F

(X)

(X_F)

(X_R)

$(X_F^{s_F})$

$(X_F^{d_F})$

Y_j

β_g, β_f

Γ_j

ν

$\rho(\nu, \varepsilon)$

$\sigma^2_{u_{d_i}}$

$\sigma^2_{u_{s_i}}$

$\sigma^2_{u_{r_i}}$

$\sigma^2_{f_i}$

$\sigma^2_{s_i}$

$\sigma^2_{F_i}$

u_s = pseudo-static nodal displacement of free node;

u_F = free nodal displacement;

$\{X\}$ = vector of absolute displacements;

$\{X_F\}$ = vector of absolute free displacements;

$\{X_R\}$ = vector of restrained displacements;

$\{X^s_F\}$ = vector of pseudo-static displacement;

$\{X^d_F\}$ = vector of dynamic displacement;

Y_j = generalized modal displacement;

β_g, β_f = empirical parameters describing spectral density function;

Γ_j = modal participation factor;

ν = separation distance;

$\rho(\nu,f)$ = coherency of ground acceleration for frequency f and station seperation ν;

$\sigma^2_{u_{d_i}}$ = variance of dynamic displacement;

$\sigma^2_{u_{s_i}}$ = variance of psuedo-static displacement;

$\sigma^2_{u_{f_i}}$ = variance of free dynamic displacement;

$\sigma^2_{f_i}$ = variance of dynamic end force;

$\sigma^2_{s_i}$ = variance of psuedo-static end force;

$\sigma^2_{F_i}$ = variance of end force;

$\sigma^2_{F_x}$

σ^2_{Fxd}

σ^2_{Fxs}

σ^2_{Fxc}

$\sigma^2_{F_y}$

$\sigma^2_{F_z}$

σ^2_{Fzs}

σ^2_{Fzd}

σ^2_{Fzc}

$\sigma^2_{M_x}$

$\sigma^2_{M_y}$

σ^2_{Mys}

$\sigma^2_{F_x}$ = variance of member shear forces in the direction of local x-axis;

σ^2_{Fxd} = variance of the dynamic component of member shear forces in the direction of local x-axis;

σ^2_{Fxs} = variance of the static component of member shear forces in the direction of local x-axis;

σ^2_{Fxc} = covariance of the static-dynamic component of member shear forces in the direction of local x-axis;

$\sigma^2_{F_y}$ = variance of shear forces in the direction of local y-axis;

$\sigma^2_{F_z}$ = variance of axial forces;

σ^2_{Fzs} = variance of the static component of member shear forces in the direction of local z-axis;

σ^2_{Fzd} = variance of the dynamic component of member axial forces;

σ^2_{Fzc} = covariance of the static dynamic component of member shear forces in the direction of local z-axis;

$\sigma^2_{M_x}$ = variance of bending moment about local x-axis;

$\sigma^2_{M_y}$ = variance of bending moment about local y-axis;

σ^2_{Mys} = variance of static component of member bending moments about local y-axis

σ^2_{Myc}

σ^2_{Myd}

$\sigma^2_{M_z}$

$\sigma^2_{M_w}$

$\sigma^2_x(H)$

$\sigma^2_x(G)$

$\sigma^2_1(*), \sigma^2_2$

$\sigma^2_x(NON), \sigma$

$\sigma^2_x(w)$

ω

ω_g, ω_f

ω_j

$[\Psi]$

ζ_j

Subscript

F, FF

FR, RF

R, RR

σ^2_{Myc} = covariance of the static-dynamic component of the bending mome about y-axis

σ^2_{Myd} = variance of dynamic component of member axial forces;

$\sigma^2_{M_z}$ = variance of torsional moment;

$\sigma^2_{M_w}$ = variance of warping moment;

$\sigma^2_*(H)$ = variance of any response due to fully correlated case;

$\sigma^2_*(G)$ = variance of any response due to general case;

$\sigma^2_1(*), \sigma^2_2(*)$ = variance of any response due to ground motion 1 and 2;

$\sigma^2_*(NON), \sigma^2_*(ST)$ = variance of any response due to nonstationary and stationary excitations;

$\sigma^2_*(w)$ = variance of any response due to wave propogation case;

ω = circular frequency (rad/sec);

ω_g, ω_f = empirical parameters describing spectral density function;

ω_j = modal circular frequency;

$[\Psi]$ = eigenvectors;

ζ_j = modal damping ratio;

Subscripts

F, FF = quantity corresponding to free displacement;

FR, RF = quantity corresponding to free and restrained displacement or vice versa;

R, RR = quantity corresponding to restrained displacement;

Superscri

.

-

"

T

Superscripts

$\cdot$	= first partial derivative with respect to time;
$\ddot{}$	= second partial derivative with respect to time;
$''$	= second partial derivative with respect τ;
T	= matrix transpose.

1.1 LITER

Li

very impor

lifelines

Th

structur

or under

to the sp

and desig

Th

of ground

strong g

variatio

accounte

motion a

obtained

determi

travell

variatio

seismic

(Dusseau

Californ

to dete

the two

presente

CHAPTER 1

GENERAL INTRODUCTION

1.1 LITERATURE REVIEW

Lifeline systems such as bridges and pipelines are part of the very important infrastructures serving society. The ability of these lifelines to function after an earthquake is of great importance.

The difference between lifeline systems and conventional structures is that typical lifelines extends for large distances above or under the ground surface. Because of this, they are very sensitive to the spatial variation of earthquake ground motion, and their analysis and design should take this into consideration.

The traditional method of analyzing structures under the effect of ground motion is to perform time history analysis based on recorded strong ground motion. For a long structure with multiple supports, the variation of seismic ground motion due to travelling waves can be accounted for by considering the recorded time history as the input motion at one support, with the input motion at the other supports being obtained by considering a delay in the arrival of the shear waves. This deterministic approach, however, is only capable of representing travelling waves, which is only one feature of realistic space-time variation of ground motion.

A comprehensive deterministic study on the effect of unequal seismic support motion was conducted on two steel deck arch bridges (Dusseau and Wen, 1985). In that study the Cold Spring Canyon Bridge in California and the New River Gorge Bridge in West Virginia were studied to determine the effect of unequal support motion on the responses of the two bridges. An outline of the conclusions of this study will be presented in Chapter 4.

In

lifeline

response o

by means

(1982). H

multiple-

obtained

I

motion, H

seismic

stresses

frequency

motion o

in the l

by Hari

Based on

In recent years, studies have been conducted on the response of lifeline structures using stochastic models of ground motion. The response of a suspension bridge subject to multiple support excitations by means of random vibration theory was conducted by Abdel-Ghaffar (1982). He found that the response values associated with correlated multiple-support excitations are significantly different from those obtained through the uncorrelated case.

In a study on the response of a burried pipline to random ground motion, Hindy and Novak (1980) concluded that the lack of correlation of seismic excitation could produce excessive stresses in the pipe. These stresses depend on the degree of correlation of the excitation and its frequency content.

The effects of spatially varying stochastic model of ground motion on the responses of pipelines and bridges of various span lengths in the longitudinal, lateral and vertical directions were also studied by Harichandran and wang (1988), and also by Zerva and Wen (1988). Based on these, the following conclusions can be made:

1. The assumption of perfectly correlated earthquake ground motion is not always safe in the seismic evaluation of pipelines.
2. The effect of differential ground motion is not significant for typical single-span, simply supported bridges, and assumming identical support excitations will lead to conservative stress response estimates. The assumption of perfectly correlated support motion is therefore a valid approximation for spans up to 200 m.
3. The spatial variation of earthquake ground motion is important for the analysis of indeterminate structures, and

Al

considerin

on the res

1.2 OBJE

In

Spring Ca

the effec

formulat

element a

obtained

commonly

analyzed

induces

1.3 ORG

here.

bridges

model is

work.

coordin

descrip

using

derivia

neglecting this can result in significant error in stress estimation.

All the above mentioned studies indicate the importance of considering the effect of spatial variations of earthquake ground motion on the response of long structures.

1.2 OBJECTIVE AND SCOPE

In this study the models of two deck arch bridges, the Cold Spring Canyon Bridge and the New River Gorge Bridge are examined under the effect of partially correlated multiple support excitation. The formulation of the equations of motions is developed using finite element and random vibrations methods. The responses of the bridges are obtained for different types of ground motion inputs, including those commonly used in current practice. The responses of the bridges are analyzed and compared to determine the worst type of ground motion that induces the highest responses.

1.3 ORGANIZATION

A brief summary of the contents of each chapter is presented here.

Chapter 2 covers in some detail the description of the two bridges. The method used by Dusseau (1985) to obtain the one-plane model is discussed in some detail, since this same model is used in this work. Also, the chapter contains discussions about the local and global coordinate system, transformations and stiffness matrices. A description of the computer program used in the analysis is provided.

Chapter 3 presents the development of the equations of motions using finite element and random vibration methods. Detailed deriviations of the response components is presented. The model used

for the c

discussed.

In

bridges ar

types of

structura

assumptio

is checke

conducted

I

are summ

proceed a

for the cross spectral density function of the ground acceleration is discussed.

In Chapter 4, results of fairly extensive analysis of the two bridges are presented. The responses of the two bridges to different types of ground motions are discussed in detail. The effects of structural stiffness and shear wave velocity are studied. The assumption that the ground motion constitute a stationary random field is checked. A comparison between this study and the deterministic study conducted by Dusseau and Wen (1985) is presented.

In Chapter 5, major conclusions of the results from this study are summarized. the avenues in which future research in this area may proceed are also discussed.

Th

Spring Ca

(Dusseau

modeling t

(Dusseau

have the

analyze t

T

of arch s

T

this stu

their mai

T

the anal

coordina

two-dime

2.1 ARC

used in

structu

bridges

1700 ft

conditi

arch co

CHAPTER 2

ARCH BRIDGES AND BRIDGE MODELING

This chapter contains a summary of description of the Cold Spring Canyon Bridge (CSCB) and the New River Gorge Bridge (NRGB) (Dusseau and Wen, 1985). Also, this chapter contains the procedure of modeling the (CSCB) and (NRGB) into in-plane and out-of-plane models (Dusseau and Wen, 1985), so that the reader of this dissertation will have the full information to understand the models that are used to analyze the two bridges.

The first section of this chapter discusses the basic features of arch structures and their classification.

The second section describes the two deck arch bridges used in this study, and includes the geometric parameters of the bridges and their main structural components.

The third section discusses the type of finite element used in the analysis, their stiffness matrices, and the local and global coordinate systems.

The fourth section discusses the modeling of the two bridges as two-dimensional planar structures.

2.1 ARCH BRIDGES

Arch Bridges made of steel and reinforced concrete have been used in transportation networks throughout the world. With the use of structural steel it is possible to economically construct long span arch bridges ranging from a minimum of about 190 ft. to a maximum of about 1700 ft. With present high-strength steels and under favorable soil conditions, spans of the order of 2000 ft. are feasible for economical arch construction.

Cr

bending

location

the pres

loaded pa

with no

the secti

tension

differs

2.1.1 C

horizon

points t

indeterm

is a th

degrees

a one a

when th

arch is

through

springi

because

elevat

extreme

types

Cross sections of the arch are designed for axial thrust, bending moment and shear forces, with magnitudes depending on the location of the pressure line (funicular polygon of applied loads). If the pressure line coincides with the axis of the arch (as in uniformly loaded parabolic arches), all cross sections are subject to compression with no moment or shear. If the pressure line falls within the kern of the section, there will exist thrust, bending moment and shear, but no tension on the cross section. Finally, if the shape of the structure differs from the pressure line, moment may become dominant.

2.1.1 CLASSIFICATION OF ARCH BRIDGES

Arch Bridges are classified as trussed or solid ribbed. If the horizontal thrust is taken by structural ties between the reaction points then the arch is referred to as a tied arch.

Arches are also classified according to the degrees of static indeterminancy. A fixed arch in which rotation is prevented at the ends is a three degrees indeterminate structure. A one-hinged arch is a two degrees indeterminate structure. A two-hinged, and three-hinged arch is a one and zero degrees indeterminate structure, respectively.

In addition arch bridges are classified as "deck construction" when the arches are entirely below the deck, "through arch", when the arch is entirely above the deck and the tie is at deck level, "half through arch" when the deck is at some intermediate elevation between springing and crown.

In this study we are concerned with the deck arch bridges, because the mass of the bridge is concentrated in the deck at a high elevation from the springing. This makes the deck arch bridges extremely vulnerable to seismic ground motion relative to the other types of arch bridges. Figure 2-1 shows a typical deck arch bridge.

2.2 DECK

In

Bridge (CS

West Virgi

2.2.1 CO

Th

Californi

major st

minimum y

the CSCB,

Figure 2.

length, 1

an over a

rectangu

abutment

total ar

polynom

hinges a

feet ab

minimize

the mai

despite

with on

equally

2.2 DECK ARCH BRIDGES USED IN THE STUDY

In this study two bridges were chosen: The Cold Springs Canyon Bridge (CSCB) in California and the New River Gorge Bridge (NRGB), in West Virgina, the worlds longest steel deck arch Bridge.

2.2.1 COLD SPRING CANYON BRIDGE

The Bridge is located about 13.5 miles North of Santa Barbara, California. It is a two lane solid-ribbed steel deck arch bridge. All major structural steel members are made of A373 steel which has a minimum yield strength of 33 ksi. Figure 2-2 shows an elevation view of the CSCB, while Figure 2-3 depicts a typical cross section. As shown in Figure 2-2, the bridge consists of 19 panels with two of 46.5 feet length, 13 of 63.64 feet length and four of 74.385 feet length, yielding an over all length of 1217.8 feet. The two hinge arch consists of two rectangular steel box girders spaced 26 feet apart and hinged at their abutments. The arch has 11 panels of 63.64 feet length, yielding a total arch span of 700 feet.

The configuration of the arch is based on a seventh degree polynomial with the southern hinges being 46.48 feet above the northern hinges and with the rise at the highest point of the arch being 144.5 feet above the northern hinges, seventh degree polynomial was used to minimize dead load moments in the arch. This configuration also makes the main span column heights symmetric about the center of the arch span despite the overall deck slope of 6.64%.

The arch ribs are connected laterally by a system of crossframes with one crossframe at each panel point and three crossframes spaced equally between panel points. The ribs are also connected laterally by

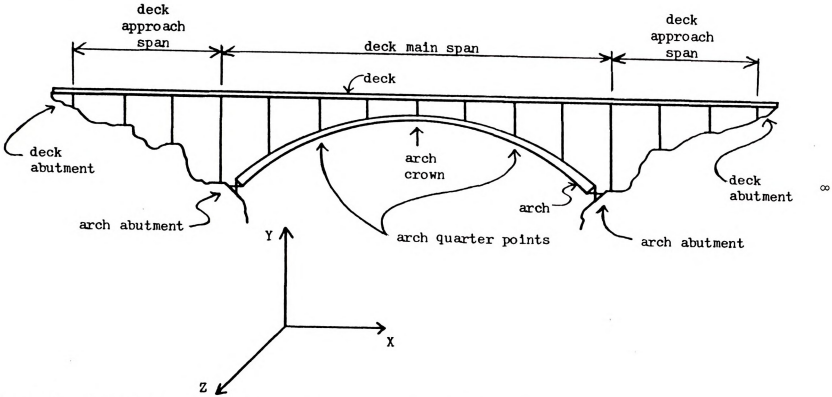

Figure 2-1: Typical Deck Arch Bridge (Excerpted from Dusseau (1985))

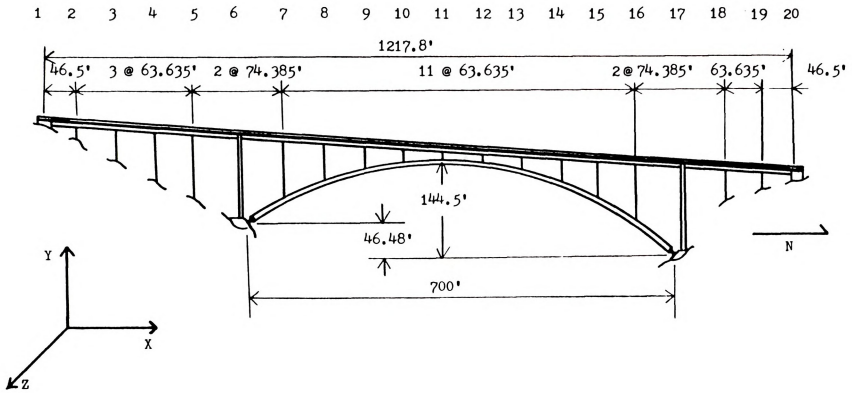

Figure 2-2: CSCB Elevation View (Excerpted from Dusseau (1985))

Floorb

Arch Rib

Figure

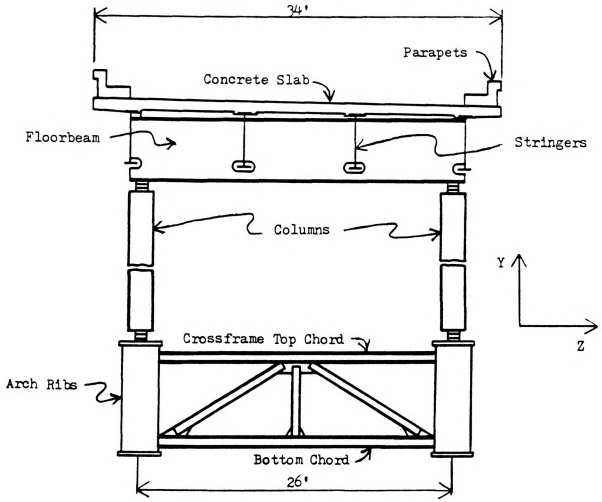

Figure 2-3: CSCB Typical Cross-Section. (Excerpted from Dusseau (1985)

top and b

arch ribs

as sides.

T

19 are s

The tower

that are

two steel

and concr

T

which ac

the latt

divided

panel po

moment a

provide

and a sy

2.2.2 T

arch c

Virgini

A steel

a typic

arch in

girder

panel i

top and bottom lateral bracing which, along with crossframes and the arch ribs, creates a box shaped cross-section with the arch ribs acting as sides.

The columns located at panel points 2 to 5, 7 through 16, 18 and 19 are steel box sections with hinge connections at the top and bottom. The towers at panel points 6 and 17 consist of steel box section columns that are rigidly fastened at their bases and are connected laterally by two steel box girders, intermediate struts, composite steel box girder, and concrete slab at the top.

The deck consists of a 7 inch two-way reinforced concrete slab which acts compositely with four longitudinal plate girder stringers, the latter being supported by plate girder floorbeams. The deck is divided into three continuous segments by hinged tower connections at panel points 6 and 17, which provide a release for in plane bending moment and warping bimoment at these points.

Between panel points 11 and 12, a system of cable x-bracing is provided between the deck and the arch in the longitudinal direction, and a system of cable v-bracing in the lateral direction.

2.2.2 THE NEW RIVER GORGE BRIDGE

The New River Gorge Bridge is a four lane, box truss, steel deck arch carrying U.S. 19 over New River Gorge and Route 82 in West Virginia. The principal material used in the bridge is ASTM A588 grade A steel with a minimum yield stress of 50 ksi.

Figure 2-4 shows an elevation view of NRGB, while Figure 2-5 is a typical cross-section. As shown in the figures, both the deck and the arch in the NRGB are essentially box trusses consisting of four box girder chords connected by lateral and vertical truss members. Each panel in the deck is divided into 6 subpanels, while the arch panels are

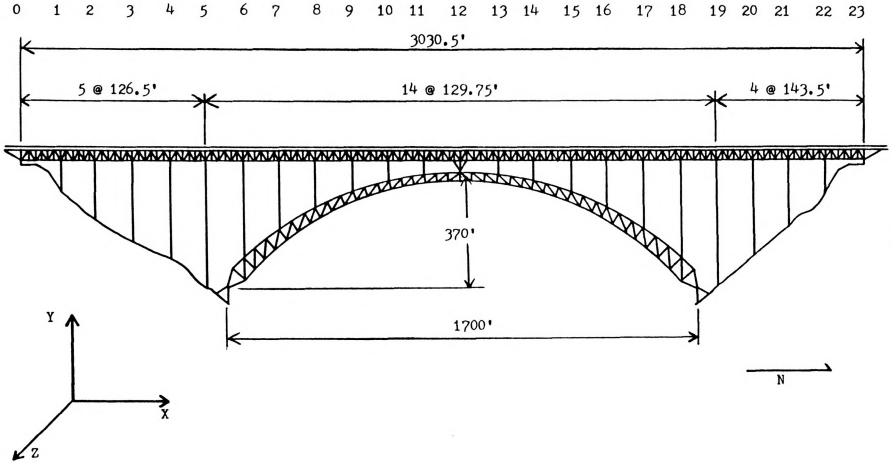

Figure 2-4: NRGB Elevation View (Excerpted from Dusseau (1985))

Figure

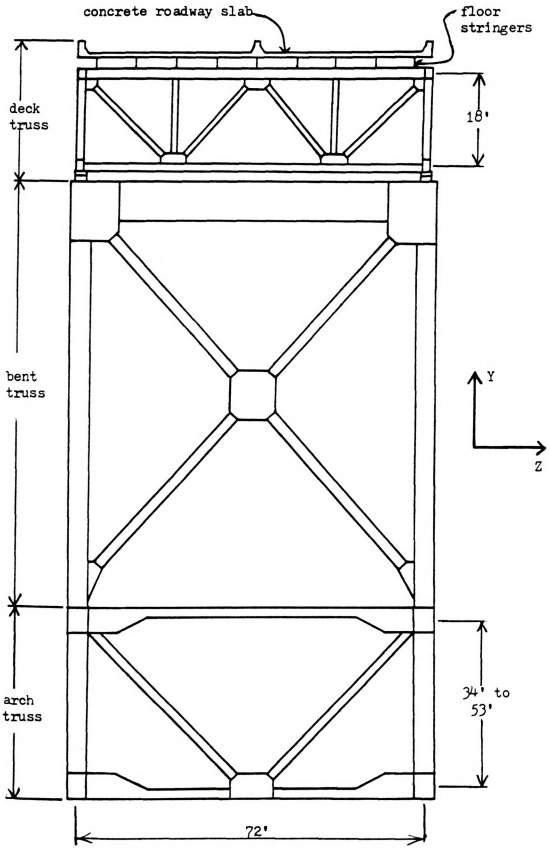

Figure 2-5: NRGB Typical Cross-section. (Excerpted from Dusseau (1985)

divided i

panels in

panels i

panels in

bridge s

panels, e

71.5 feet

T

centered

of 370 f

panel po

columns

connect

and sout

from the

5 and 19

are pin

span dec

joints

releases

2.3 BE

2.3.1

analysi

and T.

Transla

divided into 1½ or 3 subpanels. The deck in the NRGB consists of four panels in the north approach span, each of length 143.5 feet, five panels in the south approach span, each of length 126.5 feet, and 14 panels in the main span, each of length 129.75 feet, yielding a total bridge span of 3030.5 feet. The two hinged arch consists of 12 center panels, each of length 129.75 feet, and two end panels, each of length 71.5 feet, yielding a total arch span of 1700 feet.

The configuration of the arch is based on a symmetric five centered series of circular arcs which results in a maximum arch height of 370 feet above the hinges. The deck and arch are connected at each panel point in the main span by bents consisting of two box section columns joined laterally by diagonal truss elements. Similar bents connect the deck to concrete pedestals at each panel point in the north and south approach spans. The approach span deck segments are isolated from the main span deck segments by expansion joints at the top of bents 5 and 19. At these points, the bottom chords of the approach span deck are pinned to the top of the bents while the bottom chords of the main span deck are attached to the bents by rollers. Thus the expansion joints provide deck axial force, bending moment and warping bimoment releases at these points.

2.3 BEAM ELEMENT, STIFFNESS MATRIX, LOCAL AND GLOBAL COORDINATES

2.3.1 BEAM ELEMENT WITH WARPING AND SHEAR DEFORMATION

The Beam Element used in performing the random vibration analysis of the two bridges includes the warping deformation (W.F. Chen and T. Atsuta 1977). Each node has seven degrees of freedom: Translations U_x, U_y, and U_z, rotations Θ_x, Θ_y and Θ_z and warping


Theta-xj

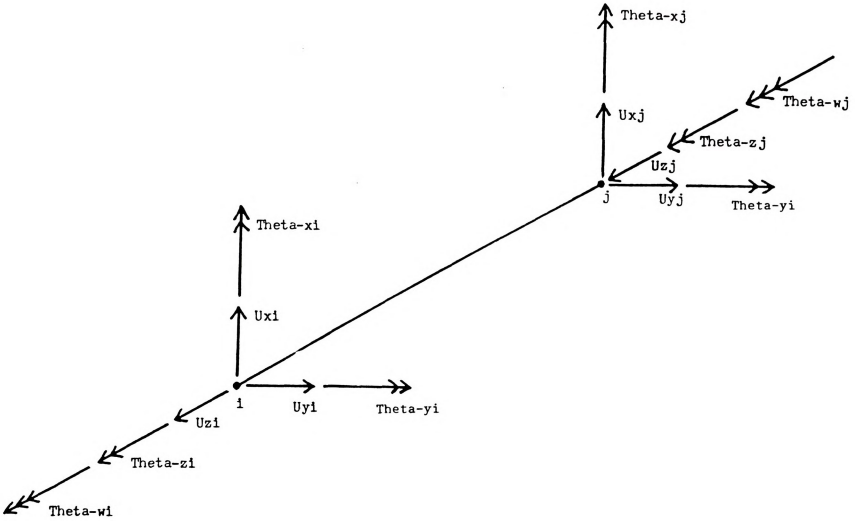

Figure 2-6: LINSTRUC Straight Beam Element End Displacements
(Excerpted from Dusseau (1985))

displacer

stiffness

and the l

with three

model the

2.3.2 ST

T

1977) in

account

matrix ar

K(3,3) =

K(3,10) =

K(4,4) =

K(4,11) =

K(7,7) =

K(4,7) =

K(7,11)

K(7,14)

K(1,1) =

displacement Θ_w. The shear deformation is also included in the stiffness matrix formulation. Figure 2-6 illustrates the beam element and the local coordinate system. Also, a standard space truss element with three translational degrees of freedom at each node is used to model the truss members.

2.3.2 STIFFNESS MATRIX

The stiffness matrix used in this study (W.F. Chen and T. Atsuta 1977) includes the warping deformation, with some modification to account for shear deformation. The non-zero entries of the stiffness matrix are listed below.

$$K(3,3) = K(10,10) = \frac{EA}{L} \tag{2.1}$$

$$K(3,10) = K(10,3) = -\frac{EA}{L} \tag{2.2}$$

$$K(4,4) = K(11,11) = \frac{12EI_w}{L^3} + \frac{36}{30}\frac{GK_t}{L} \tag{2.3}$$

$$K(4,11) = K(11,4) = -K(4,4) \tag{2.4}$$

$$K(7,7) = K(14,14) = \frac{4EI_w}{L} + \frac{4}{30} GK_t L \tag{2.5}$$

$$K(4,7) = K(7,4) = K(4,14) = K(14,4) = \frac{6EI_w}{L^2} + \frac{3}{30} GK_t \tag{2.6}$$

$$K(7,11) = K(11,7) = K(11,14) = K(14,11) = -K(4,7) \tag{2.7}$$

$$K(7,14) = K(14,7) = \frac{2EI_w}{L} - \frac{GK_t L}{30} \tag{2.8}$$

$$K(1,1) = K(8,8) = \frac{12EI_{yy}}{L^3\,(1+2.0\,G_1)} \tag{2.9}$$

$$G_1 = \frac{6EI_{yy}}{GA_x L_y^2} \tag{2.10}$$

K(1,8) =

K(1,5) =

K(8,5) =

K(5,5) =

K(5,12)

K(2,2) =

K(2,9) =

K(2,6)

K(9,6)

K(6,6)

K(6,13)

where

$$K(1,8) = K(8,1) = \frac{-12EI_{yy}}{L^3\ (1+2.0\ G_1)} \tag{2.11}$$

$$K(1,5) = K(5,1) = K(1,12) = K(12,1) = \frac{6EI_{yy}}{L^2\ (1+2.0\ G_1)} \tag{2.12}$$

$$K(8,5) = K(5,8) = K(8,12) = K(12,8) = \frac{-6EI_{yy}}{L^2\ (1+2.0\ G_1)} \tag{2.13}$$

$$K(5,5) = K(12,12) = \frac{4EI_{yy}\ (1+G_1/2.0)}{L\ (1+2.0\ G_1)} \tag{2.14}$$

$$K(5,12) = K(12,5) = \frac{2EI_{yy}\ (1+G_1/2.0)}{L\ (1+2.0\ G_1)} \tag{2.15}$$

$$K(2,2) = K(9,9) = \frac{12EI_{xx}}{L^3\ (1.0+2.0\ G_2)} \tag{2.16}$$

$$G_2 = \frac{6EI_{xx}}{GA_yL^2_x} \tag{2.17}$$

$$K(2,9) = K(9,2) = - \frac{12EI_{xx}}{L^3\ (1.0+2.0\ G_2)} \tag{2.18}$$

$$K(2,6) = K(6,2) = K(2,13) = K(13,2) = \frac{-6EI_{xx}}{L^2\ (1.0+2.0\ G_2)} \tag{2.19}$$

$$K(9,6) = K(6,9) = K(9,13) = K(13,9) = \frac{6EI_{xx}}{L^2\ (1.0+2\ G_2)} \tag{2.20}$$

$$K(6,6) = K(13,13) = \frac{4EI_{xx}\ (1.0+G_2/2.0)}{L\ (1.0+2.0\ G_2)} \tag{2.21}$$

$$K(6,13) = K(13,6) = \frac{2EI_{xx}\ (1.0-G_2)}{L\ (1.0+2.0\ G_2)} \tag{2.22}$$

where I_w - warping moment of inertia.

K_t - torsional constant.

G_1

coo

I

stiffnes

elements.

2.3.3 LC

used in

the K no

the coor

planes

study, t

coordin

element.

2.4 MOI

and the

very im

degree

computa

the tw

degree

repres

Dusseau

next f

(1985)

G_1 and G_2 dimensionless shear constants with respect to y and x coordinates.

If the warping moment of inertia is equal to zero then the stiffness matrix will be the same as for the standard space frame elements.

2.3.3 LOCAL AND GLOBAL COORDINATE AXES

Figure 2-7 illustrates the local and global coordinate system used in the analysis. The transformation matrix formulation is based on the K node method (W.Weaver Jr., and J.M. Gere, 1965). This method was the coordinates of a third point that lies in one of the principal planes of the member but is not on the member axis itself. In this study, the third point must lie in the x-z plane of the elements local coordinate system, and it cannot lie on the centroidel z axes of the element.

2.4 MODELING OF THE TWO BRIDGES

As mentioned earlier the Cold Spring Canyon Bridge in California and the New River Gorge Bridge in West Virginia were studied. It was very important that the models of both bridges have the fewest number of degrees of freedom. It would have been very difficult from a computational time point of view to study the probabilistic response of the two bridges without having a model of the bridges with reduced degrees of freedom. The so-called "one-plane-model" is used to represent each bridge, and the structural parameters derived by Wen and Dusseau (1985) for the two bridges were used. For completeness, the next few sections give a summary of the method used by Wen and Dusseau (1985) to model the two bridges, so that the reader will have a clear

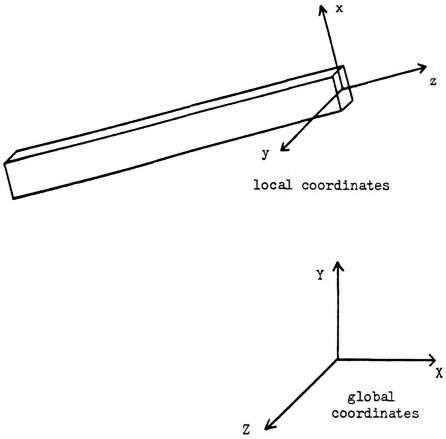

Figure 2-7: Local Coordinate Axes. (Excerpted from Dusseau (1985))

idea of th

detail is

2.4.1 VE

Th

and was u

horizont

freedom i

global Z

T

model an

directio

translat

d.o.f.'s

2.4.2 A

necessa

deck con

CSCB we

girders.

CSCB an

segment

(1985).

length

bridge.

segmen

cantil

idea of the "one-plane-model" approach which was used in this study.More detail is given in Dusseau (1985).

2.4.1 VERSIONS OF THE ONE-PLANE MODEL

The first version of the one-plane model is the "in-plane" model and was used in the analysis of the two bridges in the X-Y plane for the horizontal ground motion. Each node has two translational degrees of freedom in the Global X and Y directions and one rotation about the global Z axes.

The second version of the one-plane model is the "out-of-plane" model and was used in the analysis of the two bridges in the lateral direction. Each node has four degrees-of-freedom (d.o.f.): one translational d.o.f. in the direction of the Z axis; two rotational d.o.f.'s about the X and Y axes and one warping d.o.f.

2.4.2 ARCH AND DECK EQUIVALENT BEAM STIFFNESSES

To use the one-plane models for the NRGB and CSCB, it was necessary to determine the equivalent beam stiffnesses for the arch and deck components of both bridges. The stiffnesses of the deck for the CSCB were based on the composite action of the concrete slab and steel girders. To derive the equivalent beam stiffnesses for the arch of the CSCB and both the arch and deck of the NRGB, special "cantilevered" segments of the arch and deck components were analyzed by Dusseau (1985).

Each cantilevered segment of arch or deck was one panel in length and included all of the structural components in the actual bridge. The member stiffnesses and lengths used in these cantilevered segments were determined as follows: for the deck in the NRGB, three cantilevered segments were selected to derive the equivalent bean

stiffness
the deck;
abutmen
stronges
was usec
arch, av
quarter
cantilev

applied
girders
cantilev
rotatio
For the
connect
each ca
girder

applie
displac
For th
moments
free e
For th
girder
loads
and 2-

the ar

stiffnesses that will represent the properties of all existing panels in the deck; for the arch in the NRGB, the cantilevered segment near the abutment was used to derive the equivalent beam properties of the strongest section of the arch, and a segment at the crown of the arch was used to represent the weakest section in the arch; for the CSCB arch, average member stiffnesses and lengths in the end panels, in the quarter point panels and in the crown were used to develop three cantilevered segments, respectively.

Each cantilevered segment was "fixed" at one end and loads were applied at the other end. For the CSCB arch which consists of two box girders connected by lateral members, "fixing" one end of each cantilevered segment meant preventing all translations and global z axis rotations of the box girders at one end as shown in Figure 2-8a.
For the NRGB deck and arch, which each consist of four box girder chords connected by lateral and vertical truss members, "fixing" one end of each cantilevered segment meant preventing all translations of these box girder chords at one end as shown in Figure 2-8b.

With one end "fixed", a series of equivalent beam loads were applied to the free end of each cantilevered segment and the resulting displacements were then used to determine equivalent beam stiffnesses. For the CSCB arch assembly, which contains two box girders, forces and moments equivalent to the desired beam end loads were applied at the free ends of the box girder ribs, as depicted in Figures 2-8a and 2-9. For the NRGB arch and deck assemblies, each of which has four box girders chords, equivalent beam end loads were derived by applying point loads to the free ends of the box girder chords as shown in Figures 2-8b and 2-10.

After fixing the cantilevered section at one end and performing the analysis due to different loading conditions at the other end, the

Figure

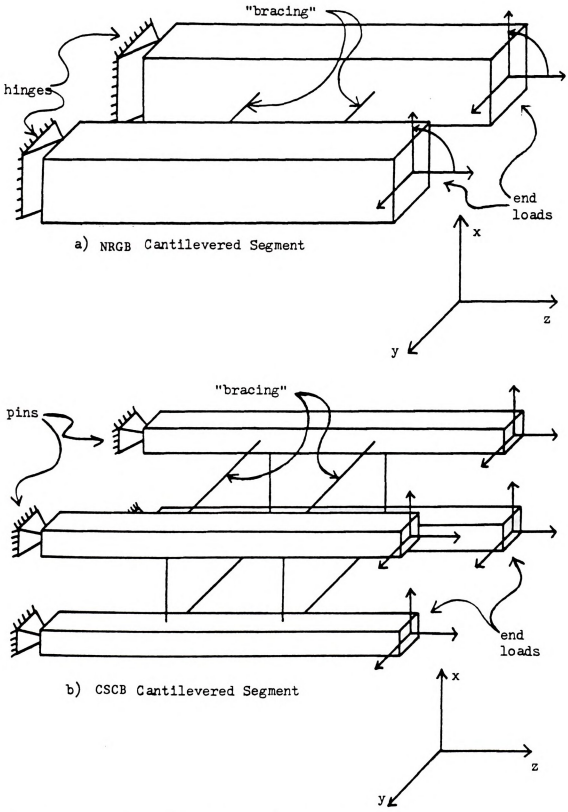

Figure 2-8: Cantilevered Segment End Fixity.

(Excerpted from Dusseau (1985))

Figure

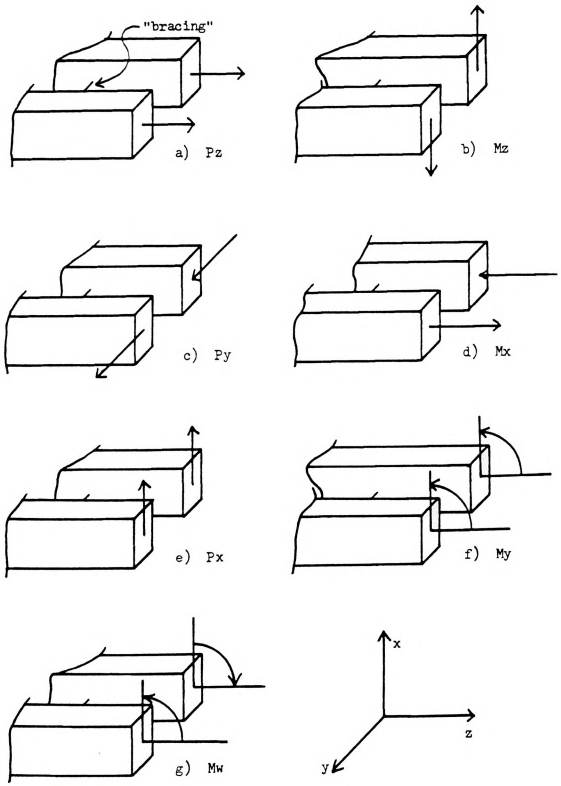

Figure 2-9: CSCB Cantilevered Segment End Loads

(Excerpted from Dusseau (1985))

Figure

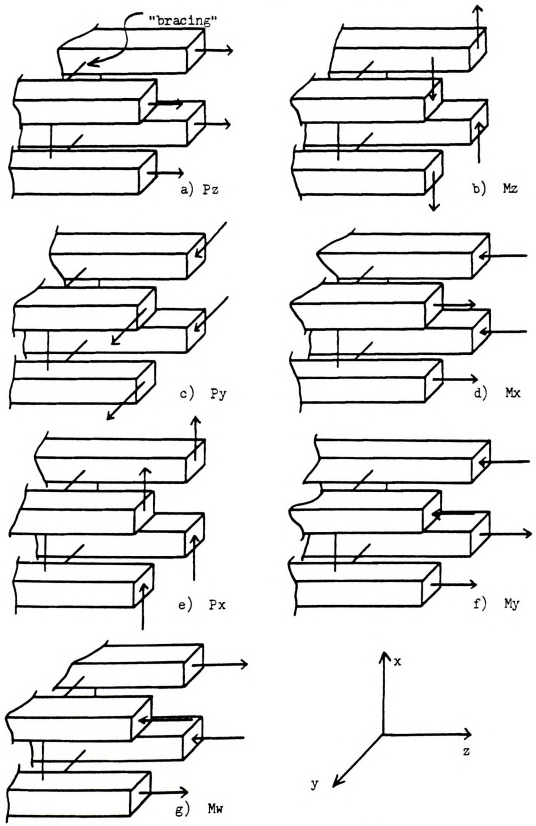

Figure 2-10: NRGB Cantilevered Segment End Loads

(Excerpted from Dusseau (1985))

fixed a

displace

displace

end dis

stiffne

bridges

axial

(see Fi

aspeci

calcula

where

moment

the NF

and 2.

torsio

where

canti

the f

resul

fixed and loaded ends were reversed so that two sets of end displacements were obtained. For the in-plane model the two sets of end displacements were the same. For the out-of-plane model the two sets of end displacements were different, and the equivalent straight beam stiffnesses were based on the larger set of end displacements for both bridges.

To determine the axial area of the equivalent beam element, an axial force P was applied to the free end of each cantilevered segment (see Figures 2-9a and 2-10a). Knowing the axial displacement due to aspecified axial force, the area of an equivalent beam element is calculated using the formula

$$A_z = \frac{P\ell}{\delta E} \tag{2.23}$$

where P is the applied force δ is the calculated axial displacement.

Similarly, to determine the torsional constant K_t, a torsional moment M_x was applied to the free end of each cantilevered segment of the NRGB and CSCB arches, where warping was ignored (see Figures 2-9b and 2-10b). The resulting rotation θ_z was used to calculate the torsional constant by the formula

$$K_t = \frac{M_z L}{G\theta_z} \tag{2.24}$$

where G is the shear modulus.

In order to determine the out-of-plane shear area A_y for each cantilevered segment, an equivalent beam shear force P_y was applied to the free end of each cantilevered segment (see Figures 2-9c and 2-10c) resulting in a translation D_p and a rotation R_p. Similarly, an

equivale

resultin

types of

The two

the sy

the sam

be sol

element

of thr

called

expres

Substi

Finall

equivalent bending moment M_z was applied (see Figures 2-9d and 2-10d) resulting in a translation D_m and a rotation R_m.

The two pair of flexibility equations that govern these two types of loading are

$$D_p = \frac{P_y L^3}{3EI_{xx}} + \frac{P_y L}{GA_y} \tag{2.25}$$

$$R_p = \frac{P_y L^2}{2EI_{xx}} \tag{2.26}$$

$$D_m = \frac{M_x L^2}{2EI_{xx}} \tag{2.27}$$

$$R_m = \frac{M_x L}{EI_{xx}} \tag{2.28}$$

The two unknowns in the last four equations are I_{xx} and A_y. Because of the symmetry of the flexibility equations, (2.26) and (2.27) will yield the same results, thus only equations (2.25), (2.26) and (2.28) need to be solved in order to achieve equivalence. Letting the length of the element be a variable equations (2.25), (2.26) and (2.28) yield a system of three equations with three unknowns I_{xx}, A_y and L_{ex}, where L_{ex} is called the "effective" beam length with respect to out-of-plane motion.

Dividing equation (2.26) by (2.28) yields the following expression for L_{ex}.

$$L_{ex} = \frac{2R_p M_x}{P_y R_m} \tag{2.29}$$

Substituting (2.29) into (2.28) yields the expression for I_{xx}.

$$I_{xx} = 2 R_p M_x^2 / (E P_y R_m^2) \tag{2.30}$$

Finally, equation (2.25) yields the following expression for A_y.

I_{yy}, sh

obtained

shown in

equiva

determi

each ca

in an a

M_w was

and a w

types

$$A_y = P_y L_{ex} / \left(G \left(D_p - \frac{P_y L_{ex}^3}{3EI_{xx}} \right) \right) \qquad (2.31)$$

Similar expressions for moment of inertia with respect to y axes I_{yy}, shear area A_x and the in- plane "effective" beam length L_{ey} were obtained using similar procedures. The applied free end forces are shown in Figures 2-9e, 2-9f, 2-10e and 2-10f.

For the deck in the NRGB, where warping was not ignored, the equivalent beam warping constant I_w and torsion constant K_t were determined by applying an equivalent beam torque M_z to the free end of each cantilevered segment (see Figures 2-9b and 2-10b), which resulted in an axial rotation R_t and a warping displacement W_t. Then, a bimoment M_w was applied (see Figures 2-9g and 2-10g), resulting in a rotation R_w and a warping displacement M_w.

The two pairs of stiffness equations that governs these two types of loadings are

$$M_z = \left(\frac{12EI_w}{L^3} + \frac{36}{30} \frac{GK_t}{L} \right) R_T - \left(\frac{6EI_w}{L^2} + \frac{3}{30} GK_t \right) W_t \qquad (2.32)$$

$$0 = \left(\frac{-6EI_w}{L^2} - \frac{3}{30} GK_t \right) R_t + \left(\frac{4EI_w}{L} + \frac{4}{30} GK_t L \right) W_t \qquad (2.33)$$

$$0 = \left(\frac{12EI_w}{L^3} + \frac{36}{30} \frac{GK_t}{L} \right) R_w - \left(\frac{6EI_w}{L^2} + \frac{3}{30} GK_t \right) W_w \qquad (2.34)$$

$$M_w = \left(\frac{-6EI_w}{L^2} - \frac{3}{30} GK_t \right) R_w + \left(\frac{4EI_w}{L} + \frac{4}{30} GK_t L \right) M_w \qquad (2.35)$$

In these

symmetry

the same

need to

letting

(2.33) a

where L

torsion,

followi

$L_{EW} = \int$

where A

B

C

$K_t =$ $\frac{}{G}$

for al

bridge

In these four equations, the two unknowns are K_t and I_w. Because of symmetry of stiffness equations, equations (2.33) and (2.34) will yield the same results. Therefore, only equations (2.32), (2.33) and (2.35) need to be solved to achieve equivalence. As in the case of bending, by letting the length of the element L be a variable in equations (2.32), (2.33) and (2.35), three equations in the three unknowns K_t, I_w and Lew, where Lew is the "effective" beam length with respect to warping and torsion, were obtained.

Solving equations (2.32), (2.33) and (2.35) results in the following expressions for Lew, K_t and I_w.

$$Lew = \sqrt{(-B + (B^2 - 4\,AC)} \;/\; 2A \tag{2.36}$$

$$\text{where } A = (-R_m\, W_t\, M_z) + (W_m\, R_t\, M_z) + (M_w\, W_t^2) \tag{2.37}$$

$$B = 8W_t\, M_w\, R_t \tag{2.38}$$

$$C = -15\, M_w\, R_t^2 \tag{2.39}$$

$$K_t = \frac{30M_z Lew\,(-3R_t + 2W_t Lew)}{G(36R_t - 3W_t Lew)(-3R_t + 2W_t Lew) + (6R_t - 3W_t Lew)(3R_t - 4W_t Lew)} \tag{2.40}$$

$$I_w = \frac{(GK_t^2 Lew)\,(3R_t - 4W_t^2 Lew)}{(60E)\,(-3R_t + 2W_t Lew)} \tag{2.41}$$

By deriving the beam equivalent stiffness and effective length for all segments of the arch and deck, the equivalence between the real bridge structure and the model is assured.

were cl

stiffnes

by usir

and weal

panels

panels

and Lev

were di

average

Thus,

five pa

corresp

element

2.4.3

calcul

the c

strin

cross-

moder

four

cross

and t

Since

0 to

As mentioned earlier, two cantilevered segments of the NRGB arch were chosen to represent the strongest and weakest sections. The stiffness of intermediate segments were calculated at segments midpoints by using linear interpolation between the stiffnesses of the strongest and weakest sections. The straight beam elements representing the end panels in the NRGB arch were 1½ subpanels in length, while the other panels were 3 subpanels. For this case the equivalent lengths Lex, Ley and Lew, which were calculated for the midpoints of the end elements, were divided by two.

For the CSCB arch, the three cantilevered segments were based on average member sizes and lengths over five of the eleven arch panels. Thus, the stiffnesses for the straight beam elements representing these five panels were taken to be the same as the values calculated for the corresponding cantilevered segments. For the intermediate straight beam elements, the stiffnesses were determined by linear interpolation.

2.4.3 MODELING OF THE DECK OF THE CSCB BRIDGE

Equivalent straight beam stiffnesses for the CSCB deck were calculated based on the composite action of the four floor stringers and the concrete roadway deck. Because there are four average floor stringer cross-sections in the CSCB deck and hence four average deck cross-sections, four sets of deck stiffnesses were calculated.

Since the roadway slab can be expected to crack under relatively moderate loads, the first step in calculating the stiffnesses of the four CSCB deck cross-sections was an estimation of the portion of the cross-sectional area of the roadway slab that would be in compression and thus contributing to overall deck stiffness at any given time. Since the portion of the slab area in compression could be anything from 0 to 100%, a compromise value of 50% was chosen. This assumption

coupled

"effecti

by a fac

four fl

to calcu

torsion

beams,

with the

string

convers

divide

effecti

center

calcula

channe

a recta

inerti

the st

of on

dimens

warpi

consta

semi-r

warpi

connec

only

joints

coupled with a modular ratio of steel to concrete of 10, led to an "effective" modular ratio of 20. Thus the area of concrete was reduced by a factor of 20 and then used in conjunction with the areas of the four floor stringers, the slab reinforcing steel and the deck laterals to calculate the axial area, shear areas, moments of inertia and the torsion constant for each deck cross-section.

In determining the warping constants for the equivalent deck beams, each deck cross-section was first converted to a channel section with the concrete roadway slab acting as the channel web and the outside stringers acting as the channel flanges. The first step in this conversion was to reduce the area of concrete by a factor of 20 and then divide by 28 feet (the distance between the outside stringers) to get an effective channel web thickness. Next, the average distance from the center of the roadway slab to the bottoms of the floor stringers was calculated and used as a channel flange width. Then, an effective channel flange thickness was calculated by determining the thickness of a rectangular flange moment of inertia equal to 1.33 times the moment of inertia of one floor stringer. The factor of 1.33 was based on 100% of the stiffness of one exterior floor stringer plus 33% of the stiffness of one interior floor stringer. Finally, with all of the channel dimensions determined, the values were substituted into the general warping constant formula for a channel section and thus the warping constants for the four deck cross-sections were determined.

The deck expansion connection at panel point 1 was modeled as semi-rigid with global X axis translation, Y and Z axis rotations, and warping displacements of the deck, allowed at this point. The bearing connection at panel point 20 was also modeled as semi-rigid but with only Y and Z axis rotations and warping displacements allowed. The deck joints at panel points 6 and 17 were modeled such that no Z axis moments

or warp

decks ar

2.4.4 M

main sp

truss e

the col

and bot

to be t

panel p

the CSC

one la

dimens

result

beams

L is t

12 in

in the

simil

2.4.5

and r

deck

bimom

or warping bimoments could be transferred between the approach span decks and the main span deck.

2.4.4 MAIN SPAN COLUMN AND CABLE MODELING

Except for the columns at panel points 11 and 12, each pair of main span columns at a given panel point were represented by a single truss element in the CSCB models. Truss elements were chosen because the columns in the CSCB (excluding the towers) are hinged at both top and bottom. The cross-sectional area of these truss elements was taken to be twice the cross-sectional area of one column.

The systems of columns and transverse cables (Figure 2-11) at panel points 11 and 12 were each represented by a single beam element in the CSCB models. A pair of truss elements representing one column and one lateral cable as illustrated in Figure 2-12 were analyzed in two dimensions. Loads P_y and P_z were applied in turn at the free joint resulting in translations D_y and D_z. The axial areas of the equivalent beams at panel points 11 and 12 were determined using $A=2P_yL/(ED_y)$ where L is the distance between the arch and deck nodes at panel points 11 and 12 in the one plane models of the CSCB.

The moment of inertia about the global X axis, the shear area in in the global Z direction and the effective length were determined in similar way as discussed in section 2.4.2.

2.4.5 CSCB APPROACH SPAN MODELING

The approach spans in the CSCB were represented by translation and rotation springs. These springs were located at the centroid of the deck at panel points 6 and 17. Because of the Z axis moment and the bimoment releases in the deck at panel points 6 and 17. Because of the

Z axis m

and 17,

these po

parallel

inertia

the rep

represe

springs

transl

17, the

with t

element

centr

approa

elemer

deck a

in the

the di

the s

displ

axis

repr

$S_y = F_y$

calc

Z axis moment and the bimoment releases in the deck at panel points 6 and 17, no Z axis rotation springs or warping springs were needed at these points to represent the approach spans.

The beam elements used to represent the approach span decks were parallel with the global X axis and were of equal length. The moment of inertia with respect to Y axis and the Z axis shear area were taken as the represented segment properties. The other section properties were represented as part of the stiffnesses of the translation and rotation springs at panel points 6 and 17 as described below.

In order to derive the stiffnesses of the X and Y axis translation springs and X axis rotation springs at panel points 6 and 17, the north and south approach spans were analyzed in their entirety with the tower columns, tower struts and deck represented as beam elements and the remaining columns represented as truss elements. The centroid of the continuous beam that represented the deck in each approach span was fastened to the tops of the columns using rigid elements. Three loads were then applied in turn at the centroid of the deck at panel point 6 in the south approach span and at panel point 17 in the north approach span. The first load applied was a force F_x in the direction of the global X axis, which resulted in a displacement D_x, the second load was a Y direction force F_y which resulted in a displacement D_y and the third load was a moment M_x about the global X axis which resulted in a rotation ϕ_x.

The stiffnesses of the X and Y axis translation springs representing each approach span were determined by $S_x=F_x/D_x$ and $S_y=F_y/D_y$, respectively. The stiffness of the X axis rotation spring was calculated using $R_x=M_x/\phi_x$. The X axis translation and rotation springs

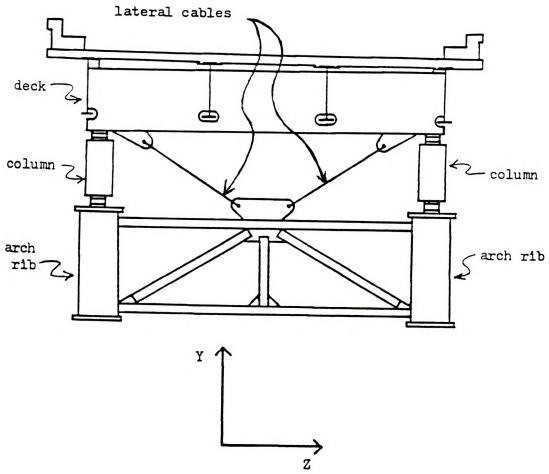

Figure 2-11: CSCB Lateral Cables. (Excerpted from Dusseau (1985))

a)

b

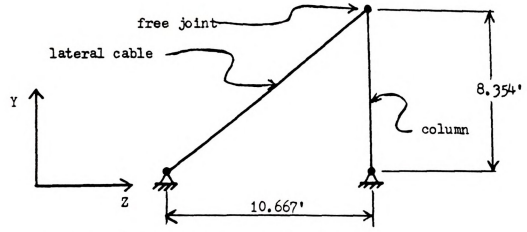

a) Lateral Cable Model

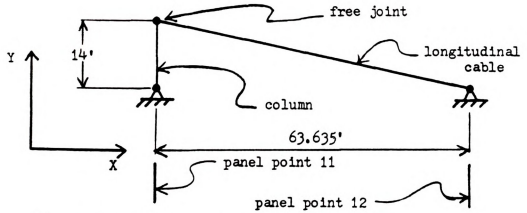

b) Longitudinal Cable Model 1

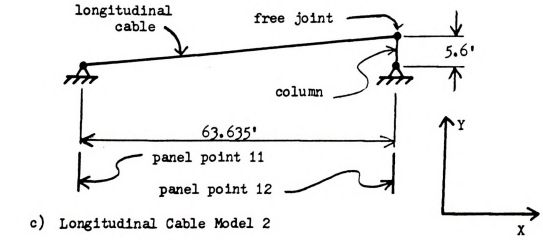

c) Longitudinal Cable Model 2

Figure 2-12: CSCB Cable Models. (Excerpted from Dusseau (1985))

were re

using A

be 10 f

(L=10 f

y axis

(Figure

global

result

the z

determ

the y

while

the f

elemen

2.4.6

per f

dead

for

appro

node

17 fc

and

were represented by beam elements. The axial areas were calculated using $A=\frac{L\,S_x}{E}$, where L is the length of the beam element and was taken to be 10 feet. The torsion constants were determined using $K_t=(L\ R_x)/G$ (L=10 feet).

To derive the stiffnesses of the Z axis translation springs and y axis rotation springs at panel points 6 and 17, only the towers (Figure 2-13) were analyzed. First, a force F_z in the direction of global Z axis then a moment M_y about the y axis were applied separately resulting in a displacement D_z and a rotation ϕ_y, respectively. Then the z axis translation springs and the Y axis rotation springs were determined using $S_z=F_z/D_z$ and $R_y=M_y/\phi_y$. The torsional constant about the y axis of the beam element was determined using $K_T=(L\ R_y)/G$, (L=10), while the axial area of the Z direction beam element was calculated by the formula $A=(10\ S_z)/E$. All other stiffness elements for the beam elements representing the CSCB approach span were taken to be zero.

2.4.6 CSCB MASS DISTRIBUTION

The lumped nodal masses were based on the average dead weights per foot (Merritt, F.S., 1972) of the bridge components. These average dead load weights per foot are 3930 pounds, 5335 pounds and 210 pounds for the arch, deck and columns, respectively. Portions of the CSCB approach span deck, tower and column masses were lumped at the deck nodes at panel point 6 for the south approach span, and at panel point 17 for the north approach span. For the north span, half of the deck and tower masses and one-fourth of the column masses were lumped at

Dec

Tower

Figur

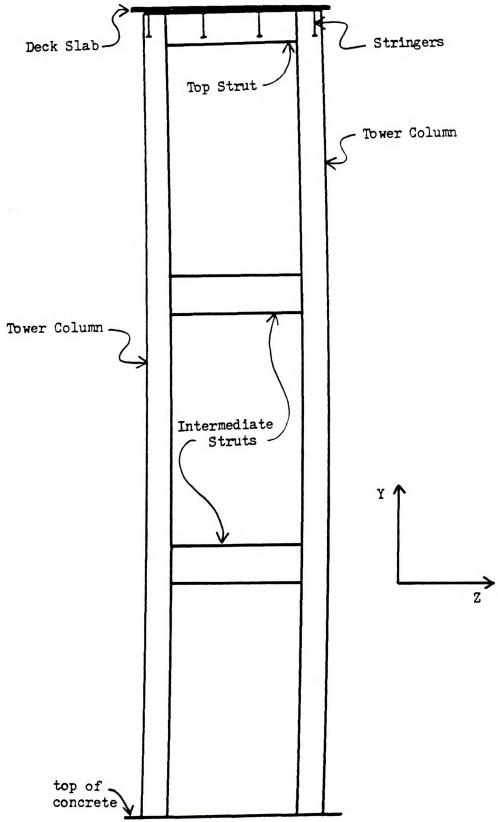

Figure 2-13 CSCB Tower Elevation View. (Excerpted from Dusseau (1985))

panel po

half of

lumped a

2.4.7 I

equival

11. Th

longitu

shown

connect

finite

specif

Table

2.4.8

the NI

numbe

repre

to th

relea

span

Figu

the

indi

spec

panel point 17 in the x and y directions. For the south approach span, half of deck and tower masses and one-fourth of the column masses were lumped at panel point 6 (Figure 2-2).

2.4.7 FINAL CSCB MODEL

The one-plane model of the CSCB is shown on Figure 2-14. The equivalent beam elements of the arch and the deck are numbered from 1 to 11. The two truss elements representing the cables which transfer longitudinal loads from the deck to the arch are labelled 1 and 2. Also shown are the two deck moment releases resulting from the hinge connection at the towers. Figure 2-15 shows the numbering used in the finite element model. The stiffness properties of all the elements are specified in Table 2-1. The listings for the lumped masses are shown in Table 2-2.

2.4.8 FINAL NRGB MODEL

The same procedures were used to derive the one-plane model of the NRGB. The equivalent beam elements of the deck and the arch are numbered from 1 to 14 (see Figure 2-16). The two truss elements representing the cables which transfer longitudinal loads from the deck to the arch are labelled 1 and 2. The deck axial force and moment releases resulting from the expansion joints at the ends of the main span are also shown.

The numbering used in the finite element model is shown in Figure 2-17. The masses lumped at each node of the model are based on the total weights of the arch, main span deck, approach span decks and individual bents.

The lumped masses and the element stiffness parameters are specified in Tables 2-3 and 2-4.

Table 2-

Table 2-1 Element Stiffness Parameters for CSCB

		ASB	AGXS	AGYS	I_{xx}	I_{yy}	KTS	IWS
Truss Elem	1	0.014	-	-	-	-	-	-
	2	0.014	-	-	-	-	-	-
Column	3	0.667	-	-	-	-	-	-
	4	0.667	-	-	-	-	-	-
	5	0.667	-	-	-	-	-	-
	6	0.667	-	-	-	-	-	-
	7	0.667	-	-	-	-	-	-
	8	0.667	-	-	-	-	-	-
	9	0.667	-	-	-	-	-	-
	10							
Deck	1	2.227	0.451	1.589	225.820	8.320	0.126	720.685
Member	2	2.201	0.451	1.551	225.820	7.631	0.126	702.852
	3	2.167	0.451	1.528	219.204	7.435	0.126	683.990
	4	2.167	0.451	1.528	219.204	7.435	0.126	683.990
	5	2.167	0.451	1.528	219.204	7.435	0.126	683.990
	6	2.167	0.451	1.528	219.204	7.435	0.126	683.992
	7	2.167	0.451	1.528	219.204	7.435	0.126	683.992
	8	2.167	0.451	1.528	219.204	7.435	0.126	683.992
	9	2.167	0.451	1.528	219.204	7.435	0.126	683.992
	10	2.201	0.451	1.551	222.521	7.631	0.126	702.852
	11	2.227	0.451	1.589	225.821	8.320	0.126	720.685
	12	0.667	0.000	0.021	274.624	0.000	1.604	0.000
	13	0.667	0.000	0.021	274.624	0.000	1.604	0.000
	14	0.009	0.000	1.540	220.602	0.000	3434.668	0.000
	15	0.250	0.000	0.000	0.000	0.000	1.329	0.000
	16	0.002	0.000	0.000	0.000	0.000	0.000	0.000
	17	2.174	0.000	1.548	221.584	0.000	2017.002	0.000
	18	0.250	0.000	0.000	0.000	0.000	1.329	0.000
	19	0.017	0.000	0.000	0.000	0.000	0.000	0.000
	20	4.752	2.810	0.382	997.029	57.039	33.047	0.000
	21	5.549	2.811	0.342	1165.350	74.760	37.615	0.000
	22	6.347	2.813	0.302	1333.680	92.481	42.183	0.000
	23	5.960	2.818	0.282	1184.220	83.812	39.954	0.000
	24	5.573	2.812	0.261	1034.750	75.143	37.725	0.000
	25	5.187	2.812	0.241	885.285	66.474	35.496	0.000
	26	5.573	2.812	0.261	1034.750	75.143	37.725	0.000
	27	5.960	2.813	0.282	1184.220	83.812	39.954	0.000
	28	6.347	2.813	0.302	1333.680	92.481	42.183	0.000
	29	5.549	2.811	0.342	1165.350	74.760	37.615	0.000
	30	4.752	2.810	0.382	997.029	57.039	33.047	0.000

Table 2-

Node
8
12
13
14
15
16
17
18
19
20
21
22

Table

Nod

Table 2-2 Lumped Masses for CSCB

Node	Mass	Node	Mass
8	62.429	23	10.619
12	11.977	24	7.587
13	8.358	25	10.643
14	10.886	26	8.474
15	8.507	27	10.730
16	10.731	28	8.874
17	8.201	29	10.886
18	10.643	30	8.764
19	7.439	31	11.977
20	10.619	35	25.166
21	6.876		
22	6.919		

Table 2-3 Lumped Masses for NRGB

Node	Mass	Node	Mass
9	62.8167	10	70.5313
33	62.816	12	66.235
11	65.953	14	63.421
31	65.953	16	61.067
13	57.021	18	59.399
29	57.021	20	58.576
15	49.833	22	56.902
27	49.933	24	58.576
17	44.499	26	59.399
25	44.499	28	61.067
19	40.675	30	63.421
23	40.675	32	66.235
21	36.703	34	70.531
8	79.040	36	77.513

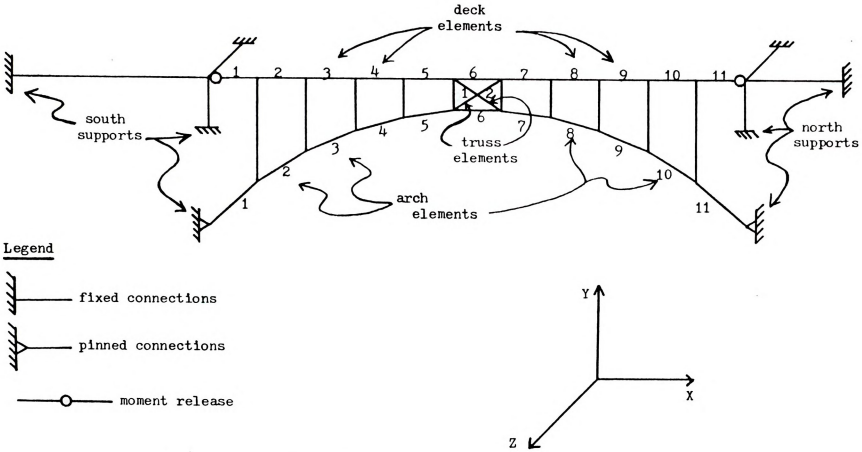

Figure 2-14: CSCB One-plane Model (Excerpted from Dusseau (1985))

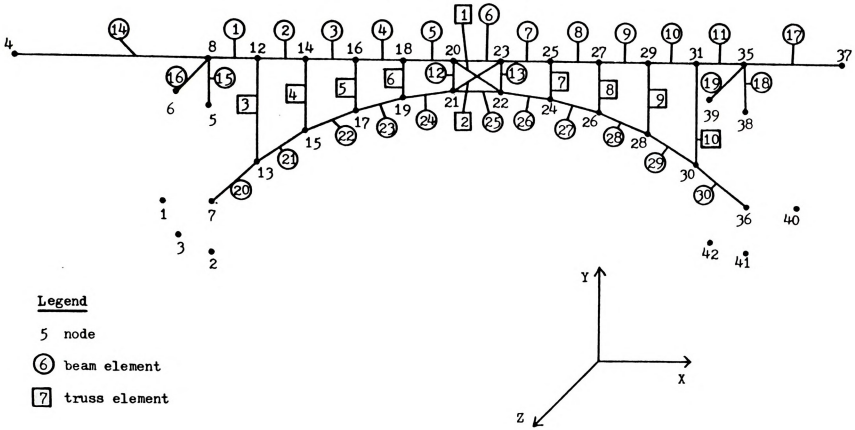

Figure 2-15: CSCB Node and Element Numbers (Excerpted from Dusseau (1985))

Table

Truss	
Beam M	

Table 2-4 Element Stiffness Parameters for NRGB

	ASB	AGXS	AGYS	I_{xx}	I_{yy}	KTS	IWS
Truss Members							
1	1.956	-	-	-	-	-	-
2	1.956	-	-	-	-	-	-
Beam Members							
1	0.996	0.304	0.118	1304.52	80.654	12.804	82338
2	0.996	0.304	0.118	1304.52	80.654	12.804	82338
3	0.996	0.304	0.118	1304.52	80.654	12.804	82338
4	0.996	0.304	0.118	1304.52	80.654	12.804	82338
5	0.996	0.304	0.118	1304.52	80.654	12.804	82338
6	0.996	0.304	0.118	1304.52	80.654	12.804	82338
7	0.996	0.304	0.118	1304.52	80.654	12.804	82338
8	0.996	0.304	0.118	1304.52	80.654	12.804	82338
9	0.996	0.304	0.118	1304.52	80.654	12.804	82338
10	0.996	0.304	0.118	1304.52	80.654	12.804	82338
11	0.996	0.304	0.118	1304.52	80.654	12.804	82338
12	0.996	0.304	0.118	1304.52	80.654	12.804	82338
13	0.996	0.304	0.118	1304.52	80.654	12.804	82338
14	0.996	0.304	0.118	1304.52	80.654	12.804	82338
15	3.529	0.000	0.550	3459.72	0.000	0.000	0
16	3.437	0.000	0.587	3438.65	0.000	0.000	0
17	3.395	0.000	0.803	3201.43	0.000	0.000	0
18	4.061	0.000	0.792	3115.42	0.000	0.000	0
19	4.914	0.000	1.531	5805.94	0.000	0.000	0
20	5.922	0.000	0.182	2655.29	0.000	0.000	0
21	3.042	0.000	0.769	6020.25	0.000	3960.960	0
22	5.922	0.000	0.182	2655.29	0.000	0.000	0
23	4.914	0.000	1.531	5805.94	0.000	0.000	0
24	4.061	0.000	0.792	3115.42	0.000	0.000	0
25	3.395	0.000	0.803	3201.43	0.000	0.000	0
26	3.437	0.000	0.587	3438.65	0.000	0.000	0
27	3.529	0.000	0.550	3459.75	0.000	0.000	0
28	0.000	0.000	0.000	0.00	0.000	347.475	0
29	0.085	0.000	0.000	0.00	0.000	0.000	0
30	0.003	0.000	0.000	0.00	0.000	0.000	0
31	0.000	0.000	0.000	0.00	0.000	352.731	0
32	0.089	0.000	0.000	0.00	0.000	0.000	0
33	0.003	0.000	0.000	0.00	0.000	0.000	0
34	14.428	0.484	1.622	24946.80	9774.56	1355.360	0
35	13.836	0.482	1.537	23921.40	8823.50	1277.170	0
36	13.077	0.480	1.428	22608.40	7605.71	1177.040	0
37	12.366	0.478	1.327	21377.80	6464.36	1083.190	0
38	11.689	0.475	1.230	20206.30	5377.82	993.854	0
39	11.036	0.473	1.136	19076.60	4329.99	907.700	0
40	10.399	0.472	1.045	17973.20	3306.59	823.553	0
41	10.399	0.471	1.045	17973.20	3306.59	823.553	0
42	11.036	0.473	1.136	19076.60	4329.99	907.700	0
43	11.689	0.475	1.230	20206.30	5377.82	993.854	0
44	12.366	0.478	1.327	31277.80	6464.36	1083.190	0
45	13.077	0.480	1.428	22608.40	7605.71	1177.040	0
46	13.836	0.482	1.537	23921.40	8823.50	1277.170	0
47	14.428	0.484	1.622	24946.80	9774.56	1355.360	0

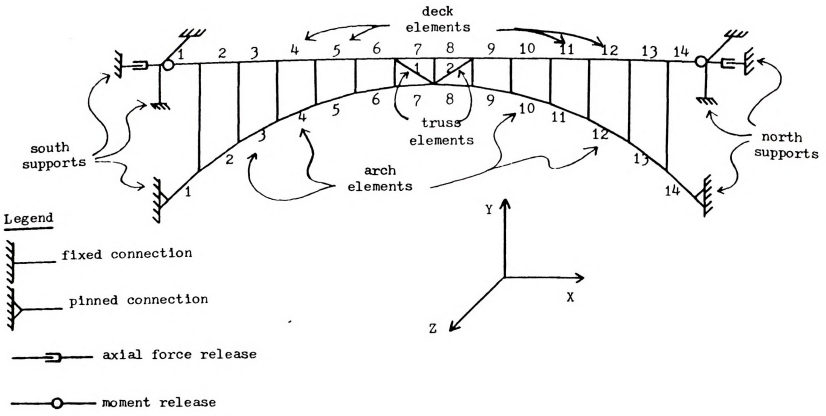

Figure 2-16: NRGB One-plane Model (Excerpted from Dusseau (1985))

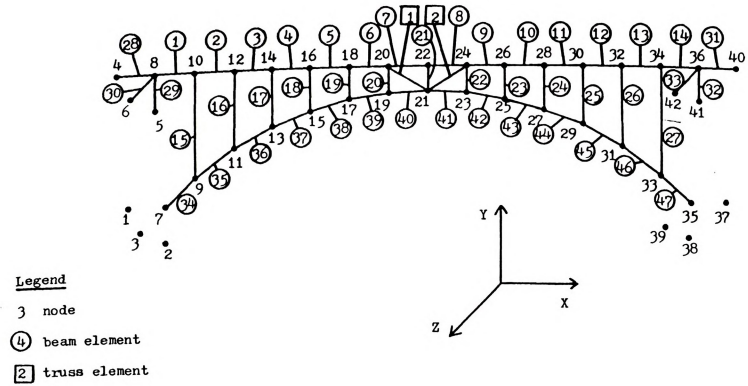

Figure 2-17: NRGB Node and Element Numbers (Excerpted from Dusseau (1985))

2.5 LI

Robert
unequa
program
a. It
de
le
be
b. It
de
co
if
ar
tr
a
c
c. I
r

2.5.

each
are
ther
main
coli
betw
wer

2.5 LINSTRUC PROGRAM

The LINSTRUC Program was developed by Ralph A. Dusseau and Robert K. Wen (1985) to perform the analysis of arch bridges subject to unequal seismic support motions using time-history analysis. The program has the following special features:

a. It uses a straight beam element with both shear and warping deformation with "effective" member lengths. These effective lengths were used to achieve equivalence between the stiffnesses of beam elements in the model and in the real structure.

b. It has a "master" and "slave" node feature, which allows the user to declare a displacement at a given node (slave) to be equal to the corresponding displacement at another (master) node. For example, if node 21 is slave to node 26 with respect to X and Y translation and Z rotation, then these displacements will be the same for the two nodes, and a rotation at node 26 will not cause corresponding X and Y translations at node 21. Thus slave nodes cannot be used to create rigid links in the program.

c. It has a static condensation procedure that allows the user to remove some nodel degrees-of-freedom before dynamic analysis.

2.5.1 FURTHER REDUCTION IN THE DEGREES-OF-FREEDOM

In the CSCB, the deck and arch are connected by two columns at each panel point. Assuming that the axial deformation of these columns are nominal and that the deck and arch cross-sections do not deform, then the deck, the arch and the two columns at each panel point must maintain a parallelogram configuration under all loads. Since the columns in the CSCB are truss members which allow no shear transfer between the deck and the arch, the pair of column at each panel point were represented in the model by a single truss element. In order to

maintai

necessa

the sam

models,

panel

both th

maintain the parallelogram configuration described above, it was necessary to require the arch and deck nodes at each panel point to have the same longitudinal X-axis rotation.

To further reduce the number of degrees-of-freedom in the bridge models, the additional requirement that the arch and deck nodes at each panel point have the same vertical Y-axis translation was imposed for both the NRGB and CSCB models.

3.1 PI

elemen

motion

are

where

entr

free

equa

+

CHAPTER 3

RANDOM VIBRATION ANALYSIS

3.1 FINITE ELEMENT FORMULATION OF EQUATIONS OF MOTION

The model of the two bridges are discretized into finite elements as shown in Figure 3-1 and Figure 3-2. The equations of motions of a multiple degree-of-freedom system subject to support motion are

$$[M]\{\ddot{X}\} + [C]\{\dot{X}\} + [k]\{X\} = \{0\} \tag{3.1}$$

where $[M]$ = lumped or consistant mass matrix

$[C]$ = damping matrix

$[k]$ = stiffness matrix

$\{X\}$, $\{\dot{X}\}$, $\{\ddot{X}\}$ are the absolute displacements, velocity and acceleration vectors

By partitioning the matrices $[M]$, $[C]$ and $[k]$ such that the entries of these matrices correspond to the partioning of $\{X\}$ into the free displacements $\{X_F\}$, and restrained displacements $\{X_R\}$, the equations of motion may be expressed as

$$\begin{bmatrix} [M_{RR}] & [M_{RF}] \\ [M_{FR}] & [M_{FF}] \end{bmatrix} \begin{Bmatrix} \{\ddot{X}_R\} \\ \{\ddot{X}_F\} \end{Bmatrix} + \begin{bmatrix} [C_{RR}] & [C_{RF}] \\ [C_{FR}] & [C_{FF}] \end{bmatrix} \begin{Bmatrix} \{\dot{X}_R\} \\ \{\dot{X}_F\} \end{Bmatrix}$$

$$+ \begin{bmatrix} [k_{RR}] & [k_{RF}] \\ [k_{FR}] & [k_{FF}] \end{bmatrix} \begin{Bmatrix} \{X_R\} \\ \{X_F\} \end{Bmatrix} = \begin{Bmatrix} \{0\} \\ \{0\} \end{Bmatrix} \tag{3.2}$$

where (X

(

Thus

pseudo

Then,
follo

the

The
str

where $\{X_F\}$, $\{\dot{X}_F\}$, $\{\ddot{X}_F\}$ are the absolute displacement, velocity and acceleration vectors of free nodes

$\{X_R\}$, $\{\dot{X}_R\}$, $\{\ddot{X}_R\}$ are the absolute displacement, velocity and acceleration vectors of restrained (support) nodes due to ground motion

Thus $$\{X\} = \begin{Bmatrix} \{X_R\} \\ \{X_F\} \end{Bmatrix} \tag{3.3}$$

The free nodal displacement vectors $\{X_F\}$ can be decomposed into pseudo-static $\{X_F^s\}$ and dynamic $\{X_F^d\}$ components

$$\{X_F\} = \{X_F^s\} + \{X_F^d\} \tag{3.4}$$

Then, the total absolute displacement vector may be written in the following form

$$\{X\} = \begin{Bmatrix} \{X_R\} \\ \{X_F\} \end{Bmatrix} = \begin{Bmatrix} \{X_R\} \\ \{X_F^s\} + \{X_F^d\} \end{Bmatrix} \tag{3.5}$$

The pseudo-static displacements $\{X_F^s\}$ are the displacements of the free structural nodes due to static support displacements $\{X_R\}$. These are obtained from the static equilibrium equations of the structure with no applied external loads, i.e.,

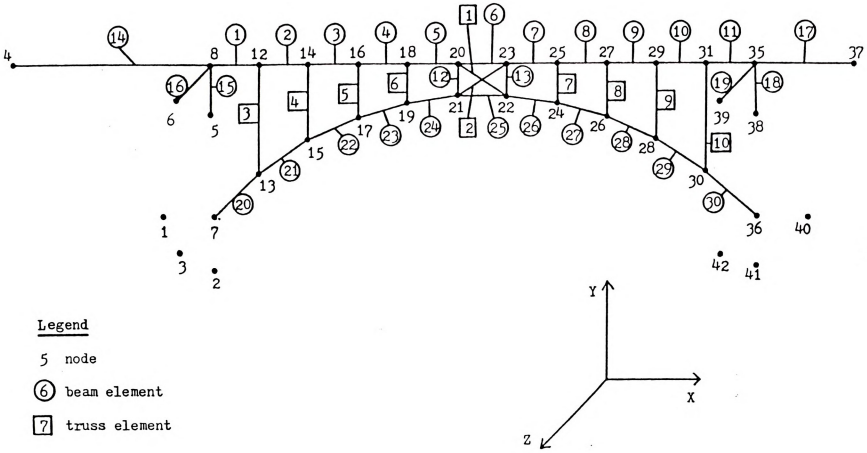

Figure 3-1: Finite Element Model of CSCB

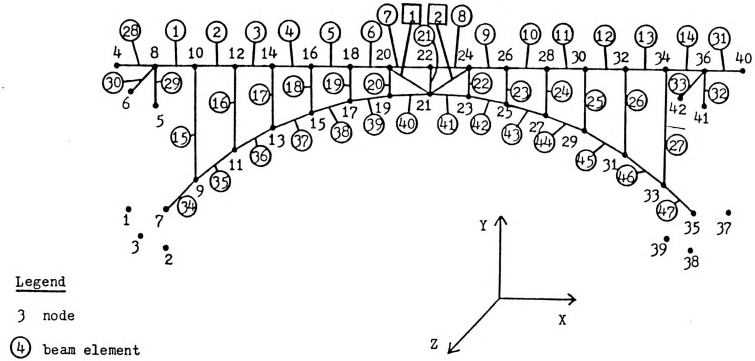

Figure 3-2: Finite Element Model of NRGB

Taking

and so

Subst

The

$$\begin{bmatrix} [k_{RR}] & [k_{RF}] \\ [k_{FR}] & [k_{FF}] \end{bmatrix} \begin{Bmatrix} (X_R) \\ (X_F^s) \end{Bmatrix} = \begin{Bmatrix} 0 \\ 0 \end{Bmatrix} \tag{3.6}$$

Taking the second system of equations (3.6), gives

$$[k_{FR}]\ (X_R) + [k_{FF}]\ (X_F^s) = 0 \tag{3.7}$$

and solving for (X_F^s), yields

$$(X_F^s) = -[k_{FF}]^{-1}\ [k_{FR}]\ (X_R) \tag{3.8}$$

Substituting equation (3.5) into equation (3.2) yields

$$\begin{bmatrix} [M_{RR}] & [M_{RF}] \\ [M_{FR}] & [M_{FF}] \end{bmatrix} \begin{Bmatrix} (\ddot{X}_R) \\ (\ddot{X}_F^s) + (\ddot{X}_F^d) \end{Bmatrix} + \begin{bmatrix} [C_{RR}] & [C_{RF}] \\ [C_{FR}] & [C_{FF}] \end{bmatrix}$$

$$\begin{Bmatrix} (\dot{X}_R) \\ (\dot{X}_F^s) + (\dot{X}_F^d) \end{Bmatrix} + \begin{bmatrix} [k_{RR}] & [k_{RF}] \\ [k_{FR}] & [k_{FF}] \end{bmatrix} \begin{Bmatrix} (X_R) \\ (X_F^s) + (X_F^d) \end{Bmatrix}$$

$$= \begin{Bmatrix} (0) \\ (0) \end{Bmatrix} \tag{3.9}$$

The second system of equation in (3.9) is

$$[M_{FR}]\ (\ddot{X}_R) + [M_{FF}]\ (\ddot{X}_F^s) + [M_{FF}]\ (\ddot{X}_F^d)$$

$$+ [C_{FR}]\ (\dot{X}_R) + [C_{FF}]\ (\dot{X}_F^s) + [C_{FF}]\ (\dot{X}_F^d)$$

+ [k

Separat

(3.8) g

= [

+ [

secon

of li

motio

=

3.2

expa

und

exp

$$+ [k_{FR}] \{X_R\} + [k_{FF}] \{X_F^s\} + [k_{FF}] \{X_F^d\} = \{0\} \qquad (3.10)$$

Separating the dynamic response from static response and using equation (3.8) gives

$$[M_{FF}] \{\ddot{X}_F^d\} + [C_{FF}] \{\dot{X}_F^d\} + [k_{FF}] \{X_F^d\}$$

$$= [- M_{FR} + [M_{FF}] [k_{FF}]^{-1} [k_{FR}]] \{\ddot{X}_R\}$$

$$+ [- [C_{FR}] + [C_{FF}] [k_{FF}]^{-1} [k_{FR}]] \{\dot{X}_R\} \qquad (3.11)$$

For stiffness proportional damping, for which $[C] = \alpha [k]$, the second term of the right hand side is equal to zero; and for other forms of light damping it may be neglected. Thus, the final equations of motions for the free displacements become

$$[M_{FF}] \{\ddot{X}_F^d\} + [C_{FF}] \{\dot{X}_F^d\} + [k_{FF}] \{X_F^d\}$$

$$= [[M_{FF}] [k_{FF}]^{-1} [k_{FR}] - [M_{FR}]] \{\ddot{X}_R\} \qquad (3.12)$$

3.2 MODAL ANALYSIS AND NORMAL COORDINATES

Using normal coordinates, the dynamic displacements can be expanded in terms of the undamped free vibration mode shapes; thus for undamped harmonic free vibration the dynamic displacements may be expressed as

in whic

(Y) ar

free v

Subst

eigen

The

ω_j a

into

$$\{X_F^d\} = [\Psi]\ \{Y\}\ e^{i\omega t} \tag{3.13}$$

in which $[\Psi] = [\{\psi_1\}\ \{\psi_2\}\ \ldots\ \{\psi_n\}]$ is the matrix of mode shapes and $\{Y\}$ are the normal coordinates.

The mode shape vectors $\{\psi_i\}$ are obtained by solving the undamped free vibration equations of motion.

$$[M_{FF}]\ \{\ddot{X}_F^d\} + [k_{FF}]\ \{X_F^d\} = \{0\} \tag{3.14}$$

Substituting equation (3.13) into equation (3.14) yields the generalized eigenvalue problems.

$$[[k_{FF}] - [\text{diag}\ (\omega^2)]\ [M_{FF}]]\ [\Psi] = [0] \tag{3.15}$$

The solution of these equations yields the undamped natural frequencies ω_j and mode shapes, $\{\psi_j\}$, of the structure. Substituting

$$\{X_F^d\} = [\Psi]\ \{Y\} \tag{3.16}$$

into equations (3.12) yields

$$[M_{FF}]\ [\Psi]\ \{\ddot{Y}\} + [C_{FF}]\ [\Psi]\ \{\dot{Y}\} + [K_{FF}]\ [\Psi]\ \{Y\}$$

$$= [[M_{FF}]\ [k_{FF}]^{-1}\ [k_{FR}] - [M_{FR}]]\ \{\ddot{X}_R\} \tag{3.17}$$

Multipl

$[\phi]^T$ an

yield

where

Multiplying equation (3.17) through by the transpose of the modal vector $[\psi]^T$ and making use of the orthogonality conditions

$$\begin{aligned} (\psi_j)^T [M_{FF}] (\psi_k) &= 0 \\ (\psi_j)^T [C_{FF}] (\psi_k) &= 0 \qquad \text{for } J \neq K \\ (\psi_j)^T [k_{FF}] (\psi_k) &= 0 \end{aligned} \tag{3.18}$$

yields the uncoupled model equations

$$M_j \ddot{Y}_j + C_j \dot{Y}_j + k_j Y_j = F_j \tag{3.19}$$

where the scalor quantities

$$M_j = (\psi_j)^T [M_{FF}] (\psi_j) \tag{3.20}$$

$$C_j = (\psi_j)^T [C_{FF}] (\psi_j) \tag{3.21}$$

$$k_j = (\psi_j)^T [k_{FF}] (\psi_j) \tag{3.22}$$

$$F_j = (\psi_j)^T [[M_{FF}] [k_{FF}]^{-1} [k_{FR}] - [M_{FR}]] (\ddot{X}_R) \tag{3.23}$$

are the

Dividir

where

In p

rati

is c

mat

the

are the generalized mass, damping, stiffness and excitation force. Dividing equation (3-19) by M_j gives

$$\ddot{Y}_j + 2\,\zeta_j\,\omega_j\,\dot{Y}_j + \omega_j^2\,Y_j = G_j \tag{3.24}$$

where

$$G_j = \frac{1}{M_j}\,(\psi_j)^T[[M_{FF}][k_{FF}]^{-1}[k_{FR}] - [M_{FR}]](\ddot{X}_R) = (\Gamma_j)^T(\ddot{X}_R) \tag{3.25}$$

$$2\,\zeta_j\omega_j = \frac{C_j}{M_j} \tag{3.26}$$

$$\omega_j^2 = \frac{k_j}{M_j} \tag{3.27}$$

$$(\Gamma_j) = \frac{1}{M_j}\,[[M_{FF}]\,[k_{FF}]^{-1}\,[k_{FR}] - [M_{FR}]]^T\,(\psi_j) \tag{3.28}$$

In practice it is common to assume typical values for the modal damping ratios ζ_j rather than to assemble the physical damping matrix [C]. It is convenient to collect the modal participation factors (Γ_j) into a matrix

$$[\Gamma] = [(\Gamma_1)\ (\Gamma_2)\ \ldots\ (\Gamma_n)] \tag{3.29}$$

then, the right hand side of equation (3.24) may be written as

$$(G) = [\Gamma]^T\,(\ddot{X}_R) \tag{3.30}$$

r is th

mode sh

3.3 Re

and

Then,

u_F,

the

whe

(3.

The modal participation factor matrix [Γ] is of size r x n where r is the number of restrained degrees-of-freedom and n is the number of mode shapes considered in the analysis.

3.3 RANDOM VIBRATION ANALYSIS

For notational convenience, let

$$X_F^d = u_d$$

$$X_F^s = u_s$$

and

$$X_F = u_F$$

Then, according to equation (3.4)

$$u_F = u_d + u_s \tag{3.31}$$

u_F, u_d and u_s are functions of time t. For the i^{th} degree of freedom, the autocorretation function of the displacement is defined as

$$R_{u_{F_i}}(\tau) = E\,[u_{F_i}(t)\; u_{F_i}(t+\tau)] \tag{3.32}$$

where τ is time delay. Substituting equation (3.31) into equation (3.32) yields

where

For

Th

th

$$R_{u_{F_i}}(\tau) = E\,[[u_{d_i}(t) + u_{s_i}(t)]\,[u_{d_i}(t+\tau) + u_{d_i}(t+\tau)]]$$

$$= E\,[u_{d_i}(t)\,u_{d_i}(t+\tau)] + E\,[u_{d_i}(t)\,u_{s_i}(t+\tau)]$$

$$+ E\,[u_{s_i}(t)\,u_{d_i}(t+\tau)] + E\,[u_{s_i}(t)\,u_{s_i}(t+\tau)]$$

$$= R_{u_{d_i}}(\tau) + R_{u_{d_i}\,u_{s_i}}(\tau) + R_{u_{s_i}\,u_{d_i}}(\tau) + R_{u_{s_i}}(\tau) \qquad (3.33)$$

where

$R_{u_{d_i}}(\tau)$ is the autocorrelation of the dynamic component of the displacements

$R_{u_{s_i}}(\tau)$ is the autocorrelation of the static component of displacements

$R_{u_{s_i}\,u_{d_i}}(\tau)$ and $R_{u_{d_i}\,u_{s_i}}(\tau)$ are the cross correlation between static and dynamic components.

For a stationary response

$$R_{u_{d_i}\,u_{s_i}}(\tau) = R_{u_{s_i}\,u_{d_i}}(-\tau) \qquad (3.34)$$

The fourier transform of equation (3.33) yields the spectral density of the free displacements

For st

where

i^{th} f

whe

$$S_{u_{F_i}}(\omega) = S_{u_{d_i} u_{d_i}}(\omega) + S_{u_{d_i} u_{s_i}}(\omega)$$

$$+ S_{u_{s_i} u_{d_i}}(\omega) + S_{u_{s_i} u_{s_i}}(\omega) \qquad (3.35)$$

For stationary response, the cross spectral density are related through

$$S_{u_{d_i} u_{s_i}}(\omega) = S^{*}_{u_{s_i} u_{d_i}}(-\omega) \qquad (3.36)$$

where the asterisk denotes the complex conjugate. The variance of the i^{th} free displacement can be obtained by integrating equation (3.35)

$$\sigma^2_{u_{F_i}} = \int_{\infty}^{\infty} S_{u_{d_i} u_{d_i}}(\omega)\, d\omega + \int_{-\infty}^{\infty} S_{u_{s_i} u_{s_i}}(\omega)\, d(\omega)$$

$$+ 2\, \mathrm{Re} \left[\int_{-\infty}^{\infty} S_{u_{s_i} u_{d_i}}(\omega)\, d\omega \right]$$

$$= \sigma^2_{u_{d_i}} + \sigma^2_{u_{s_i}} + 2\, \mathrm{cov}\,(u_{s_i}, u_{d_i}) \qquad (3.37)$$

where Re [ ] denotes the real part of the argument

$\sigma^2_{u_{s_i}}$, $\sigma^2_{u_{d_i}}$ = variances of the pseudo-static and dynamic displacements for the i^{th} degree of freedom.

and

3.3.1

i^{th} d

Usin

or

Sub

and

$\text{cov}\,(u_{s_i}, u_{d_i})$ = covariance between the static and dynamic displacements for the i^{th} degree of freedom.

3.3.1 THE VARIANCE OF DYNAMIC DISPLACEMENTS

The autocorrelation function of the dynamic displacement for the i^{th} degree of freedom is defined as

$$R_{u_{d_i}}(\tau) = E\,[u_{d_i}(t)\; u_{d_i}(t+\tau)] \tag{3.38}$$

Using the normal coordinates

$$\{u_d\} = [\Psi]\;\{Y\}$$

or

$$u_{d_i} = \psi_{ij}\; Y_j \tag{3.39}$$

Substituting equation (3.39) into (3.38) gives

$$R_{u_{d_i}}(\tau) = E\left[\sum_{j=1}^{n} \psi_{ij}\; Y_j(t) \sum_{k=1}^{n} \psi_{ik}\; Y_k(t+\tau)\right]$$

$$= \sum_{j=1}^{n} \sum_{k=1}^{n} \psi_{ij}\; \psi_{ik}\; E\,[Y_j(t)\; Y_k(t+\tau)] \tag{3.40}$$

Where t

the ana

equati

where

respo

where

excit

Subst

$R_{u_{d_i}}$

The

equ

Where the index n is equal to the number of mode shapes considered in the analysis.

The equation of motion for the j^{th} mode corresponding to equation (3.24) can be solved using Duhamel's integral

$$Y_j(t) = \int_{-\infty}^{\infty} G_j(t - \theta)\, h_j(\theta)\, d\theta \tag{3.41}$$

where $h_j(\theta)$ is the impulse response function for mode j. h (θ_j) is the response Y_j in equation (3.24) due to an impulse excitation $G_j = \delta(t)$, where $\delta(t)$ is the Dirac delta function. The response for a general excitation is given by the superposition integral in equation (3.41). Substituting equation (3.41) into equation (3.40), yields

$$R_{u_{d_i}}(\tau) = \sum_{j=1}^{n} \sum_{k=1}^{n} \psi_{ij}\psi_{ik}\, E\left[\int_{-\infty}^{\infty} G_j(t - \theta_1)\, h_j(\theta_1)\, d\theta_1 \int_{-\infty}^{\infty} G_k(t + \tau - \theta_2)\, h_k(\theta_2)\, d\theta_2\right] \tag{3.42}$$

The impulse response function does not depend on time lag τ, thus equation (3.42) becomes

$R_{u_{d_1}}$ (r

Refer

and

Ther

$$R_{u_{d_i}}(\tau) = \sum_{j=1}^{n} \sum_{k=1}^{n} \psi_{ij}\psi_{ik} \int_{-\infty}^{\infty} \int_{-\infty}^{\infty} h_j(\theta_1)\, h_k(\theta_2) \cdot E\,[G_j(t - \theta_1)$$

$$G_k(t + \tau - \theta_2)]\ \ d\theta_1\, d\theta_2 \tag{3.43}$$

Referring to equation (3.30), we can write the following

$$G_j(t - \theta_1) = \left\{\Gamma_j\right\}^T \left\{\ddot{X}_R(t - \theta_1)\right\} \tag{3.44}$$

and

$$G_k(t + \tau - \theta_2) = \left\{\Gamma_k\right\}^T \left\{\ddot{X}_R(t + \tau - \theta_2)\right\} \tag{3.45}$$

Then, from equation (3.43)

$$E\,[G_j(t - \theta_1)\, G_k(t + \tau - \theta_2)]$$

$$= E\left[\sum_{\ell=1}^{r} \Gamma_{\ell j}\, \ddot{X}_{R\ell}(t - \theta_1) \sum_{m=1}^{r} \Gamma_{mk}\, \ddot{X}_{Rm}(t + \tau - \theta_2)\right]$$

$$= \sum_{\ell=1}^{r} \sum_{m=1}^{r} \Gamma_{\ell j}\, \Gamma_{mk}\, E\,[\ddot{X}_{R\ell}(t - \theta_1)\, \ddot{X}_{Rm}(t + \tau - \theta_2)]$$

$$= \sum_{\ell=1}^{r} \sum_{m=1}^{r} \Gamma_{\ell j}\, \Gamma_{mk}\, R_{\ddot{X}_{R\ell}\ddot{X}_{Rm}}(\tau - \theta_2 + \theta_1) \tag{3.46}$$

Putting

The s

degre

autoc

Subs

wit

Eq

Putting equations (3.43) and (3.46) together gives

$$R_{u_{d_i}}(\tau) = \sum_{j=1}^{n}\sum_{k=1}^{n}\sum_{\ell=1}^{r}\sum_{m=1}^{r} \psi_{ij}\psi_{ik}\Gamma_{\ell j}\Gamma_{mk} \int_{-\infty}^{\infty}\int_{-\infty}^{\infty} R_{\ddot{X}_{R\ell}\ddot{X}_{Rm}}(\tau - \theta_2 + \theta_1)\, h_j(\theta_1)\, h_k(\theta_2)\, d\theta_1\, d\theta_2 \qquad (3.47)$$

The spectral density function of the dynamic displacement for the i^{th} degree of freedom is obtained through the fourier transform of the autocorrelation function as follows

$$S_{u_{d_i}}(\omega) = \frac{1}{2\pi}\int_{-\infty}^{\infty} R_{u_{d_i}}(\tau)\, e^{-i\omega\tau}\, d\tau \qquad (3.48)$$

Substituting equation (3.47) into equation (3.48) gives

$$S_{u_{d_i}}(\omega) = \frac{1}{2\pi}\sum_{j=1}^{n}\sum_{k=1}^{n}\sum_{\ell=1}^{r}\sum_{m=1}^{r} \psi_{ij}\psi_{ik}\,\Gamma_{\ell j}\Gamma_{mk} \int_{\infty}^{\infty}\int_{-\infty}^{\infty}\int_{\infty}^{\infty} R_{\ddot{X}_{R\ell}\ddot{X}_{Rm}}(\tau - \theta_2 + \theta_1)\, h_j(\theta_1)\, h_k(\theta_2)\, e^{-i\omega\tau}\, d\theta_1\, d\theta_2\, d\tau \qquad (3.49)$$

with the change of variables

$$\tau - \theta_2 + \theta_1 = \gamma$$

Equation (3.49) can be written in the form

$$S_{u_{d_i}}(\omega) = \frac{1}{2\pi} \sum_{j=1}^{n} \sum_{k=1}^{n} \sum_{\ell=1}^{r} \sum_{m=1}^{r} \psi_{ij}\psi_{ik}\,\Gamma_{\ell j}\Gamma_{mk}$$

$$\int_{\infty}^{\infty} \int_{-\infty}^{\infty} \int_{\infty}^{\infty} R_{\dot{X}_{R\ell}\dot{X}_{Rm}}(\gamma)\, h_j(\theta_1)\, h_k(\theta_2)\, e^{-i\omega(\gamma + \theta_2 - \theta_1)}$$

$$d\theta_1\, d\theta_2\, d\gamma$$

$$= \sum_{j=1}^{n} \sum_{k=1}^{n} \sum_{\ell=1}^{r} \sum_{m=1}^{r} \psi_{ij}\psi_{ik}\,\Gamma_{\ell j}\Gamma_{mk} \left[\int_{-\infty}^{\infty} h_j(\theta_1)\, e^{i\omega\theta_1}\, d\theta_1\right]$$

$$x \left[\int_{-\infty}^{\infty} h_k(\theta_2)\, e^{-i\omega\theta_2}\, d\theta_2\right]\left[\frac{1}{2\pi} \int_{-\infty}^{\infty} R_{\dot{X}_{R\ell}\dot{X}_{Rm}}(\gamma)\, e^{-i\omega\gamma} d\gamma\right] \quad (3.50)$$

The impulse response function $h_j(\theta)$ and the frequency response function $H_j(\omega)$ are related through

$$h_j(\theta) = \frac{1}{2\pi} \int_{-\infty}^{\infty} H_j(\omega)\, e^{i\omega\theta}\, d\omega \quad (3.51)$$

$$H_j(\omega) = \int_{-\infty}^{\infty} h_j(\theta)\, e^{-i\omega\theta}\, d\theta \quad (3.60)$$

Using equations (3.51), (3.60) and (3.48) we can write

$$\int_{-\infty}^{\infty} h_j(\theta_1)\, e^{i\omega\theta_1}\, d\theta_1 = H_j(-\omega) \tag{3.61}$$

$$\int_{-\infty}^{\infty} h_k(\theta_2)\, e^{-i\omega\theta_2}\, d\theta_2 = H_k(\omega) \tag{3.62}$$

$$\frac{1}{2\pi}\int_{-\infty}^{\infty} R_{\ddot{X}_{R\ell}\ddot{X}_{Rm}}(\gamma)\, e^{-i\omega\gamma}\, d\gamma = S_{\ddot{X}_{R\ell}\ddot{X}_{Rm}}(\omega) \tag{3.63}$$

Then, equation (3.50) takes the form

$$S_{u_{d_i}}(\omega) = \sum_{j=1}^{n}\sum_{K=1}^{n}\sum_{\ell=1}^{r}\sum_{m=1}^{r} \psi_{ij}\,\psi_{ik}\,\Gamma_{\ell j}\,\Gamma_{mk}\,H_j(-\omega)\,H_k(\omega)\, S_{\ddot{X}_{R\ell}\ddot{X}_{Rm}}(\omega) \tag{3.64}$$

This equation represents the transfer relation between power spectral density function of the stationary random excitation $\{\ddot{X}_R\}$ and the response $u_{d_i}(t)$.

The variance of the free dynamic displacement response $u_{d_i}(t)$ with zero mean is

$$\sigma^2_{u_{d_i}} = \int_{-\infty}^{\infty} S_{u_{d_i}}(\omega)\, d\omega \tag{3.65}$$

Substituting equation (3.64) into (3.65) gives

$$\sigma^2_{u_{d_i}} = \sum_{j=1}^{n} \sum_{k=1}^{n} \sum_{\ell=1}^{r} \sum_{m=1}^{r} \psi_{ij}\, \psi_{ik}\, \Gamma_{\ell j}\, \Gamma_{mk} \int_{-\infty}^{\infty} H_j(-\omega) H_k(\omega)\, S_{\ddot{X}_{R\ell}\ddot{X}_{Rm}}(\omega)\, d\omega \qquad (3.66)$$

The modal frequency response function $H_j(\omega)$ may be obtained from equation (3.51), or more directly from the decoupled equations of motions, equation (3.24), and has the form

$$H_j(\omega) = \frac{1}{(\omega_j^2 - \omega^2) + 2i\zeta_j\omega_j\omega} \qquad (3.67)$$

3.3.2 VARIANCES OF PSEUDO-STATIC DISPLACEMENT

The static displacements of the free nodes due to static support motion is determined by equation (3.8)

$$\{X_F^S\} = -[K_{FF}]^{-1}\,[K_{FR}]\,\{X_R\}$$

using the same notation for X_F^S as in paragraph 3.3 ($X_F^S = U_S$), and letting $[A] = -[K_{FF}]^{-1}\,[K_{FR}]$ for notational convenience, gives

$$\{U_S\} = [A]\,\{X_R\} \qquad (3.68)$$

[A] is

freedo

of-fr

the f

displ

words

to a

The

degr

Usi

[A] is an nxr matrix, where n is equal to the number of degrees-of-freedom for the free nodes, and r is the restrained (support) degrees-of-freedom. Each column in [A] represents the static displacements of the free nodes due to a unit value of the corresponding support displacement, while all other support displacement are zero. In other words, the r^{th} column represents the displacements of the free nodes due to a unit static displacement of the r^{th} ground degree of freedom only.

Equation (3.68) can be written in scalar form as

$$u_{s_i} = \sum_{\ell=1}^{r} A_{i\ell} X_{R\ell} \tag{3.69}$$

The autocorrelation function of pseudo-static displacements for the i^{th} degree of freedom previously defined in equation (3.33) is

$$R_{u_{s_i}}(\tau) = E\left[u_{s_i}(t)\, u_{s_i}(t+\tau)\right]$$

Using equation (3.69) gives

$$R_{u_{s_i}}(\tau) = E\left[\sum_{\ell=1}^{r} A_{i\ell} X_{R\ell}(t) \sum_{m=1}^{r} A_{im} X_{Rm}(t+\tau)\right]$$

$$= \sum_{\ell=1}^{r} \sum_{m=1}^{r} A_{i\ell} A_{im}\, E\left[X_{R\ell}(t)\, X_{Rm}(t+\tau)\right]$$

$$= \sum_{\ell=1}^{r} \sum_{m=1}^{r} A_{i\ell} A_{im} R_{X_{R\ell} X_{Rm}}(\tau) \tag{3.70}$$

The spectral density function of the pseudo-static displacement is obtained through the fourier transform of equation (3.70)

$$S_{u_{s_i}}(\omega) = \sum_{\ell=1}^{r} \sum_{m=1}^{r} A_{i\ell} A_{im} S_{X_{R\ell} X_{Rm}}(\omega) \tag{3.71}$$

The spectral density function of support displacements $S_{X_{R\ell} X_{Rm}}(\omega)$ is related to the acceleration spectra through

$$S_{X_{R\ell} X_{Rm}}(\omega) = \frac{1}{\omega^4} S_{\ddot{X}_{R\ell} \ddot{X}_{Rm}}(\omega) \tag{3.72}$$

Thus equation (3.71) can be written as

$$S_{u_{s_i}}(\omega) = \sum_{\ell=1}^{r} \sum_{m=1}^{r} A_{i\ell} A_{im} \frac{1}{\omega^4} S_{\ddot{X}_{R\ell} \ddot{X}_{Rm}}(\omega) \tag{3.73}$$

The variance of the pseudo-static displacement of the i^{th} degree of freedom is

$$\sigma^2_{u_{s_i}} = \sum_{\ell=1}^{r} \sum_{m=1}^{r} A_{i\ell} A_{im} \int_{-\infty}^{\infty} \frac{1}{\omega^4} S_{\ddot{X}_{R\ell} \ddot{X}_{Rm}}(\omega)\, d\omega \tag{3.74}$$

3.3.3

displa

From

From

Sub

S

3.3.3 COVARIANCE OF PSEUDO-STATIC AND DYNAMIC DISPLACEMENT

Using equations 3.33 the cross correlation of static and dynamic displacements is

$$R_{u_{s_i} u_{d_i}}(\tau) = E\left[u_{s_i}(t)\, u_{d_i}(t+\tau)\right] \tag{3.75}$$

From equation (3.39)

$$u_{d_i}(t+\tau) = \psi_{ij} Y_j(t+\tau)$$

From equation (3.69)

$$u_{s_i}(t) = A_{i\ell}\, S_{R\ell}(t)$$

Substituting equations (3.39) and (3.69) into (3.75) yields

$$R_{u_{s_i} u_{d_i}}(\tau) = E\left[\sum_{\ell=1}^{r} A_{i\ell}\, X_{R\ell}(t) \sum_{k=1}^{n} \psi_{ik} Y_k(t+\tau)\right]$$

$$= \sum_{\ell=1}^{r} \sum_{k=1}^{n} A_{i\ell}\, \psi_{ik}\, E\left[X_{R_\ell}(t)\, Y_k(t+\tau)\right] \tag{3.76}$$

Substituting equation (3.41) into 3.76 yields

$$R_{u_{s_i} u_{d_i}}(\tau) = \sum_{\ell=1}^{r} \sum_{k=1}^{n} A_{i\ell}\, \psi_{ik} E\left[X_{R\ell}(t) \int_{-\infty}^{\infty} G_k(t+\tau-\theta) h_k(\theta)\, d\theta \right] \quad (3.77)$$

Using equation (3.45) gives

$$R_{u_{s_i} u_{d_i}}(\tau) = \sum_{\ell=1}^{r} \sum_{k=1}^{n} A_{i\ell}\, \psi_{ik} E\left[X_{R\ell}(t) \int_{-\infty}^{\infty} \sum_{m=1}^{r} \Gamma_{mk}\, \ddot{X}_{Rm}(t+\tau-\theta) h_k(\theta)\, d\theta \right.$$

$$= \sum_{\ell=1}^{r} \sum_{k=1}^{n} \sum_{m=1}^{r} A_{i\ell}\, \psi_{ik}\, \Gamma_{mk} \int_{-\infty}^{\infty} E[X_{R\ell}(t)\, \ddot{X}_{Rm}(t+\tau-\theta)]\, h_k(\theta)\, d\theta$$

$$= \sum_{\ell=1}^{r} \sum_{k=1}^{n} \sum_{m=1}^{r} A_{i\ell}\, \psi_{ik}\, \Gamma_{mk} \int_{-\infty}^{\infty} R_{X_{R\ell} \ddot{X}_{Rm}}(\tau-\theta) h_k(\theta)\, d\theta \quad (3.78)$$

Consider $f(\tau) = \int_{-\infty}^{\infty} R_{X_{R\ell} \ddot{X}_{Rm}}(\tau-\theta) h_k(\theta)\, d\theta$ (3.79)

The fourier transform of equation (3.79) is

$$f(\omega) = \frac{1}{2\pi} \int_{-\infty}^{\infty} \int_{-\infty}^{\infty} R_{X_{R\ell} \ddot{X}_{Rm}}(\tau-\theta)\, h_k(\theta) e^{-i\omega\tau}\, d\theta\, d\tau \quad (3.80)$$

Let $\tau - \theta = \tau'$

Then $d\tau = d\tau'$ (3.81)

Substituting equations (3.81) into equation (3.80) gives

$$f(\omega) = \int_{-\infty}^{\infty} h_k(\theta)d\theta \frac{1}{2\pi} \int_{-\infty}^{\infty} R_{X_{R\ell}\ddot{X}_{Rm}}(\tau')e^{-i\omega(\tau'+\theta)}d\tau'$$

$$= \int_{-\infty}^{\infty} h_k(\theta)e^{-i\omega\theta}d\theta \frac{1}{2\pi} \int_{-\infty}^{\infty} R_{X_{R\ell}\ddot{X}_{Rm}}(\tau') e^{-i\omega\tau'}d\tau'$$

$$= H_k(\omega) S_{X_{R\ell}\ddot{X}_{Rm}}(\omega) \qquad (3.81)$$

Now, taking the fourier transform of equation (3.78) and considering equation (3.81) we have

$$S_{u_{s_i}u_{d_i}}(\omega) = \sum_{\ell=1}^{r} \sum_{k=1}^{n} \sum_{m=1}^{r} A_{i\ell}\psi_{ik}\Gamma_{mk} H_k(\omega) S_{X_{R\ell}\ddot{X}_{Rm}}(\omega) \qquad (3.82)$$

The covariance of pseudo-static and dynamic displacements is

$$\text{cov}(u_{s_i},u_{d_i}) = \sum_{\ell=1}^{r} \sum_{k=1}^{n} \sum_{m=1}^{r} A_{i\ell}\psi_{ik}\Gamma_{mk} \int_{-\infty}^{\infty} H_k(\omega) S_{X_{R\ell}\ddot{X}_{Rm}}(\omega) \quad (3.83)$$

In this equation, we have to express $S_{X_{R\ell}\ddot{X}_{Rm}}(\omega)d\omega$ through the spectrum density function of the ground acceleration. Starting with

$$R_{X_{R\ell}X_{Rm}}(\tau) = E[X_{R\ell}(t) X_{Rm}(t+\tau)] \qquad (3.84)$$

Differentiating twice with respect to τ gives

$$R''_{X_{R\ell}X_{Rm}}(\tau) = E\,[X_{R\ell}(t)\,\ddot{X}_{Rm}(t+\tau)] \tag{3.85}$$

differentiating equation (3.84) once with respect to τ gives

$$R'_{X_{R\ell}X_{Rm}}(\tau) = E\,[X_{R\ell}(t)\,\dot{X}_{Rm}(t+\tau)]$$

$$= E\,[X_{R\ell}(t-\tau)\,\dot{X}_{Rm}(t)] \tag{3.86}$$

differentiating equation (3.86) again with respect to τ yields

$$R''_{X_{R\ell}X_{Rm}}(\tau) = -E\,[\dot{X}_{R\ell}(t-\tau)\,\dot{X}_{Rm}(t)]$$

$$= -E\,[\dot{X}_{R\ell}(t)\,\dot{X}_{Rm}(t+\tau)] \tag{3.87}$$

Comparing equations (3.85) and (3.87) shows that

$$R''_{X_{R\ell}X_{Rm}}(\tau) = E\,[X_{R\ell}(t)\,\ddot{X}_{Rm}(t+\tau)] = -E\,[\dot{X}_{R\ell}(t)\dot{X}_{Rm}(t+\tau)] \tag{3.88}$$

or

$$R''_{X_{R\ell}X_{Rm}}(\tau) = R_{X_{R\ell}\ddot{X}_{Rm}}(\tau) = -R_{\dot{X}_{R\ell}\dot{X}_{Rm}}(\tau) \tag{3.89}$$

Taking the fourier transform of equation (3.89) given

$$S_{X_{R\ell}\ddot{X}_{Rm}}(\omega) = -S_{\dot{X}_{R\ell}\dot{X}_{Rm}}(\omega) \tag{3.90}$$

The autocorrelation function $R_{\dot{X}_{R\ell}\dot{X}_{Rm}}(\tau)$ can be expressed in the following form.

$$R_{\dot{X}_{R\ell}\dot{X}_{Rm}}(\tau) = \int_{-\infty} S_{\dot{X}_{R\ell}\dot{X}_{Rm}}(\omega)\, e^{i\omega\tau}\, d\omega \tag{3.91}$$

Then

$$R_{X_{R\ell}\ddot{X}_{Rm}}(\tau) = \int_{-\infty}^{\infty} -S_{\dot{X}_{R\ell}\dot{X}_{Rm}}(\omega) e^{i\omega\tau}\, d\omega \tag{3.92}$$

The auto correlation function of support displacement is expressed as

$$R_{X_{R\ell}X_{Rm}}(\tau) = \int_{-\infty}^{\infty} S_{X_{R\ell}X_{Rm}}(\omega)\, e^{i\omega\tau}\, d\omega \tag{3.93}$$

Differentiating equation (3.93) twice with respect to τ yields

$$R''_{X_{R\ell}X_{Rm}}(\tau) = \int_{-\infty}^{\infty} -\omega^2 S_{X_{R\ell}X_{Rm}}(\omega)\, e^{i\omega\tau}\, d\omega \tag{3.94}$$

Using equations (3.88), (3.91) and 3.94) show that

$$S_{\dot{X}_{R\ell}\dot{X}_{Rm}}(\omega) = \omega^2\, S_{X_{R\ell}X_{Rm}}(\omega) \tag{3.95}$$

Also, from equation (3.72)

$$S_{X_{R\ell}X_{Rm}}(\omega) = \frac{1}{\omega^4} \; S_{\ddot{X}_{R\ell}\ddot{X}_{Rm}}(\omega)$$

Then, from the above two equations, it shows that

$$S_{\dot{X}_{R\ell}\dot{X}_{Rm}}(\omega) = \frac{1}{\omega^2} \; S_{\ddot{X}_{R\ell}\ddot{X}_{Rm}}(\omega) \tag{3.96}$$

Now using, equation (3.90) yields

$$S_{\ddot{X}_{R\ell}\ddot{X}_{Rm}}(\omega) = -\frac{1}{\omega^2} \; S_{\ddot{X}_{R\ell}\ddot{X}_{Rm}}(\omega) \tag{3.97}$$

Substituting equation (3.97) into equation (3.83) gives

$$\sigma^2_{u_{s_i}u_{d_i}} = \sum_{\ell=1}^{r} \sum_{k=1}^{n} \sum_{m=1}^{r} A_{i\ell} \, \psi_{ik} \, \Gamma_{mk} \int_{-\infty}^{\infty} H_k(\omega) \left(\frac{-1}{\omega^2}\right) S_{\ddot{X}_{R\ell}\ddot{X}_{Rm}}(\omega) \, d\omega \tag{3.98}$$

Using the same procedure, it can be shown that the covariance of dynamic and pseudo-static displacement is

$$\text{cov}\,(u_{d_i}, u_{s_i}) = \sum_{\ell=1}^{r} \sum_{k=1}^{n} \sum_{m=1}^{r} A_{i\ell}\psi_{ik}\Gamma_{mk} \int_{-\infty}^{\infty} H_k(\omega) \left(\frac{-1}{\omega^2}\right) S_{\ddot{X}_{R\ell}\ddot{X}_{Rm}}(\omega) d\omega \tag{3.99}$$

3.3.4 THE VARIANCE OF DYNAMIC END FORCES

The eigenvectors represent the displaced shapes of the nodal points for each mode in the global coordinate system. Each node had a number of displacement vectors equal to the number of degrees of

freedo

extra

displ

to th

wher

syst

The

wh

st

ei

ar

de

d

freedom. In order to calculate the element end forces, we need to extract the values of the eigenvectors corresponding to the nodal displacements at the two ends of the members and transform these values to the local coordinate system through

$$\{D_m\} = [T]\ \{D_G\} \tag{3.100}$$

where $\{D_m\}$ is the vector of nodal displacement in the local coordinate system

$[T]$ is the transformation matrix

$\{D_G\}$ is the vector of nodal displacement in the global coordinate systems.

The element end forces are then given by

$$\{f\} = [K]\{D_m\} \tag{3.101}$$

where $\{f\}$ is the vector of element end forces $[K]$ is the element of stiffness matrix.

This sequence of operations is performed for all the eigenvectors, or for the subset of them that are to be used in the analysis. Finally, the variances of each end force may obtained as described below.

Let F_{ij} be the end force of the element corresponding to the i^{th} degree of freedom of a given element and the j^{th} eigenvector. F_{ij} is

calculated by equation (1.105). The autocorrelation function of the i^{th} dynamic end force is defined as

$$R_{f_i f_i}(\tau) = E\left[\sum_{j=1}^{n} F_{ij}\, Y_j(t) \sum_{k=1}^{n} F_{ik}\, Y_k\,(t+\tau)\right]$$

$$= \sum_{j=1}^{n} \sum_{k=1}^{n} F_{ij}\, F_{ik}\, E\,[Y_j(t)\, Y_k\,(t+\tau)]$$

$$= \sum_{j=1}^{n} \sum_{k=1}^{n} F_{ij}\, F_{ik}\, R_{Y_j Y_k}(\tau) \qquad (3.102)$$

Using the same procedure as in section 3.3.1, it can be shown that the variance of this end force is

$$\sigma^2_{f_i}(\tau) = \sum_{j=1}^{n} \sum_{k=1}^{n} \sum_{\ell=1}^{r} \sum_{m=1}^{r} F_{ij}\, F_{ik} \Gamma_{\ell j} \Gamma_{mk} \int_{-\infty}^{\infty} H_j(-\omega) H_k(\omega)\, S_{X_{R\ell} X_{Rm}}\, d\omega \qquad (3.103)$$

3.3.5 THE VARIANCE OF STATIC END FORCES

To determine the static nodal displacements in the global coordinates, we use equation (3.69)

$$\{u_s\} = [A]\{X_R\}$$

We then determine the element end forces due to the movement of each support in the local coordinate system in the same manner as explained earlier.

Let S_{ij} be the static end force of the element corresponding to the i^{th} degree of freedom of a given element and the j^{th} degree of freedom of ground motion.

Then, the autocorrelation function of the i^{th} component of the static end forces is defined as

$$R_{s_i s_i}(\tau) = E\left[\sum_{\ell=1}^{r} S_{i\ell}\, X_{R\ell}(t) \sum_{m=1}^{r} S_{im}\, X_{Rm}\,(t+\tau)\right]$$

$$= \sum_{\ell=1}^{r}\sum_{m=1}^{r} S_{i\ell}\, S_{im}\, E\,[X_{R\ell}(t)\, X_{Rm}(t+\tau)]$$

$$= \sum_{\ell=1}^{r}\sum_{m=1}^{r} S_{i\ell}\, S_{im}\, R_{X_{R\ell}X_{Rm}}(\tau) \qquad (3.104)$$

Using the same procedures as in section 3.3.2, it can be shown that the variance of the i^{th} pseudo-static end force of a given element is

$$\sigma^2_{s_i} = \sum_{\ell=1}^{r}\sum_{m=1}^{r} S_{i\ell} S_{im} \int_{-\infty}^{\infty} \frac{1}{\omega^4}\, S_{\ddot{X}_{R\ell}\ddot{X}_{Rm}}(\omega)\, d\omega \qquad (3.105)$$

3.3.6 THE COVARIANCE OF PSEUDO-STATIC AND DYNAMIC FORCES

The cross correlation function of pseudo-static and dynamic forces is defined as

$$R_{s_i f_i}(\tau) = E\left[\sum_{\ell=1}^{r} S_{i\ell} X_{R\ell}(t) \sum_{k=1}^{n} F_{ik} Y_k(t+\tau)\right]$$

$$= \sum_{\ell=1}^{r}\sum_{k=1}^{n} S_{i\ell} F_{ik}\, E\left[X_{R\ell}(t)\, Y_k(t+\tau)\right] \qquad (3.106)$$

Using the same procedure as in section 3.3.3, it can be shown that the covariance between the pseudo-static and dynamic end forces is expressed as:

$$\text{cov}\,(S_i, f_i) = \sum_{\ell=1}^{r}\sum_{k=1}^{n}\sum_{m=1}^{r} S_{i\ell} F_{ik} \Gamma_{mk} \int_{-\infty}^{\infty} H_k(\omega)\left(\frac{-1}{\omega^2}\right) S_{X_{R\ell} X_{Rm}}(\omega)\, d\omega \qquad (3.107)$$

3.3.7 SUMMARY

The variance of the displacement or rotation of the i^{th} degree of freedom in the global coordinate system is expressed in the following form

$$\sigma^2_{u_{f_i}} = \sigma^2_{u_{d_i}} + \sigma^2_{u_{s_i}} + 2\,\text{cov}\,(u_{s_i}, u_{d_i})$$

where

$$\sigma^2_{u_{d_i}} = \sum_{j=1}^{n}\sum_{k=1}^{n}\sum_{\ell=1}^{r}\sum_{m=1}^{r} \psi_{ij}\psi_{ik}\Gamma_{\ell j}\Gamma_{mk} \int_{-\infty}^{\infty} H_j(-\omega)\, H_k(\omega)\, S_{\ddot{X}_R\ddot{X}_{R\ell}\ddot{X}_{Rm}}(\omega)\, d\omega$$

$$\sigma^2_{u_{s_i}} = \sum_{\ell=1}^{r}\sum_{m=1}^{r} A_{i\ell}A_{im} \int_{-\infty}^{\infty} \frac{1}{\omega^4}\, S_{\ddot{X}_R\ddot{X}_{R\ell}\ddot{X}_{Rm}}(\omega)\, d\omega$$

$$\operatorname{cov}(u_{s_i}, u_{d_i}) = \sum_{\ell=1}^{r}\sum_{k=1}^{n}\sum_{m=1}^{r} A_{i\ell}\psi_{ik}\Gamma_{mk} \int_{-\infty}^{\infty} H_k(\omega)\left(\frac{-1}{\omega^2}\right) S_{\ddot{X}_R\ddot{X}_{R\ell}\ddot{X}_{Rm}}(\omega)\, d\omega$$

The variance of the i^{th} component of end forces for each finite element is expressed in the following form

$$\sigma^2_{F_i} = \sigma^2_{f_i} + \sigma^2_{s_i} + 2\operatorname{cov}(s_i, f_i)$$

where

$$\sigma^2_{f_i} = \sum_{j=1}^{n}\sum_{k=1}^{n}\sum_{\ell=1}^{r}\sum_{m=1}^{r} F_{ij}F_{ik}\Gamma_{\ell j}\Gamma_{mk} \int_{-\infty}^{\infty} H_j(-\omega)H_k(\omega)\, S_{\ddot{X}_R\ddot{X}_{R\ell}\ddot{X}_{Rm}}(\omega)\, d\omega <$$

$$\sigma^2_{s_i} = \sum_{\ell=1}^{r}\sum_{m=1}^{r} S_{i\ell}S_{im} \int_{-\infty}^{\infty} \frac{1}{\omega^4}\, S_{\ddot{X}_R\ddot{X}_{R\ell}\ddot{X}_{Rm}}(\omega)\, d\omega$$

$$\operatorname{cov}(s_i, f_i) = \sum_{k=1}^{n}\sum_{\ell=1}^{r}\sum_{m=1}^{r} F_{ik}S_{i\ell}\Gamma_{mk} \int_{-\infty}^{\infty} H_k(-\omega)\left(\frac{-1}{\omega^2}\right) S_{\ddot{X}_R\ddot{X}_{R\ell}\ddot{X}_{Rm}}(\omega)\, d\omega$$

All the above mention notations were previously identified.

3.4 THE INPUT MOTION

In order to solve this problem using the probabilistic approach we must have a mathematical model for the acceteration spectrum of the ground motion $S_{\ddot{X}_{R\ell}\ddot{X}_{Rm}}(\omega)$. For stationary excitation, the displacement and velocity spectrum are related to the acceleration spectrum by equation (3.72) and (3.95), respectively.

The ground motion model used in this study is that proposed by Harichandran and Vanmarcke (1986). The model considered the spatial as well as the temporal variation of earthquake ground motion, and was based on the analysis of recordings made by the SMART-1 seismograph array in Lotung, Taiwan. In this model the cross spectral density function between the acceleration of two locations A and B is expressed as

$$S_{\ddot{X}_A\ddot{X}_B} = S_{\ddot{X}}(\omega)\ \rho\ (\nu,\ f = \frac{\omega}{2\pi})\ e^{-\frac{i\omega\nu}{v}} \tag{3.108}$$

where

$$\rho(\nu,f) = A\ \exp\left[\frac{-2\nu}{\alpha\theta(f)}(1-A+\alpha A)\right]+(1-A)\exp\left[\frac{-2\nu}{\theta(f)}\ (1-A+\alpha A)\right] \tag{3.109}$$

$$\theta(f) = k\ \left[1 + (\frac{f}{fo})^{b}\right]^{-\frac{1}{2}} \tag{3.110}$$

A, α, k, fo and b are model parameters where typical values are shown in Table 3-1 (Harichandran 1988). The function $\rho(\nu,f)$ with these parameters are plotted in Figure 3-3(a) and (b).

accele

The

S-(ω
X

wher

and

ir

e

s

T

F

i

$S_{\ddot{x}}(\omega)$ - is the auto spectral density function of ground acceleration.

ν - seperation between locations A and B

f - Linear frequency

v - apparent wave propogation velocity in the direction AB.

The functional form suggested by Claugh and Penzien (1974) is used for $S_{\ddot{x}}(\omega)$:

$$S_{\ddot{x}}(\omega) = |H_1(\omega)|^2 \; |H_2(\omega)|^2 \; S_o \tag{3.111}$$

where $|H_1(\omega)|^2$ is the Kanai-Tajimi spectrum function and has the form

$$|H_1(\omega)|^2 = \frac{(1+4\beta_g^2 [\omega/\omega_g]^2)}{\left(1- \left[\frac{\omega}{\omega_g}\right]2\right)^2 + 4\beta_g^2 \left[\frac{\omega}{\omega_g}\right]^2} \tag{3.112}$$

and

$$|H_2(\omega)|^2 = \frac{(\omega/\omega_f)^4}{\left(1- \left[\frac{\omega}{\omega_f}\right]2\right)^2 + 4\beta_f^2 \left[\frac{\omega}{\omega_f}\right]^2} \tag{3.113}$$

in which ω_g, ρ_g ω_f ρ_f and S_o are model parameters that can be estimated by fitting the above function to observed acceleration spectra. Two acceleration spectra with the parameters given in Table 3-2 were used in this study. These spectra are plotted in Figure 3-4 . Ground motion 1 has a wide excitation frequency range and is characteristic of motion recorded on rock, while ground motion 2 has a narrow excitation frequency range is charactertistic of motion on soil. For the values of S_o given in Table 3-2, the variances of ground acceleration (area under the spectrum in equation (3.111) are 2π gal^2

for a

is re

are

Note

tota

subs

3-5

tha

ove

was

for all the events. The variances of ground displacements $S_X(\omega)$ which is related to the acceleration spectrum. $S_{\ddot{X}}(\omega)$, through

$$S_X(\omega) = \frac{1}{\omega^4} S_{\ddot{X}}(\omega)$$

are $1.09(10)^{-7}$ and $4.09(10)^{-7}$ m^2 for spectra 1 and 2, respectively. Note that although the normalized acceleration spectra have the same total power for both events, the corresponding displacement spectra have substantially different total power as depicted in Figure 3-5.

3-5 COMPUTATIONAL PROCEDURES.

The LINSTRUC computer program (Dusseau 1985) was modified so that it can be used on the VAX/VMS. The program was used to obtain the overall stiffness and mass matrices. The computational procedures that was used is summarized here.

1. Compute the eigenvalues and the eigenvectors using the generalized Jacobi method (Bathe, K.J. 1982).
2. Calculate matrix [A] using equation (3.8). In the case of CSCB, [A] is a 58 x 2 matrix. The entry A_{ij} is the free nodal displacement at mode i due to a unit support displacement at j.
3. Calculate the entries of the modal participation factor matrix [Γ] using equation (3.28).
4. Calculate the integrals $\int_{\infty}^{\infty} H_j(-\omega)H_k(\omega)\, S_{\ddot{X}_{Rl}\ddot{X}_{Rm}}(\omega)d\omega$ and store the results in a 34 x 34 x 2 x 2 array. (The integrations were done using the IMSL subroutine "DCADRE").

5. Calculate the integrals $\int_{-\infty}^{\infty} \frac{1}{\omega^4} S_{\ddot{X}_{R\ell}\ddot{X}_{Rm}}(\omega)\, d\omega$ and store the results in 4 x 4 or 2 x 2 arrays depending on the number of moving supports.

6. Calculate the integrals $\int_{-\infty}^{\infty} H_k(-\omega) \left(\frac{-1}{\omega^2}\right) S_{\ddot{X}_{R\ell}\ddot{X}_{Rm}}(\omega)\, d\omega$ and store the results in a 34 x 2 x 2 array.

7. Calculate the variances of dynamic and static displacements, and the covariance between the static and dynamic displacement, using equations (3.66), (3.74) and (3.99).

8. Calculate the variances of members end forces using the following sequence of operations:

   a. For nodes i and j of each element extract the corresponding static and dynamic displacements from matrix [A] and from the eigenvectors. For each element the number of displacement sets of the static components is equal to the number of moving supports. For the dynamic component the number is equal to the mode shapes considered in the analysis.

   b. Transform the end displacements to the local coordinate, then determine the members end forces and store them in an array. For the static component the array is of r x q where r is the number of moving supports, and q is the number of degrees of freedom for nodes i and j, in this case 14. For the dynamic component the array is of order n x q, where n is the number of mode shapes.

c. To calculate the variance of the dynamic, static and the covariance of static-dynamic components use equations (3.103), (3.105) and (3.107), respectively.

d. To calculate the total response use equation (3.37).

Table 3-1: Model Parameters for $\rho(\nu,f)$

Model	Parameter	Ground Motion 1	Ground Motion 2
Double Exponential	A	0.626	0.355
	α	0.022	0.086
	k	19700	23100
	$f_o(H_z)$	2.02	0.55
	b	3.47	2.35

Table 3-2: Model Parameters for Autospectra

Model	Parameter	Ground Motion 1	Ground Motion 2
Double Filter	ω_g(rad/s)	20.22	5.05
	β_g	0.53	0.62
	ω_f(rad/s)	5.45	6.41
	β_f	0.46	0.27
	$S_o(gal.S^2)$	0.0957	0.3068

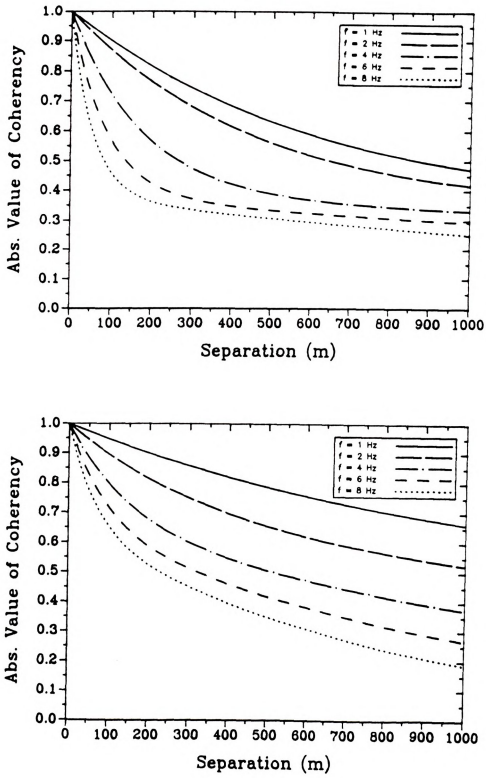

Figure 3-3: The Coherency Function $\rho(\nu,f)$. (a) Ground Motion 1; (b) Ground Motion 2.

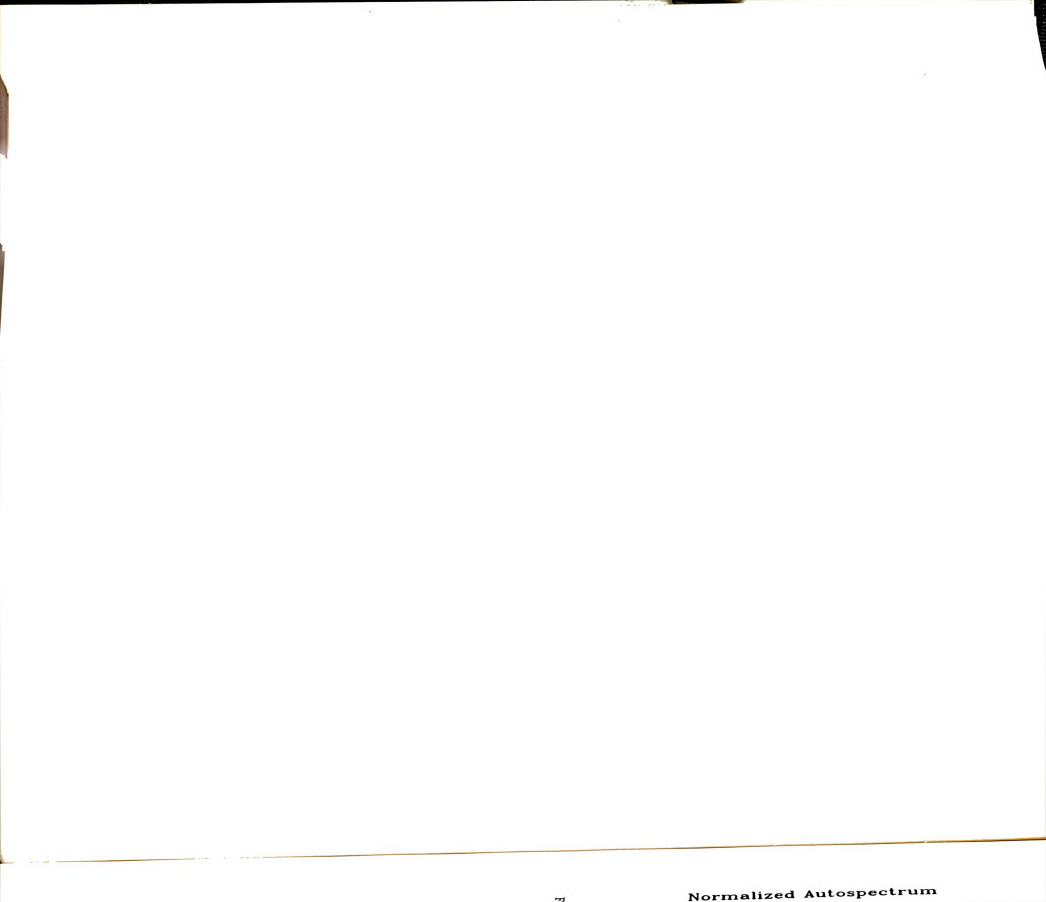
Normalized Autospectrum

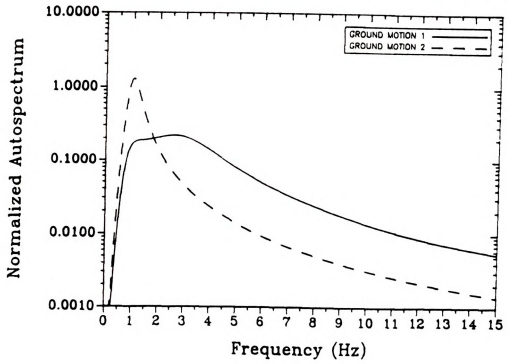

Figure 3-4: Spectra of Ground Acceleration Using Estimated Parameters.

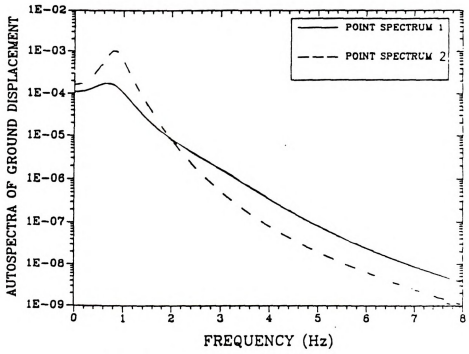

Figure 3-5: Spectra of Ground Displacement Using Estimated Parameters.

3.6 NONSTATIONARY RESPONSE

The theory developed until now is valid only for stationary excitation. Earthquake acceleration amplitudes, however, initially grow from zero, then have a steady phase and eventually decay. The excitation is therefore nonstationary. For a single degree-of-freedom system with undamped circular natural frequency ω_n and damping ratio β, the response may not attain its stationary state for very small values of $\beta\omega_n$ or small durations of strong shaking. For a multi-degree-of-freedom system, each modal response grows at a different rate, with higher modes having large natural frequencies attaining stationarity more quickly. The rate at which the total response grows depends on how much the lower modes contribute to the overall response. If the lower modes do not contribute significantly, then the total response may attain stationarity rather quickly. For the arch bridges considered in this study, the first few modes have long periods (low frequencies) and therefore may not reach stationary conditions for short earthquakes. It is therefore of interest to compute the transient response of the bridges due to nonstationary excitation.

In most earthquake engineering applications it is reasonable to account for nonstationarity in the amplitude of the ground accelerations, while the frequency content may be assumed not to change with time. For these cases the ground accelerations may be written as

$$\ddot{X}(t) = A(t)Z(t) \tag{3.114}$$

in which $Z(t)$ is a stationary process, and $A(t)$ is a temporal modulating function. Various forms have been suggested for $A(t)$ based on the fitting of modulating functions to measured accelerograms. The response

of the generalized displacement for the jth mode may then be expressed as

$$Y(t) = \int_0^t h_j(t - \tau)A(\tau)\ddot{X}(\tau)d\tau \tag{3.115}$$

where $h_j(t)$ is the impulse response function of the jth mode. For frequency domain analysis, it is convenient to define a "time-dependent frequency response function", as

$$H_j(\omega,t) = \int_0^t h_j(t - \tau)A(\tau)e^{i\omega\tau}d\tau \tag{3.116}$$

To evaluate the response variance at a given time t, the function $H_j(\omega,t)$ can be substituted for the normal frequency response function $H_j(\omega)$ in the expressions for the stationary response. The main difficulty in this is that while $H_j(\omega)$ has a closed form expression, $H_j(\omega,t)$ cannot easily be expressed in closed form for any A(t). However, a closed form expression can be derived for $H_j(\omega,t)$ if A(t) is the unit Heaviside function

$$A(t) = \begin{cases} 0, & t < 0 \\ 1, & t \geq 0 \end{cases}$$

This corresponds to an excitations that suddenly starts at time t=0 with stationary intensity, and is not the same as stationary excitation.

Gasparini and DebChaudhury (1980) considered structural response to two modulating functions A(t) using a time domain approach. The

first modulating function grew linearly from zero, then was steady and finally decayed linearly to zero, while the second began suddenly (like the Heaviside function) but decayed linearly to zero after some time. As would be intuitively expected, the initial growth of the response differed for the two modulations, but they gradually approached the same stationary value and began to decay as soon as the excitations started to decay.

The present study is concerned more with comparing the relative differences in the responses due to different models of multiple support excitation, and not so much with finding absolute response variances. Thus the exact form used for A(t) is not very crucial, and the use of a Heaviside modulating function is sufficient to assess the effect of transient modal responses.

For the Heaviside modulation, the closed form expression for $H_j(\omega,t)$ is (Lin 1963)

$$H_j(\omega,t) = H_j(\omega)\left[1 - \exp(-\omega_j\beta_j t)\exp(-i\omega t)\left[\cos \omega_{jd}t + \frac{(\omega_j\beta_j+i\omega)}{\omega_{jd}} \sin \omega_{jd}t\right]\right] \qquad (3.117)$$

The transient responses in this study are computed by replacing $H(\omega)$ in the results derived in Section 3.3, with the expression for $H(\omega,t)$ given in equation (3.117).

CHAPTER 4

ANALYSIS RESULTS

4.1 MODAL ANALYSIS

The Generalized Jacobi method was used to solve the eigenvalue problem for both bridges. All mode shapes and frequencies were extracted and considered in obtaining the response values of the two bridges for the in-plane and out-of-plane models.

4.1.1 CSCB MODE SHAPES AND NATURAL PERIODS

The first four modes for the in-plane model of the CSCB are shown in Figure 4-1. The first mode has a natural period of 2.32 seconds and is a full wave vertical motion of the deck and the arch. The second mode is a 1½ wave of vertical motion for the deck and the arch with a natural period of 1.19 seconds. The third mode has a natural period of 0.65 seconds and is characterized by large two full waves of vertical motion of the deck and the arch. Finally, the fourth mode has a natural period of 0.63 seconds and is characterized by large two full waves of vertical motion for the arch and the deck and a moderately large longitudinal translation of the deck.

Figure 4-2 illustrates the first four modes for the out-of-plane model of the CSCB. The first mode has a natural period of 2.67 seconds and is a half wave lateral motion of the deck and the arch. The second mode has a natural period of 1.54 seconds and is characterized by a large full wave lateral motion of the deck with a small lateral half wave motion of the arch. The third mode has a natural period of 1.01 seconds and is characterized by a large 1½ wave lateral motion of the deck accompanied by a small half wave lateral motion of the arch. Finally, mode four has a natural period of 0.69 seconds and is

characterized by a large half wave lateral motion of the arch accompanied by a moderately large two wave lateral motion of the deck.

4.1.2 NRGB MODE SHAPES AND NATURAL PERIODS

The first four modes for the in-plane model of the NRGB are depicted in Figure 4-3. The first mode has a natural period of 4.18 seconds and is a full wave vertical motion of the deck and the arch. Mode two is a 1½ wave vertical motion of the deck and the arch with a natural period of 2.00 seconds. The third mode has a natural period of 1.43 seconds and represents a two wave vertical motion of the deck and the arch. Finally, mode four is characterized by large horizontal motions of the deck toward the center of the bridge. This latter mode has a natural period of 1.21 seconds and also exhibits a small vertical deck and arch motion in the form of 1½ waves.

Figure 4-4 illustrates the first four modes for the out-of-plane model of the NRGB. The first mode has a natural period of 6.78 seconds and is a half wave lateral motion of the deck and the arch. Mode two has a natural period of 3.48 seconds and is a full wave lateral motion of the deck accompanied by a small full wave lateral motion of the arch. The third mode has a natural period of 2.40 seconds and is characterized by a large 1½ wave lateral motion of the deck and a small 1½ wave lateral motion of the arch. Finally, mode four has a natural period of 1.89 seconds and is characterized by a large two full wave lateral motion of the deck accompanied by a small full wave lateral motion of the arch.

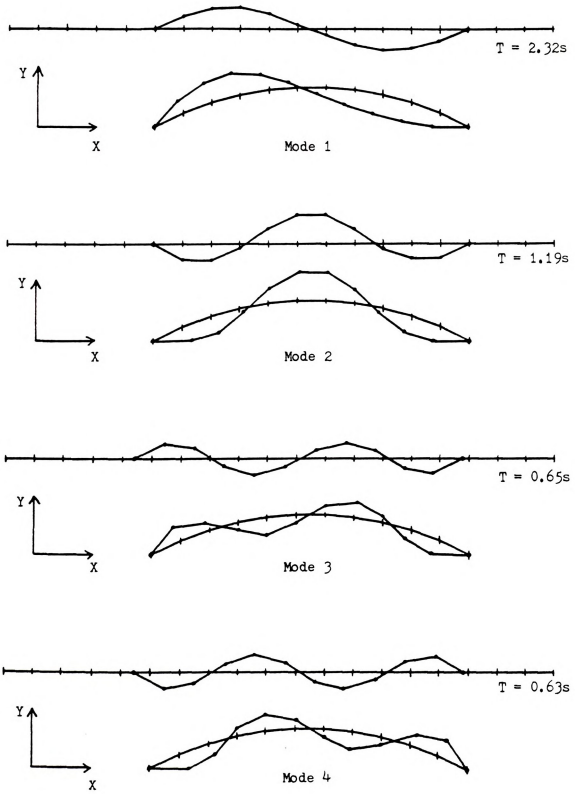

Figure 4-1: CSCB In-Plane Modes (Excerpted from Dusseau (1985))

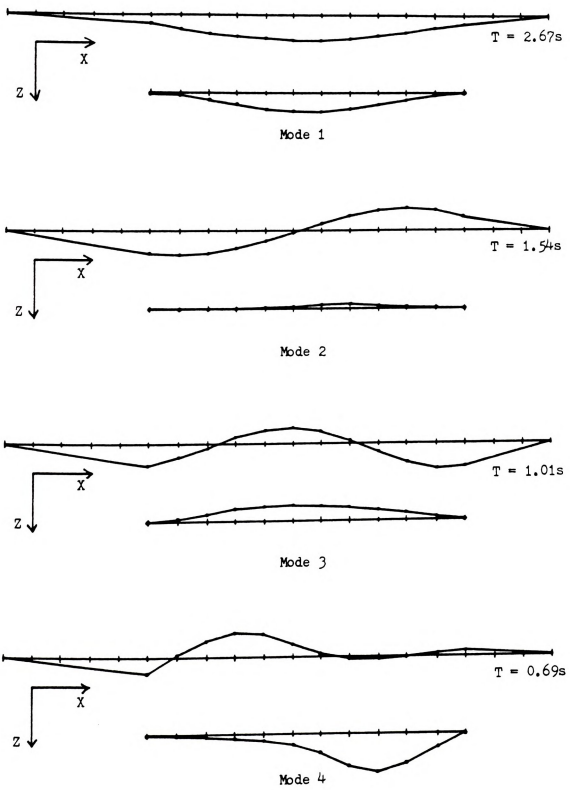

Figure 4-2: CSCB Out-Of-Plane Modes (Excerpted from Dusseau (1985))

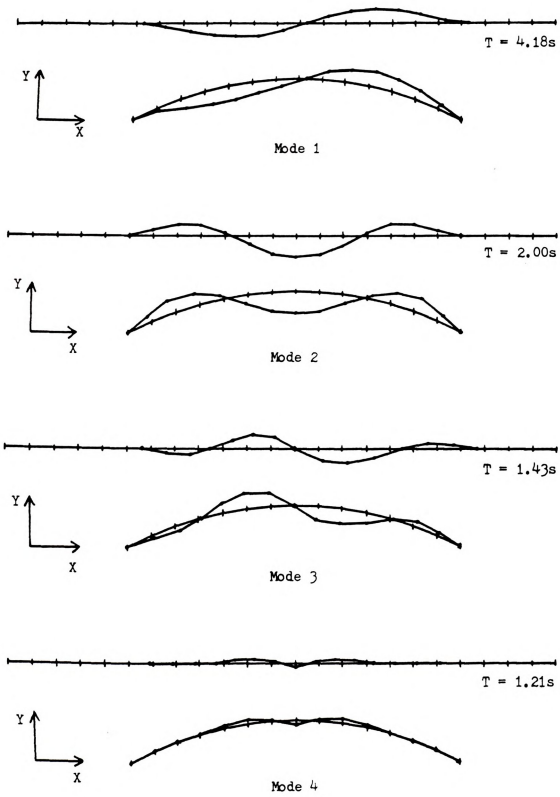

Figure 4-3: NRGB In-Plane Modes (Excerpted from Dusseau (1985))

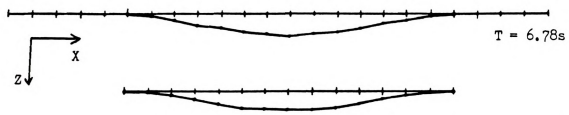

Mode 1

Mode 2

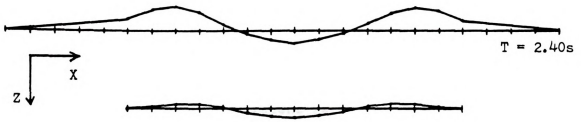

Mode 3

Mode 4

Figure 4-4: NRGB Out-Of-Plane Modes (Excerpted from Dusseau (1985))

4.2 MODELS OF GROUND MOTION

The three specialized coherency models of ground motion considered in this study are the following:

Case 1: Fully correlated ground motion. In this case we assumed that the supports of the bridges are moving identically. This corresponds to the current practice of designing bridges for earthquake ground motion. For this case the term $\rho(\nu, f=\frac{\omega}{2\pi})e^{-i\omega\nu/v}$ in equation (3.108) is equal to one.

Case 2: Wave propogation case. In this case we assumed that there is no loss of coherency between the support excitations, but there is a time delay corresponding to the time required for the seismic waves to travel from one support to another. For this case the term $\rho(\nu,f)$ in equation (3.108) is equal to one.

Case 3: The general case of ground motion. In this case, the wave propogation factor as well as the frequency-dependent spatial correlation function $\rho(\nu,f)$ were considered in the ground motion model.

In each case two different sets of ground motion parameters were used to study the responses of the two bridges (see Tables 3-1 and 3-2). Note that although the variances of ground acceleration corresponding to the two sets of parameters were normalized to be the same, the variances of ground displacements are different.

4.3 ANALYSIS RESULTS

As mentioned earlier, each bridge has two models; the in-plane model and the out-of-plane model. For the in-plane model the ground motion acceleration was applied in the global X-axis direction. For

each element, the variances of bending moments, shear and axial forces were obtained. Also, the variances of nodal rotations and displacements in the global coordinate system were determined.

For the out-of-plane model, the ground motion was applied in the global Z-axis direction. The corresponding variances of member end forces, nodal displacements and rotations were determined.

For the CSCB Bridge models only, the ground acceleration was additionally applied to the support of the approaching span to study the effect of that on the response of the CSCB.

Throughout this chapter the following symbols are used:

$\sigma^2_{F_z}$ - The variance of member shear forces in the direction of local x-axis.

$\sigma^2_{F_z}$ - The variance of axial forces.

$\sigma^2_{F_y}$ - The variance of shear forces in the direction of local y-axis.

$\sigma^2_{M_x}$ - The variance of bending moment about local x-axis.

$G^2_{M_z}$ - The variance of torsional moment.

$G^2_{M_y}$ - The variance of bending moment about local y-axis.

$G^2_{M_w}$ - The variance of warping moment.

$\sigma^2_*(w)$, $\sigma^2_*(H)$, $\sigma^2_*(G)$ - The variances of any member end forces resulting from the wave propogation case (Case 2), fully correlated case (Case 1) and general case (Case 3) of ground motion, respectively.

4.3.1 RESPONSE COMPONENTS OF CSCB AND NRGB

As discussed earlier in chapter 3, the variance of the total response consists of three components; the variance of the dynamic component, the variance of the static component and the covariance between the static and dynamic components. The relative contributions of response components were found by dividing the variance of a specific response by the variance of the total response. In CSCB Bridge, for the first set of ground motion parameters (ground motion 1), the relative contributions of dynamic and static components are shown in Tables 4-1 and 4-2. For the second set of parameters (ground motion 2) the same relative contributions are shown in Tables 4-4 and 4-5. The relative contributions of the covariance between the dynamic and static components for both ground motions are shown in tables 4-3 and 4-6, respectively.

Those tables show that the dynamic component of the response is the dominant one and represents more than 96% of the total response for most elements, except the bracing members. For the general correlation case of ground motion 1, the relative contributions of the dynamic and static variances and the covariance of the axial forces in longitudinal bracing are 78%, 8% and 12%, respectively. For ground motion 2, the same relative contributions listed in the same order are 65%, 11% and 23%. This indicates the relative sensitivity of the bracing members to statically applied support displacements, since they transfer the forces between the deck and the arch.

The variance of the static component represents the bridge response due to a pseudo-static application of differential support motion. In this case the inertia forces of the bridge mass do not contribute to the increase of the bridge response. The variance of the

Table 4-1 Relative Contributions of the Dynamic Components of CSCB Members End Forces to the General Case of Ground Motion 1.

Elements	NODE I			NODE J		
	$\frac{\sigma^2_{Fxd}(G)}{\sigma^2_{Fx}(G)}$	$\frac{\sigma^2_{Fzd}(G)}{\sigma^2_{Fz}(G)}$	$\frac{\sigma^2_{Myd}(G)}{\sigma^2_{My}(G)}$	$\frac{\sigma^2_{Fxd}(G)}{\sigma^2_{Fx}(G)}$	$\frac{\sigma^2_{Fzd}(G)}{\sigma^2_{Fz}(G)}$	$\frac{\sigma^2_{Myd}(G)}{\sigma^2_{My}(G)}$
Bracing Elements						
1		79.8			79.8	
2		77.7			77.7	
Deck Elements						
1	99.3	100.3	78.9	99.3	100.3	99.3
2	97.4	100.3	99.3	97.4	100.3	92.2
3	98.6	100.3	92.2	98.6	100.3	96.5
4	100.1	100.2	96.5	100.1	100.2	105.5
5	98.6	100.2	105.5	98.6	100.2	102.4
6	95.6	100.8	102.4	95.6	100.8	101.8
7	101.7	101.3	101.8	101.7	101.3	99.0
8	102.0	101.4	99.0	102.0	101.4	100.9
9	100.1	101.4	100.9	100.1	101.4	101.2
10	98.5	101.4	101.2	98.5	101.4	101.3
11	101.3	101.4	101.3	101.3	101.4	91.5
Arch Elements						
20	96.5	100.3	78.4	96.5	100.3	96.5
21	99.0	100.3	96.5	99.0	100.3	93.1
22	100.6	100.3	93.1	100.6	100.3	95.9
23	98.7	100.3	95.9	98.7	100.3	105.8
24	98.6	100.3	105.8	98.6	100.3	102.6
25	96.7	100.0	102.6	96.7	100.0	101.7
26	101.5	99.8	101.7	101.5	99.8	99.0
27	101.7	99.7	99.0	101.7	99.8	100.5
28	100.2	99.8	100.5	100.2	99.8	101.7
29	100.4	99.8	101.7	100.4	99.8	100.8
30	100.8	99.8	100.8	100.8	99.8	91.2

Table 4-2 Relative Contributions of the Static Components of CSCB Members End Forces to the General Case of Ground Motion 1.

Elements	NODE I			NODE J		
	$\frac{\sigma^2_{Fxs}(G)}{\sigma^2_{Fx}(G)}$	$\frac{\sigma^2_{Fzs}(G)}{\sigma^2_{Fz}(G)}$	$\frac{\sigma^2_{Mys}(G)}{\sigma^2_{My}(G)}$	$\frac{\sigma^2_{Fxs}(G)}{\sigma^2_{Fx}(G)}$	$\frac{\sigma^2_{Fzs}(G)}{\sigma^2_{Fz}(G)}$	$\frac{\sigma^2_{Mys}(G)}{\sigma^2_{My}(G)}$
Bracing Elements						
1		7.90			7.90	
2		9.50			9.50	
Deck Elements						
1	0.05	0.01	11.25	0.05	0.01	0.05
2	1.80	0.01	0.05	1.80	0.01	2.13
3	0.13	0.01	2.13	0.13	0.01	1.84
4	0.01	0.01	1.84	0.00	0.01	4.35
5	0.25	0.01	4.35	0.25	0.01	0.32
6	0.57	0.07	0.32	0.57	0.07	1.00
7	0.43	0.22	1.00	0.43	0.22	0.23
8	0.39	0.20	0.23	0.39	0.20	0.05
9	0.00	0.18	0.05	0.00	0.18	0.05
10	0.00	0.18	0.05	0.00	0.18	0.05
11	0.20	0.17	0.05	0.20	0.17	0.36
Arch Elements						
20	0.79	0.01	11.87	0.79	0.01	0.79
21	0.35	0.01	0.79	0.35	0.01	1.73
22	0.04	0.01	1.73	0.04	0.01	2.20
23	0.08	0.01	2.20	0.08	0.01	4.19
24	0.28	0.01	4.19	0.28	0.01	0.37
25	0.35	0.00	0.37	0.35	0.00	0.29
26	0.34	0.01	0.93	0.34	0.01	0.29
27	0.23	0.01	0.29	0.23	0.01	0.02
28	0.05	0.01	0.02	0.05	0.01	0.11
29	0.02	0.00	0.11	0.02	0.00	0.05
30	0.05	0.00	0.05	0.05	0.00	1.60

Table 4-3 Relative Contributions of the Static-Dynamic Components of CSCB Members End Forces to the General Case of Ground Motion 1.

Elements	NODE I			NODE J		
	$\frac{\sigma^2_{Fxc}(G)}{\sigma^2_{Fx}(G)}$	$\frac{\sigma^2_{Fzc}(G)}{\sigma^2_{Fz}(G)}$	$\frac{\sigma^2_{Myc}(G)}{\sigma^2_{My}(G)}$	$\frac{\sigma^2_{Fxc}(G)}{\sigma^2_{Fx}(G)}$	$\frac{\sigma^2_{Fzc}(G)}{\sigma^2_{Fz}(G)}$	$\frac{\sigma^2_{Myc}(G)}{\sigma^2_{My}(G)}$
Bracing Elements						
1		12.28			12.28	
2		12.77			12.77	
Deck Elements						
1	0.68	0.35	9.84	0.68	0.35	0.68
2	0.78	0.30	0.68	0.78	0.30	5.67
3	1.22	0.27	5.67	1.22	0.27	1.70
4	0.15	0.25	1.70	0.15	0.25	9.84
5	1.12	0.24	9.84	1.12	0.24	2.69
6	3.78	0.85	2.69	3.78	0.85	2.76
7	2.10	1.55	2.76	2.10	1.55	0.80
8	2.36	1.55	0.80	2.36	1.55	0.93
9	0.08	1.55	0.93	0.08	1.55	1.28
10	1.28	1.56	1.28	1.28	1.56	1.66
11	1.62	1.60	1.66	1.66	1.60	7.03
Arch Elements						
20	2.75	0.28	9.77	2.75	0.28	2.75
21	0.69	0.29	2.75	0.69	0.29	5.14
22	0.59	0.29	5.14	0.59	0.29	1.86
23	1.25	0.30	1.86	1.25	0.30	10.03
24	1.11	0.29	10.03	1.11	0.29	2.94
25	2.97	0.04	2.94	2.97	0.04	2.61
26	1.82	0.22	2.61	1.82	0.22	0.72
27	1.94	0.22	0.72	1.94	0.22	0.53
28	0.27	0.22	0.53	0.27	0.22	1.80
29	0.40	0.22	1.80	0.40	0.22	0.81
30	0.81	0.22	0.81	0.81	0.22	7.17

Table 4-4 Relative Contributions of the Dynamic Components of CSCB Members End Forces to the General Case of Ground Motion 2.

Elements	NODE I			NODE J		
	$\frac{\sigma^2_{Fxd}(G)}{\sigma^2_{Fx}(G)}$	$\frac{\sigma^2_{Fzd}(G)}{\sigma^2_{Fz}(G)}$	$\frac{\sigma^2_{Myd}(G)}{\sigma^2_{My}(G)}$	$\frac{\sigma^2_{Fxd}(G)}{\sigma^2_{Fx}(G)}$	$\frac{\sigma^2_{Fzd}(G)}{\sigma^2_{Fz}(G)}$	$\frac{\sigma^2_{Myd}(G)}{\sigma^2_{My}(G)}$
Bracing Elements						
1		66.9			66.9	
2		64.1			64.1	
Deck Elements						
1	98.6	101.2	72.5	98.6	101.2	98.6
2	83.7	101.0	98.6	83.7	101.0	90.8
3	97.3	100.9	90.8	97.3	100.9	87.0
4	100.2	100.8	87.0	100.2	100.8	112.3
5	95.3	100.7	112.2	95.3	100.7	103.8
6	92.5	102.5	103.8	92.5	102.5	104.3
7	105.7	104.3	104.3	105.7	104.3	98.3
8	103.2	104.1	98.3	103.2	104.1	102.5
9	100.2	104.0	102.5	100.2	104.0	101.4
10	92.0	103.8	101.4	92.0	103.8	102.9
11	102.9	103.8	102.9	102.9	103.8	89.4
Arch Elements						
20	94.3	101.6	72.7	94.3	101.6	94.3
21	92.5	101.7	94.3	92.5	101.7	92.0
22	101.4	101.7	92.0	101.5	101.7	85.8
23	98.0	101.8	85.8	98.0	101.8	112.2
24	94.8	101.7	112.2	94.8	101.7	104.1
25	94.3	100.2	104.1	94.3	100.2	104.1
26	105.5	98.6	104.1	105.5	98.6	98.6
27	102.8	98.6	98.6	102.8	98.6	101.4
28	100.9	98.6	101.4	100.9	98.6	101.9
29	102.2	98.7	102.0	102.2	98.7	101.3
30	101.3	98.6	101.3	101.3	98.6	89.5

Table 4-5 Relative Contributions of the Static Components of CSCB Members End Forces to the General Case of Ground Motion 2.

Elements	NODE I			NODE J		
	$\frac{\sigma^2_{Fxs}(G)}{\sigma^2_{Fx}(G)}$	$\frac{\sigma^2_{Fzs}(G)}{\sigma^2_{Fz}(G)}$	$\frac{\sigma^2_{Mys}(G)}{\sigma^2_{My}(G)}$	$\frac{\sigma^2_{Fxs}(G)}{\sigma^2_{Fx}(G)}$	$\frac{\sigma^2_{Fzs}(G)}{\sigma^2_{Fz}(G)}$	$\frac{\sigma^2_{Mys}(G)}{\sigma^2_{My}(G)}$
Bracing Elements						
1		10.41			10.41	
2		12.32			12.32	
Deck Elements						
1	0.06	0.03	12.02	0.06	0.03	0.06
2	10.30	0.02	0.06	10.30	0.02	1.80
3	0.18	0.02	1.80	0.18	0.02	4.80
4	0.00	0.01	4.79	0.00	0.01	5.61
5	0.53	0.01	5.61	0.53	0.01	0.32
6	0.77	0.13	0.32	0.77	0.13	1.07
7	0.85	0.40	1.07	0.85	0.40	0.45
8	0.37	0.36	0.45	0.37	0.36	0.10
9	0.00	0.32	0.10	0.00	0.32	0.04
10	0.87	0.29	0.04	0.87	0.29	0.46
11	0.46	0.27	0.46	0.46	0.27	1.48
Arch Elements						
20	0.87	0.05	12.20	0.87	0.05	0.87
21	1.85	0.06	0.87	1.85	0.06	1.41
22	0.07	0.07	1.41	0.07	0.07	5.51
23	0.08	0.07	5.51	0.08	0.07	5.20
24	0.65	0.07	5.20	0.65	0.07	0.36
25	0.47	0.00	0.36	0.47	0.00	1.01
26	0.76	0.03	1.01	0.76	0.03	0.51
27	0.23	0.03	0.51	0.23	0.03	0.03
28	0.12	0.03	0.03	0.12	0.03	0.09
29	0.09	0.03	0.09	0.09	0.03	0.06
30	0.06	0.03	0.06	0.06	0.03	1.48

Table 4-6 Relative Contributions of the Static-Dynamic Components of CSCB Members End Forces to the General Case of Ground Motion 2.

Elements	NODE I			NODE J		
	$\frac{\sigma^2_{Fxc}(G)}{\sigma^2_{Fx}(G)}$	$\frac{\sigma^2_{Fzc}(G)}{\sigma^2_{Fz}(G)}$	$\frac{\sigma^2_{Myc}(G)}{\sigma^2_{My}(G)}$	$\frac{\sigma^2_{Fxc}(G)}{\sigma^2_{Fx}(G)}$	$\frac{\sigma^2_{Fzc}(G)}{\sigma^2_{Fz}(G)}$	$\frac{\sigma^2_{Myc}(G)}{\sigma^2_{My}(G)}$
Bracing Elements						
1		22.73			22.73	
2		23.61			23.61	
Deck Elements						
1	1.30	1.22	15.46	1.30	1.22	1.30
2	5.96	1.03	1.30	5.96	1.03	7.45
3	2.49	0.89	7.45	2.49	0.89	8.21
4	0.21	0.81	8.21	0.21	0.81	17.86
5	4.18	0.74	17.86	4.18	0.74	4.15
6	6.72	2.60	4.15	6.72	2.60	5.32
7	6.54	4.69	5.32	6.54	4.69	1.30
8	3.59	4.46	1.30	3.59	4.46	2.59
9	0.21	4.28	2.59	0.21	4.28	1.48
10	7.19	4.14	1.48	7.19	4.14	3.40
11	3.40	4.04	3.40	3.40	4.04	9.12
Arch Elements						
20	4.79	1.67	15.08	4.79	1.67	4.79
21	5.60	1.74	4.79	5.60	1.74	6.61
22	1.52	1.77	6.61	1.52	1.77	8.65
23	1.95	1.82	8.65	1.95	1.82	17.42
24	4.56	1.81	17.42	4.56	1.81	4.51
25	5.25	0.23	4.51	5.25	0.23	5.10
26	6.25	1.35	5.10	6.25	1.35	0.86
27	3.07	1.37	0.86	3.07	1.37	1.46
28	1.03	1.36	1.46	1.03	1.36	2.05
29	2.30	1.32	2.05	2.30	1.32	1.39
30	1.39	1.33	1.39	1.39	1.33	8.99

dynamic components represent the structural response to dynamically applied differential support motion where the inertia forces come into play. The inertia forces will mainly be generated in the vertical direction as well as in the horizontal direction resulting in a much higher response of the bridge members

The difference in the relative contribution of the bracing member responses due to different ground motion parameters can be justified as follows. Although the variance of ground motion acceleration for the two sets of parameters was the same, the variance of ground displacement was higher in ground motion 2 than in ground motion 1. This difference in ground displacements causes the observed increase in the variance of the static response and in the covariance between static and dynamic responses.

4.3.2 IN-PLANE RESPONSE OF THE CSCB

As mentioned earlier, three cases of ground motion correlation were used to study the responses of the bridges. Each case has two different sets of parameters (ground motions 1 and 2). Thus the CSCB was analyzed six times for the in-plane response.

A comparison of the bridge responses due to the three correlation cases was carried by dividing the variance of the members responses due to fully corrtelated and wave propogation cases by the corresponding variances of responses of the general case. For this part of the study, the goal was to establish the correlation model of ground motion that will generate the highest structural response of the CSCB.

Tables 4-7 and 4-8 show the results of this part of the study. The entries in the tables that are shown as "-", indicate that the compared values are zero. For the deck members we notice that the axial forces were the highest in the fully correlated case where the movement of the

Table 4-7 Normalized In-plane CSCB Responses - Ground Motion 1

Elements	Shear force Fx		Axial force Fz		Moment My	
	$\frac{\sigma^2_{F_x}(w)}{\sigma^2_{F_x}(G)}$	$\frac{\sigma^2_{F_x}(H)}{\sigma^2_{F_x}(G)}$	$\frac{\sigma^2_{F_z}(w)}{\sigma^2_{F_z}(G)}$	$\frac{\sigma^2_{F_z}(H)}{\sigma^2_{F_z}(G)}$	$\frac{\sigma^2_{M_y}(w)}{\sigma^2_{M_y}(G)}$	$\frac{\sigma^2_{M_y}(H)}{\sigma^2_{M_y}(G)}$
Deck Elements						
1	1.01	0.14	0.98	1.23	1.01	0.14
2	1.14	0.08	0.98	1.24	0.94	0.60
3	1.04	0.21	0.98	1.24	1.09	0.09
4	0.98	0.11	0.98	1.26	1.00	0.63
5	1.09	0.03	0.97	1.26	1.00	0.07
6	0.92	1.61	0.97	1.28	0.96	0.10
7	1.09	0.02	0.97	1.29	0.98	0.70
8	0.94	0.16	0.97	1.29	1.10	0.08
9	1.04	0.24	0.97	1.30	0.95	0.12
10	1.14	0.08	0.97	1.30	1.00	0.17
Bracing Elements						
1			0.97	0.95		
Arch Elements						
20	1.00	0.14	1.16	0.015	1.00	0.14
21	1.14	0.06	1.16	0.012	0.94	0.10
22	1.07	0.22	1.16	0.01	1.09	0.09
23	1.00	0.08	1.16	0.01	0.99	0.63
24	1.10	0.03	1.16	0.01	1.00	0.08
25	0.92	1.60	1.16	0.008	0.93	0.11
26	1.10	0.03	1.16	0.01	0.96	0.72
27	0.97	0.11	1.16	0.01	1.10	0.08
28	1.06	0.24	1.16	0.01	0.93	0.12
29	1.14	0.06	1.16	0.03	0.99	0.16
30	0.99	0.16	1.16	0.06	-	-

Table 4-8 Normalized In-plane CSCB Responses - Ground Motion 2

Elements	Shear force Fx		Axial force Fz		Moment My	
	$\frac{\sigma^2_{F_x}(w)}{\sigma^2_{F_x}(G)}$	$\frac{\sigma^2_{F_x}(H)}{\sigma^2_{F_x}(G)}$	$\frac{\sigma^2_{F_z}(w)}{\sigma^2_{F_z}(G)}$	$\frac{\sigma^2_{F_z}(H)}{\sigma^2_{F_z}(G)}$	$\frac{\sigma^2_{M_y}(w)}{\sigma^2_{M_y}(G)}$	$\frac{\sigma^2_{M_y}(H)}{\sigma^2_{M_y}(G)}$
Deck Elements						
1	0.96	0.1	0.98	1.26	0.95	0.1
2	1.06	0.28	0.98	1.26	0.94	0.05
3	0.97	0.17	0.98	1.26	0.97	0.19
4	0.95	0.05	0.98	1.26	0.97	0.54
5	0.97	0.04	0.98	1.27	0.96	0.04
6	0.97	1.35	0.98	1.29	0.42	0.07
7	0.98	0.03	0.98	1.32	0.91	0.93
8	0.93	0.07	0.98	1.31	1.00	0.12
9	0.93	0.24	0.98	1.31	0.95	0.05
10	1.05	0.23	0.98	1.31	0.93	0.13
Bracing Elements			0.99 0.98	0.76 0.74		
Arch Elements						
20	0.93	0.09	1.10	0.03	0.95	0.09
21	1.04	0.16	1.10	0.03	0.94	0.05
22	0.97	0.23	1.10	0.023	0.97	0.19
23	0.95	0.04	1.10	0.02	0.97	0.52
24	0.97	0.05	1.10	0.015	0.96	0.05
25	0.96	1.39	1.10	0.01	0.92	0.07
26	0.98	0.04	1.10	0.01	0.91	0.87
27	0.94	0.05	1.10	0.01	1.00	0.13
28	0.94	0.32	1.10	0.01	0.94	0.05
29	1.04	0.13	1.10	0.01	0.94	0.10
30	0.94	0.10	1.10	0.01	-	-

supports are identical. The increase in the variances of the axial forces with respect to the general case ranged from 23% to 30% for ground motion 1, and 26% to 31% for ground motion 2. The second worst case was the general correlation case where the deck experienced a 2% to 3% increase in axial force responses with respect to the wave propogation case for both ground motions.

The variances of shear forces and bending moments developed in the deck members were the highest in the wave propogation case where the deck members experienced a 1% to 15% increase over the general case. For the fully correlated case, the response of shear forces and bending moments ranged from 8% to 25% of the response in the general case for most of deck member, with a few members having a 63% to 70% increase of that response.

For the arch members the variances of the axial forces were the highest in the wave propogation case, where the variances of the axial forces were 16% and 10% higher than the variances of the general case responses for ground motions 1 and 2, respectively. In the fully correlated case, the variances of axial forces ranged from 11% to 23% of the response in the wave propogation case. For ground motion 1, the variances of shear forces and bending moments were higher in the wave porpogation case by 6% to 15% in comparison with the general case, but for ground motion 2, the general case responses were higher by a maximum of 6% compared to the wave propogation case. In the fully correlated case, the variances of the shear forces and bending moments ranged from 6% to 87% of the corresponding variances in the general case of ground motion.

These results indicate that for the deck members, the worst case of ground motion for axial force response was the fully correlated one. For the arch members the worst case is the wave propogation case. The

bending moments developed in the deck members in the fully correlated case are very small relative to the other two cases. The same occured in the arch members. Consequently, we can deduce that the fully correlated case generated the highest axial force responses in the deck. Intuitively this is expected since the supports are moving identically resulting in inertia forces in the horizontal direction that have the same phase. In the wave propogation case, there is a phase shift in support motion resulting in smaller axial forces and larger bending moments and shear forces. The general case of ground motion will have a phase shift and loss of coherency between the support motions, resulting in responses similar to the wave propogation case.

For the arch members it is clear that the wave propogation case of ground motion is the worst, resulting in higher responses, especially in the arch axial forces. This shows the sensitivity of long arch structures to dynamically applied differential support motion or dynamic pinching. The dynamically applied support motion will generate inertia forces in the horizontal and vertical directions. These inertia forces coupled with the sensitivity of arch structures to differential support motion will generate the highest response in the arch members.

The response of the axial bracing members in the longitudinal direction was the highest in the general correlation case. The difference in response between the wave propogation and general case was 3% at most. The response in the fully correlated case was 6% and 25% less than the response in the general case for ground motions 1 and 2, respectively. The reason for that difference in response is that the variance of ground motion displacement is higher for ground motion 2. The higher the support displacement, the larger the longitudianl force that has to be transferred from the deck to the arch.

The vertical displacements of CSCB resulting from the two ground motions, and the comparison between the displacements from different ground motion correlations are shown on Figures 4-5 through 4-9. Figures 4-5 and 4-6 show the normalized vertical displacements of ground motion 1 and 2, respectively. The normalization was done by dividing the variances of vertical displacements for each case of ground motion correlation by the maximum value of displacement. Figure 4-5 shows that in the general case of ground motion the maximum displacement occurs at the middle of the bridge. Meanwhile for the wave propogation and fully correlated ground motions the maximum displacement occurs at the one third points. In the fully correlated ground motion the variance of the vertical displacements at midspan is very small. In ground motion 2, as shown on Figure 4-6, the maximum vertical displacements in the general and wave propogation occur at midspan point of the bridge. The response to fully correlated ground motion 2 is similar to the one for ground motion 1. Figures 4-7 and 4-8 show the comparisons between the variances of vertical displacements due to the three cases of ground motion correlation. The mormalization was done by dividing the variances of displacements resulting from the wave propogation and the fully correlated cases of ground motion by the corresponding displacements from the general case. Both figures indicate that the vertical displacement from the wave propogation and the general case are very close to each other and are much higher than the resulting displacements from the fully correlated case of ground motion. Figure 4-9 shows the comparison of the vertical displacements of ground motions 1 and 2. The comparison was done by dividing the variance of the displacement from ground motion 1 by the corresponding variance of ground motion 2 for all ground motion correlations. The figure shows that the ratios in the wave propogation and the general cases are very

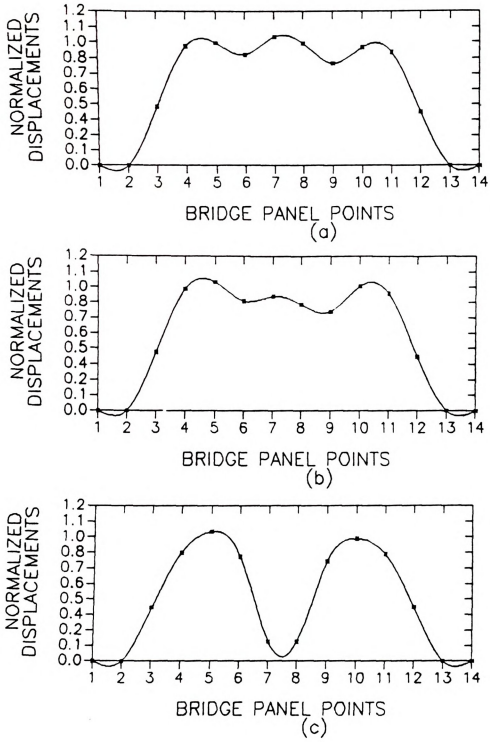

Figure 4-5: Normalized Variances of CSCB Vertical Displacements for Ground Motion 1. (a) General Case; (b) Wave Propogation Case; (c) Fully Correlated Case.

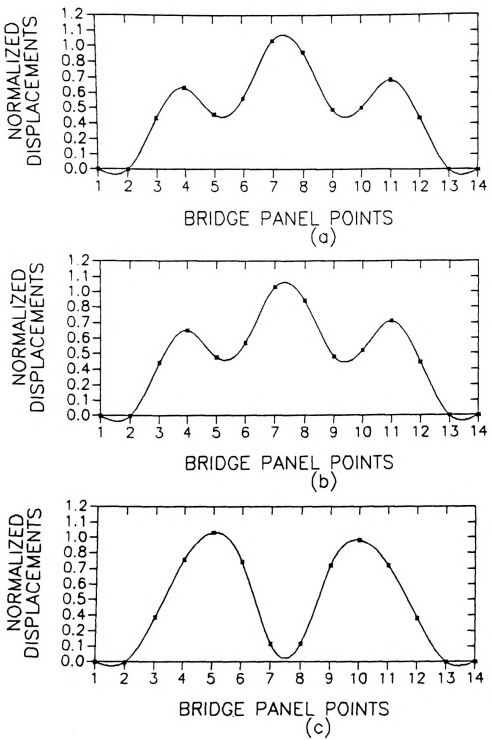

Figure 4-6: Normalized Variances of CSCB Vertical Displacements for Ground Motion 2. (a) General Case; (b) Wave Propogation Case; (c) Fully Correlated Case.

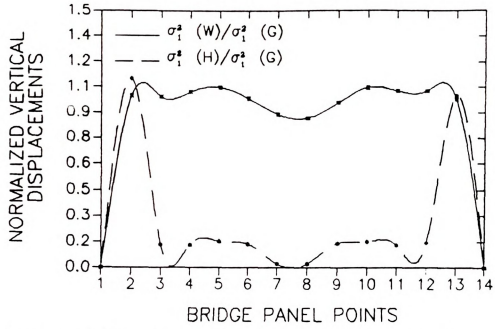

Figure 4-7: CSCB Normalized Variances of Vertical Displacements of Ground Motion 1 With Respect to the General Case.

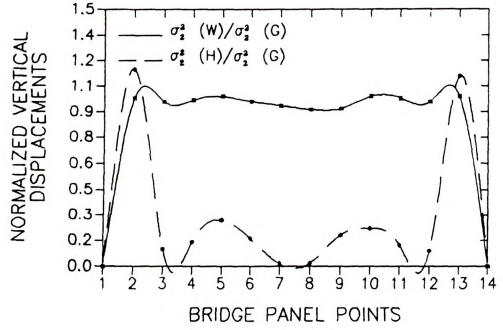

Figure 4-8: CSCB Normalized Variances of Vertical Displacements of Ground Motion 2 With Respect to the General Case.

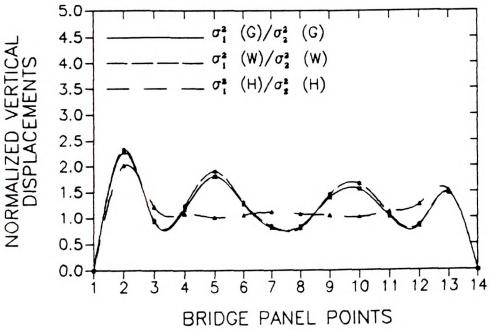

Figure 4-9: CSCB Ratios of Variances of Ground Motion 1 to Ground Motion 2 for the Three Cases of Ground Motion.

close to each other. It also shows that the displacements are higher in ground motion 1 and that the ratio is changing along the span of the bridge. Meanwhile, the ratio in the fully correlated ground motion is almost constant along the span of the bridge.

4.3.3 IN-PLANE RESPONSE OF NRGB

The comparison of the bridge responses to the three correlation cases of the two ground motions are summarized in Tables 4-9 and 4-10. For the deck members, the variances of axial forces corresponding to the

fully correlated case were 66% to 100% higher than the other two cases. The variances of shear forces and bending moments were the highest in the wave propogation case. The normalized variances of bending moments, shear and axial forces were higher than the corresponding values for the CSCB responses. The lowest values of shear forces and bending moments occured in the fully correlated case.

The responses of the arch members indicate that the highest variances of bending moments, shear and axial forces occured in the wave propogation case. The second highest responses were in the general case, and the lowest were in the fully correlated case. The variances of axial forces in the wave propogation case were about 20% and 800% higher than the responses in the general and fully correlated cases of ground motion, respectively.

The most evident difference in the responses of the two bridges is the response of the longitudinal bracing. For the CSCB, the variances of the axial forces were close to each other for ground motion 1, but, for ground motion 2, the variances of axial forces corresponding to the fully correlated case were about 25% less than the responses to the other two correlation cases of ground motion. For the NRGB, the variances of axial forces in the longitudinal bracing were the highest in the fully correlated case. The variances were 82% to 100% higher than those in the general and wave propogation cases of ground motion 1. For ground motion 2, the variances of axial forces due to fully correlated excitation were 44% to 78% higher than the variances due to the general and wave propogation excitations.

The differences in longitudinal bracing responses for the CSCB and NRGB were caused by the differences in their deck longitudinal force transfer mechanism. The CSCB deck has one expansion joint at the south abutment and a pin connection at the north abutment as shown in Figure

Table 4-9 Normalized In-plane NRGB Responses - Ground Motion 1

Elements	Shear force Fx		Axial force Fz		Moment My	
	$\frac{\sigma^2_{F_x}(w)}{\sigma^2_{F_x}(G)}$	$\frac{\sigma^2_{F_x}(H)}{\sigma^2_{F_x}(G)}$	$\frac{\sigma^2_{F_z}(w)}{\sigma^2_{F_z}(G)}$	$\frac{\sigma^2_{F_z}(H)}{\sigma^2_{F_z}(G)}$	$\frac{\sigma^2_{M_y}(w)}{\sigma^2_{M_y}(G)}$	$\frac{\sigma^2_{M_y}(H)}{\sigma^2_{M_y}(G)}$
Bracing Elements						
1			0.91	1.82		
2			0.83	2.02		
Deck Elements						
1	1.19	0.27	1.09	1.66	1.19	0.27
2	1.14	0.54	1.09	1.66	1.17	0.35
3	1.22	0.37	1.09	1.66	1.16	0.73
4	1.18	0.86	0.85	2.03	1.22	0.21
5	1.09	1.03	0.85	2.03	1.07	0.87
6	1.19	0.39	0.85	2.03	1.14	0.66
Arch Elements						
34	1.18	0.29	1.19	0.15	1.18	0.29
35	1.10	0.63	1.19	0.13	1.13	0.45
36	1.21	0.15	1.19	0.11	1.12	0.38
37	1.14	0.48	1.20	0.08	1.04	0.92
38	1.22	0.11	1.20	0.07	1.07	0.95
39	0.68	2.69	1.20	0.06	1.20	0.1
40	0.86	2.18	1.20	0.06	0.93	1.19

Table 4-10 Normalized In-plane NRGB Responses - Ground Motion 2

Elements	Shear force Fx		Axial force Fz		Moment My	
	$\frac{\sigma^2_{F_x}(w)}{\sigma^2_{F_x}(G)}$	$\frac{\sigma^2_{F_x}(H)}{\sigma^2_{F_x}(G)}$	$\frac{\sigma^2_{F_z}(w)}{\sigma^2_{F_z}(G)}$	$\frac{\sigma^2_{F_z}(H)}{\sigma^2_{F_z}(G)}$	$\frac{\sigma^2_{M_y}(w)}{\sigma^2_{M_y}(G)}$	$\frac{\sigma^2_{M_y}(H)}{\sigma^2_{M_y}(G)}$
Bracing Elements						
1			0.99	1.43		
2			0.92	1.78		
Deck Elements						
1	1.11	0.08	0.98	1.80	1.11	0.08
2	1.09	0.33	0.98	1.80	1.11	0.21
3	1.12	0.09	0.98	1.80	1.09	0.32
4	1.11	0.33	0.92	1.98	1.12	0.05
5	1.09	0.33	0.92	1.98	1.08	0.46
6	1.12	0.10	0.92	1.98	1.10	0.38
Arch Elements						
34	1.11	0.16	1.12	0.02	1.11	0.16
35	1.06	0.47	1.12	0.02	1.09	0.35
36	1.12	0.07	1.12	0.02	1.07	0.28
37	1.09	0.37	1.12	0.02	1.12	0.04
38	1.09	0.31	1.12	0.02	1.06	0.65
39	1.13	0.03	1.12	0.02	1.06	0.75
40	0.78	3.20	1.12	0.02	1.12	0.12
41	0.92	2.28	1.12	0.02	1.01	0.93

4-10. The deck longitudinal force will be mainly transferred to the support through the north abutment, and a little portion will be transferred to the arch through the bracing.

In the response of the NRGB arch, the normalized variances of shear forces and bending moments were relatively higher than for the CSCB arch responses.

This can be related to the rise to span ratio. For the NRGB the rise to span ratio is 0.22. For the CSCB the ratio is 0.21 for the south hinge and 0.14 for the north hinge. Thus, the NRGB will respond more in bending than the CSCB bridge.

The vertical displacements of NRGB resulting from the two ground motions and the comparison between the different correlations of support excitations are shown as Figures 4-11 through 4-15. Figures 4-11 and 4-12 show the normalized vertical displacements for ground motion 1 and 2, respectively. The normalization was done by dividing the variances of vertical displacements for each case of ground motion correlation by the maximum value of displacment. Figure 4-11 and 4-12 show that the maximum vertical displacments of the general and wave propogation cases occur at the one third span points. The minimum vertical displacements occurs in the middle of bridge span. For the fully correlated ground motion the maximum vertical displacement occurs at points close to the middle of the bridge, where the vertical displacement are very small.

Figures 4-13 and 4-14 show the comparison between the variances of vertical displacements due to the three cases of ground motion correlation. The normalization was done by dividing the wave propogation and fully correlated cases of ground motion by the corresponding displacements from the general case. Both figures indicate that the vertical displacements resulting from the wave propogation case were slightly higher than the displacements from the

general case for the two ground motions. The figures also show that the displacements form the fully correlated case of ground motion is much smaller comparing with the other two ground motion correlations.

Figure 4-15 shows the comparison of the vertical displacements of ground motions 1 and 2. The comparison was done by dividing the variances of the displacements from ground motion 1 by the corresponding variance of the displacement of ground motion 2 for all ground motion correlations. The figure shows that the ratio of the wave propogation and the general case are very close. It also shows that the displacements are higher in ground motion 2 by about 200% comparing with ground motion 1. For the fully correlated ground motion the difference between the two ground motions is not as high as in the other two cases. This difference in response between ground motions 1 and 2 is related to the frequency content of the ground motion.

4.3.4 OUT OF PLANE RESPONSE OF THE CSCB AND NRGB

Tables 4-11 and 4-12 show comparisons of the CSCB responses to the three correlation cases of ground motions 1 and 2, respectively. The study of the responses show that the bridge members responded differently to different ground motions. For some members the highest response was in the wave propogation case, for others it was either in the general or fully correlated case. Thus, it was difficult to predict which is the worst case for the out-of-plane response of the arch members or a group of members.

Tables 4-12 and 4-14 show comparisons of the NRGB responses for the three correlation cases of ground motions 1 and 2, respectively. The conclusions that can be drawn from the NRGB responses are the same as the ones for the CSCB responses.

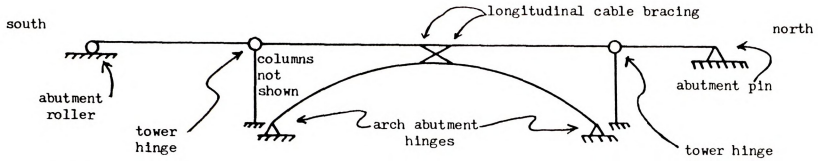

a) CSCB Transfer Mechanisms

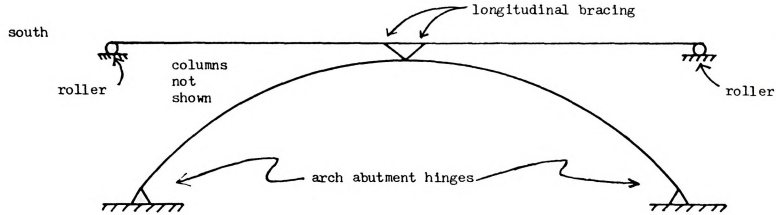

b) NRGB Transfer Mechanisms

Figure 4-10: Deck Longitudinal Force Transfer Mechanism
(Excerpted from Dusseau (1985))

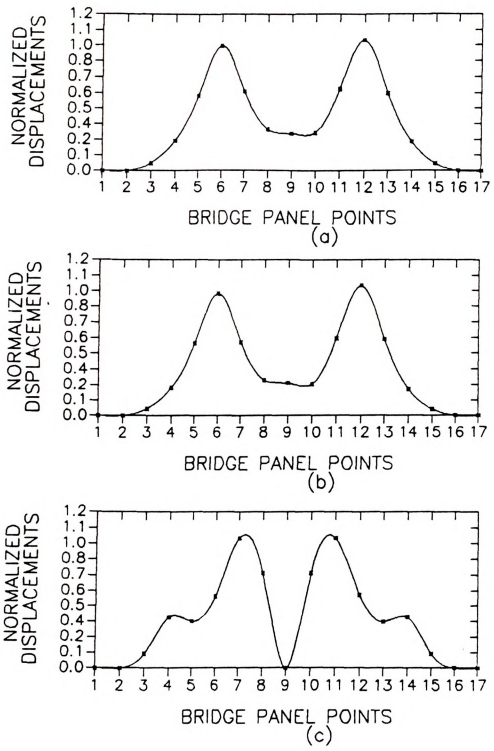

Figure 4-11: Normalized Variances of NRGB Vertical Displacements for Ground Motion 1. (a) General Case; (b) Wave Propogation Case; (c) Fully Correlated Case.

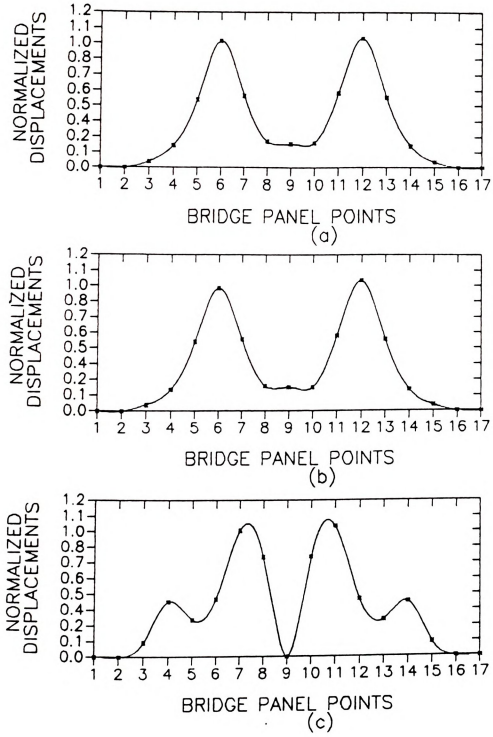

Figure 4-12: Normalized Variances of NRGB Vertical Displacements for Ground Motion 2. (a) General Case; (b) Wave Propogation Case; (c) Fully Correlated Case.

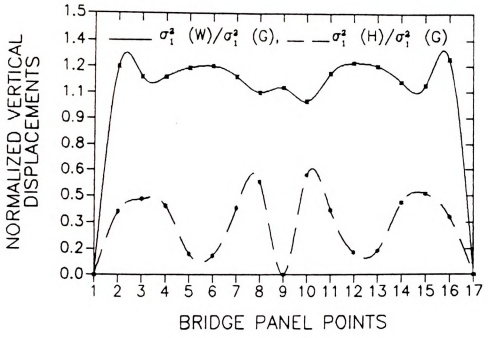

Figure 4-13: NRGB Normalized Variances of Vertical Displacements of Ground Motion 1 With Respect to the General Case.

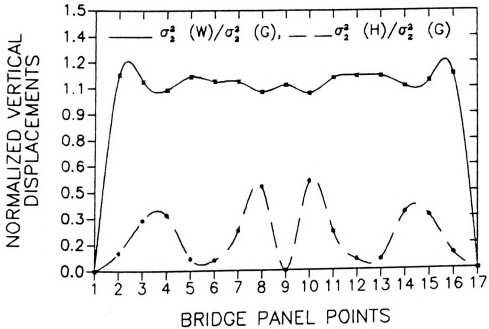

Figure 4-14: NRGB Normalized Variances of Vertical Displacements of Ground Motion 2 With Respect to the General Case.

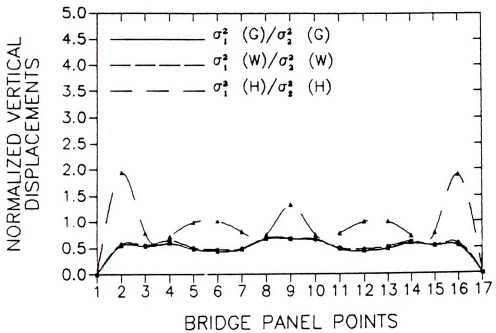

Figure 4-15: NRGB Ratios of Variances of Ground Motion 1 to Ground Motion 2 for the Three Cases of Ground Motion.

The lateral displacements of CSCB resulting from the two ground motions and the comparison between the displacement from different correlations of ground motion are shown on Figures 4-16 through 4-20. Figures 4-16 and 4-17 show the normalized lateral displacements of thearch and the deck for ground motion 1 and 2, respectively. The normalization was done by dividing the variances of lateral displacements for each case of ground motion correlation by the maximum value of displacement. Figures 4-16 and 4-17 indicate that the maximum lateral displacements in CSCB occur at points close to the midspan point

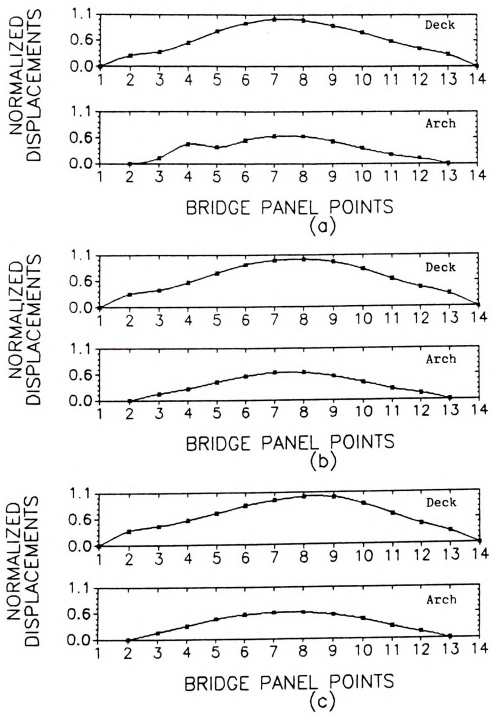

Figure 4-16: Normalized Variances of CSCB Lateral Displacements for Ground Motion 1. (a) Fully Correlated Case; (b) General Case; (c) Wave Propogation Case.

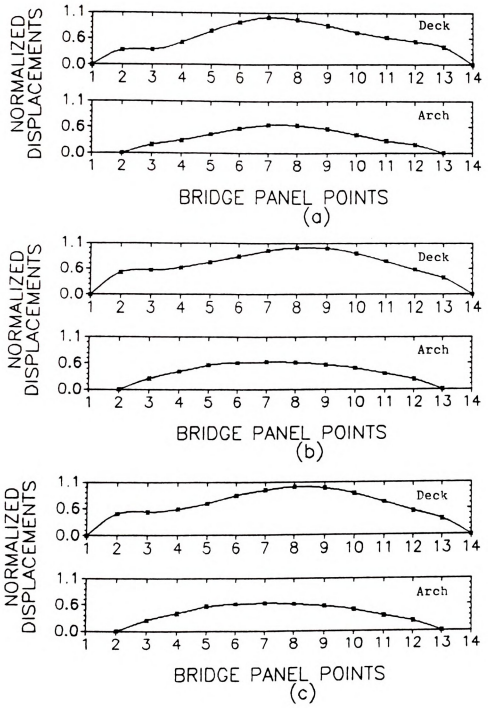

Figure 4-17: Normalized Variances of CSCB Lateral Displacements for Ground Motion 2. (a) Fully Correlated Case; (b) General Case. (c) Wave Propogation Case.

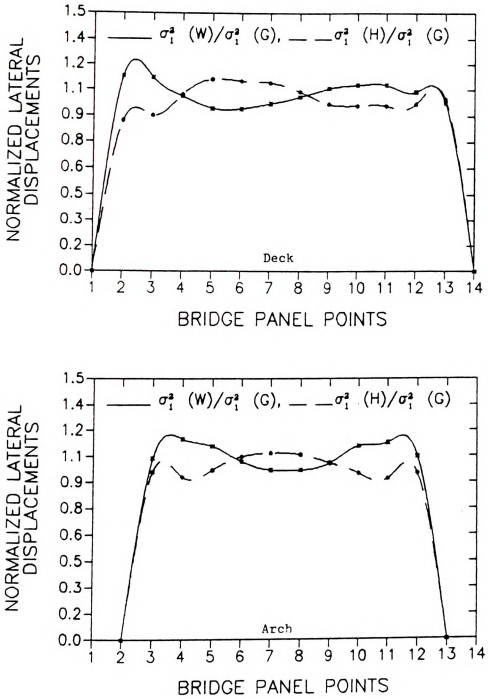

Figure 4-18: CSCB Normalized Variances of Lateral Displacements of Ground Motion 1 With Respect to the General Case.

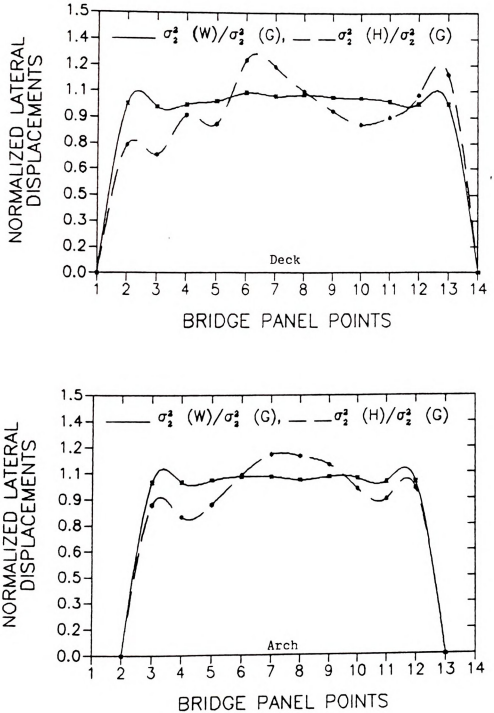

Figure 4-19: CSCB Normalized Variances of Lateral Displacements of Ground Motion 2 With Respect to the General Case.

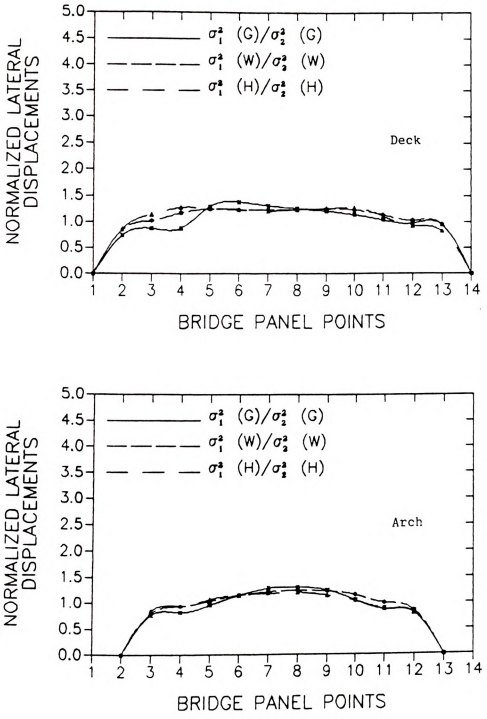

Figure 4-20: CSCB Ratios of Lateral Displacements of Ground Motion 1 to Ground Motion 2.

Table 4-11 Normalized Out-of-plane CSCB Responses - Ground Motion 1

Element	Fy		Mx		Mz		Mw	
	$\sigma^2_{F_y}(W)$	$\sigma^2_{F_y}(H)$	$\sigma^2_{M_x}(W)$	$\sigma^2_{M_x}(H)$	$\sigma^2_{M_z}(W)$	$\sigma^2_{M_z}(H)$	$\sigma^2_{M_w}(W)$	$\sigma^2_{M_w}(H)$
	$\sigma^2_{F_y}(G)$	$\sigma^2_{F_y}(G)$	$\sigma^2_{M_x}(G)$	$\sigma^2_{M_x}(G)$	$\sigma^2_{M_z}(G)$	$\sigma^2_{M_z}(G)$	$\sigma^2_{M_w}(G)$	$\sigma^2_{M_w}(G)$
Deck Elements								
1	0.81	1.52	1.07	1.02	0.80	1.31	-	-
2	0.71	1.51	1.33	0.88	1.30	0.71	1.15	0.98
3	0.89	1.20	1.01	0.95	1.10	1.25	1.10	1.00
4	1.08	1.19	1.12	1.64	0.79	1.46	1.13	0.89
5	0.75	1.56	0.99	1.21	0.73	1.32	1.05	1.17
6	1.04	0.70	2.67	0.43	0.86	1.09	0.98	1.25
7	0.90	0.92	1.06	0.84	0.89	1.08	1.17	0.81
8	0.72	1.24	0.62	1.23	1.18	0.79	0.88	0.87
9	0.95	0.91	0.71	0.80	1.22	0.77	1.21	0.86
10	1.11	0.82	1.38	0.75	1.03	0.97	0.98	0.92
11	1.10	0.89	1.02	0.95	0.82	1.06	1.12	0.89
20	1.24	0.91	1.09	0.99	1.22	0.92		
21	1.24	0.90	1.60	0.68	1.10	0.99		
22	1.10	0.97	1.10	1.00	0.99	1.07		
23	1.07	1.37	0.88	1.10	1.14	0.91		
24	1.09	0.88	0.92	1.05	1.11	1.06		
25	1.21	0.13	1.41	0.40	0.97	1.57		
26	1.30	0.85	0.91	0.98	0.75	1.39		
27	0.79	1.23	0.91	1.04	0.82	0.86		
28	0.84	0.81	1.03	0.87	1.18	0.83		
29	1.28	0.81	1.72	0.56	0.88	0.99		
30	1.11	0.80	1.05	1.00	1.09	0.91		

Table 4-12 Normalized Out-of-plane CSCB Responses - Ground Motion 2

Elements	Fy		Mx		Mz		Mw	
	$\frac{\sigma^2(W)}{F_y}$	$\frac{\sigma^2(H)}{F_y}$	$\frac{\sigma^2(W)}{M_x}$	$\frac{\sigma^2(H)}{M_x}$	$\frac{\sigma^2(W)}{M_z}$	$\frac{\sigma^2(H)}{M_z}$	$\frac{\sigma^2(W)}{M_w}$	$\frac{\sigma^2(H)}{M_w}$
	$\frac{\sigma^2(G)}{F_y}$	$\frac{\sigma^2(G)}{F_y}$	$\frac{\sigma^2(G)}{M_x}$	$\frac{\sigma^2(G)}{M_x}$	$\frac{\sigma^2(G)}{M_z}$	$\frac{\sigma^2(G)}{M_z}$	$\frac{\sigma^2(G)}{M_w}$	$\frac{\sigma^2(G)}{M_w}$
Deck Elements								
1	0.88	1.72	1.02	1.06	0.98	1.55	-	-
2	0.92	2.07	1.01	0.67	0.98	0.55	1.02	0.95
3	1.01	1.37	1.01	1.18	0.88	0.83	1.01	0.93
4	0.99	0.92	0.97	1.04	0.85	1.72	1.01	0.85
5	0.88	1.53	0.95	1.12	0.95	1.80	0.98	1.03
6	1.04	0.74	0.94	0.95	1.03	1.35	0.93	1.15
7	0.99	1.24	1.01	0.85	1.02	1.30	1.00	0.74
8	0.99	1.63	0.99	1.32	1.01	0.63	1.01	0.95
9	1.03	1.15	1.02	0.95	0.98	0.60	1.02	0.91
10	1.03	0.74	1.03	0.63	0.94	1.05	1.02	0.89
11	0.99	0.75	1.03	1.01	0.96	1.46	1.04	0.90
Arch Elements								
20	1.02	0.75	1.02	0.92	1.02	0.81		
21	1.02	0.77	1.02	0.43	1.02	1.01		
22	1.02	0.98	1.02	1.06	1.01	1.14		
23	1.02	1.17	1.01	1.34	1.01	0.86		
24	1.01	0.88	1.01	1.20	1.01	0.94		
25	1.02	0.22	0.96	0.35	1.01	1.35		
26	1.02	0.84	1.02	1.21	1.01	1.19		
27	1.01	1.04	1.02	1.22	1.02	0.97		
28	1.03	0.93	1.04	0.92	1.02	0.88		
29	1.03	0.75	1.04	0.38	1.02	1.06		
30	1.02	0.76	1.02	0.85	1.03	0.94		

Table 4-13 Normalized Out-of-plane NRGB Responses - Ground Motion 1

Elements	Fy		Mx		Mz		Mw	
	$\frac{\sigma^2(W)}{\sigma^2(G)}_{F_y}$	$\frac{\sigma^2(H)}{\sigma^2(G)}_{F_y}$	$\frac{\sigma^2(W)}{\sigma^2(G)}_{M_x}$	$\frac{\sigma^2(H)}{\sigma^2(G)}_{M_x}$	$\frac{\sigma^2(W)}{\sigma^2(G)}_{M_z}$	$\frac{\sigma^2(H)}{\sigma^2(G)}_{M_z}$	$\frac{\sigma^2(W)}{\sigma^2(G)}_{M_w}$	$\frac{\sigma^2(H)}{\sigma^2(G)}_{M_w}$
Deck Elements								
1	1.01	0.97	1.01	0.92	1.01	0.97	1.03	0.87
2	0.91	1.89	1.03	0.92	0.97	1.27	1.00	1.04
3	1.00	0.91	1.05	0.88	1.00	1.08	1.03	0.84
4	1.00	0.98	0.99	0.92	1.00	0.69	1.02	0.97
5	0.99	1.19	1.01	0.94	0.99	0.61	0.99	0.86
6	0.99	1.04	0.99	1.14	0.96	1.58	1.05	1.27
7	1.01	1.33	1.14	1.35	1.05	1.70	1.13	1.70
8	0.94	1.75	1.11	1.40	1.02	1.33	1.04	1.21
9	0.78	1.44	0.93	1.22	1.02	0.59	0.93	0.96
10	1.04	1.05	0.94	1.02	0.69	1.23	0.84	1.22
11	1.12	0.74	0.92	1.02	0.94	1.19	1.13	0.69
12	0.89	1.13	0.98	1.01	1.04	1.01	0.91	1.15
13	0.98	1.70	0.99	0.97	0.99	1.25	0.99	0.96
Arch Elements								
34	1.05	0.86	1.00	1.00	1.00	0.96		
35	1.05	0.88	1.03	1.00	1.05	0.87		
36	1.02	0.90	1.04	0.88	1.05	0.89		
37	1.05	0.83	0.99	0.93	1.04	0.95		
38	1.06	0.78	1.03	1.16	1.01	1.06		
39	1.05	0.88	1.02	1.03	0.97	1.65		
40	0.92	0.63	1.12	0.38	0.85	2.37		
41	1.01	0.65	1.04	0.47	0.99	1.48		
42	0.95	1.04	0.92	1.20	0.89	1.23		
43	1.02	0.79	1.09	0.97	0.84	1.24		
44	1.09	0.81	0.95	0.99	0.93	1.09		
45	0.89	1.07	0.78	1.31	0.95	1.01		
46	0.93	1.04	0.99	1.03	0.95	1.02		
47	0.95	1.00	1.01	0.98	0.93	1.05		

Table 4-14 Normalized Out-of-plane NRGB Responses - Ground Motion 2

Elements	Fy		Mx		Mz		Mw	
	$\sigma^2_{F_y}(W)$	$\sigma^2_{F_y}(H)$	$\sigma^2_{M_x}(W)$	$\sigma^2_{M_x}(H)$	$\sigma^2_{M_z}(W)$	$\sigma^2_{M_z}(H)$	$\sigma^2_{M_w}(W)$	$\sigma^2_{M_w}(H)$
	$\sigma^2_{F_y}(G)$	$\sigma^2_{F_y}(G)$	$\sigma^2_{M_x}(G)$	$\sigma^2_{M_x}(G)$	$\sigma^2_{M_z}(G)$	$\sigma^2_{M_z}(G)$	$\sigma^2_{M_w}(G)$	$\sigma^2_{M_w}(G)$
Deck Elements								
1	1.01	0.98	1.01	0.89	1.01	0.98	1.02	0.83
2	0.86	2.40	1.02	0.89	0.95	1.40	0.97	1.31
3	0.99	1.12	1.04	0.89	1.01	1.05	1.05	0.53
4	1.01	0.82	0.97	0.95	0.98	0.99	0.99	1.21
5	1.00	1.12	1.03	0.93	1.01	0.63	1.03	0.72
6	0.97	1.27	1.00	1.23	0.95	1.77	1.02	1.26
7	0.99	1.51	1.06	1.15	0.96	1.98	0.94	2.61
8	0.82	2.70	1.05	1.17	0.95	1.49	1.05	0.90
9	0.82	1.96	0.93	1.44	1.00	0.65	0.96	0.93
10	1.04	0.86	0.98	0.99	0.74	2.21	0.83	1.85
11	1.05	0.63	0.91	1.32	1024	1.04	1.09	0.38
12	0.88	1.56	0.94	1.20	1.00	1.01	0.87	1.66
13	0.95	1.84	0.99	0.95	0.96	1.36	1.00	0.92
14	0.98	1.02	1.00	0.93				
Arch Elements								
34	1.04	0.86	1.00	0.98	1.00	1.00		
35	1.04	0.88	1.03	0.94	1.03	0.88		
36	1.01	1.04	1.02	1.01	1.03	0.93		
37	1.05	0.66	0.97	1.11	1.02	1.03		
38	1.06	0.64	1.02	1.03	0.99	1.29		
39	1.04	0.85	1.03	0.97	0.91	2.12		
40	1.05	0.14	1.08	0.23	0.72	3.64		
41	1.05	0.22	1.06	0.31	0.89	1.91		
42	0.97	1.11	0.97	1.19	0.83	1.80		
43	1.04	0.65	1.06	0.72	0.88	1.47		
44	1.04	0.69	0.91	1.30	0.93	1.23		
45	0.89	1.42	0.84	1.71	0.96	1.09		
46	0.93	1.19	0.98	1.02	0.96	1.14		
47	0.95	1.11	0.99	0.99	0.93	1.19		

for all ground motion cases. The reason behind that is due to the fact that CSCB is not symmetric.

Figures 4-18 and 4-19 show the comparison of the lateral displacements of ground motion 1 and 2 for the arch and the deck. The comparison was done in the same way as for the in-plane response of CSCB.The figures indicate that the lateral displacements were not greatly influenced by the different ground motion cases. The lateral displacement for the three cases were within 10-15% from each other for most of bridge panel points.

Figure 4-20 shows the comparison of the lateral displacements of ground motion 1 and 2. The comparison was done in the same way as for the in-plane response. The figure indicates that the lateral displacements were larger in ground motion 1 by about 20%.

The lateral displacement response of NRGB is shown in Figures 4-21 Through 4-25. Figure 4-21 shows that the maximum displacement in the fully correlated case of ground motion 1 occured at midspan. In the other two cases, the maximum displacements in the deck occured at points closed to the supports. In the arch the maximum displacements occured at midspan. The maximum lateral displacements in ground motion 2 cccured at one quarter points in the three cases of ground motion in both the arch and the deck as shown in Figure 4-22. Figures 4-23 and 4-24 show that the maximum lateral displacements for the arch and the deck occured in the fully correlated case of ground motion. Figure 4-25 shows that the lateral displacements are about 1.5 times higher in ground motion 1 than in ground motion 2.

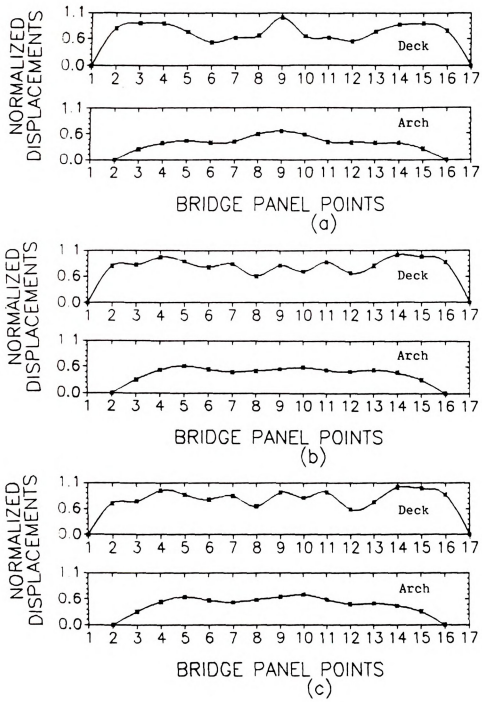

Figure 4-21: Normalized Variances of NRGB Lateral Displacements for Ground Motion 1. (a) Fully Correlated Case; (b) General Case; (c) Wave Propogation Case.

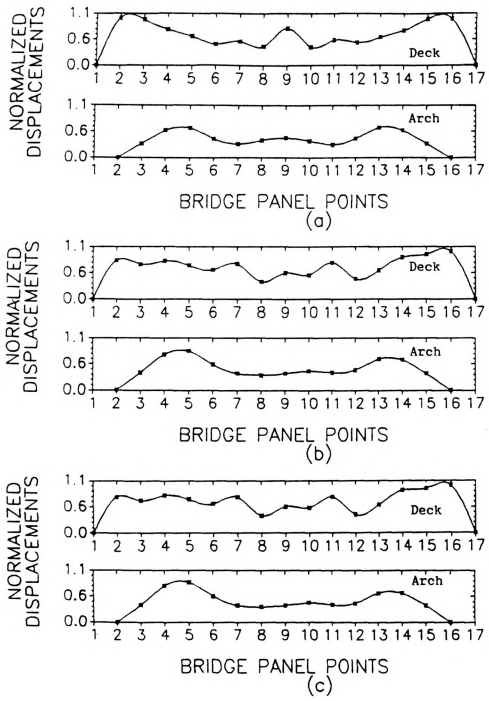

Figure 4-22: Normalized Variances of NRGB Lateral Displacements for Ground Motion 2. (a) Fully Correlated Case; (b) General Case. (c) Wave Propogation Case.

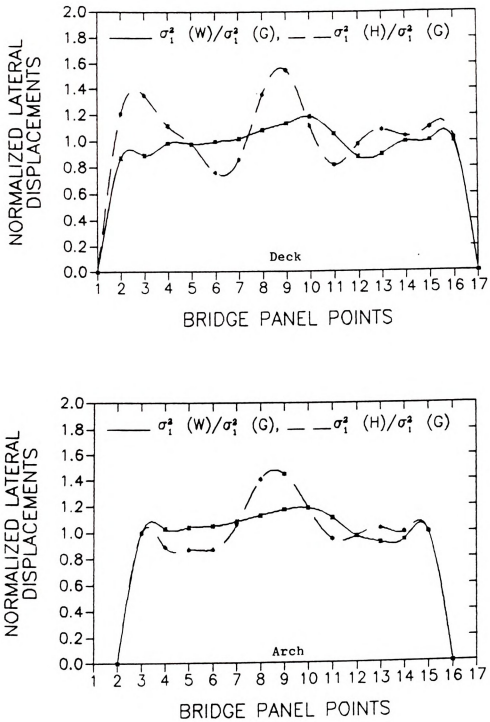

Figure 4-23: NRGB Normalized Variances of Lateral Displacements of Ground Motion 1 With Respect to the General Case.

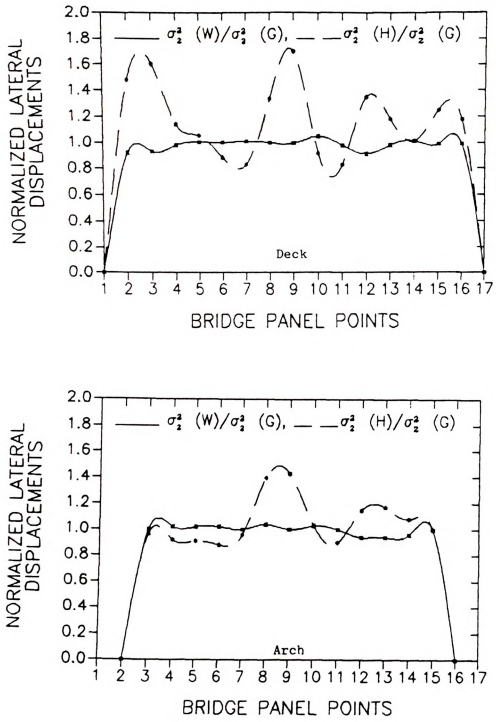

Figure 4-24: NRGB Normalized Variances of Lateral Displacements of Ground Motion 2 With Respect to the General Case.

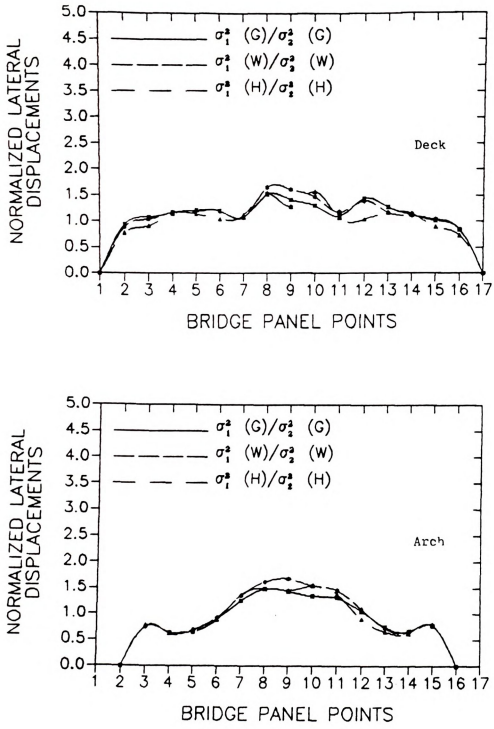

Figure 4-25: NRGB Ratios of Lateral Displacements of Ground Motion 1 to Ground Motion 2.

4.3.5 THE EFFECT OF GROUND MOTION PARAMETERS

As mentioned earlier, two sets of characteristic ground motions were used to analyze the responses of the CSCB and NRGB. The parameters characterizing these ground motions are shown in Tables 3-1 and 3-2. For both models the variances of ground acceleration (area under the spectrum) are equal, but the variance of ground displacement in ground motion 1 is larger than the variance in ground motion 2.

The comparison between the CSCB and NRGB out-of-plane and in-plane responses for the three correlation cases of ground motions 1 and 2 are shown in Tables 4-15 through Table 4-26. Tables 4-15 to 4-17 show the comparisons of the in-plane responses of CSCB to the three correlation cases of support motion in ground motions 1 and 2. The tables show that the CSCB responses were much higher in ground motion 1 in the three cases of support motion correlation. The axial forces in the arch were more than 6 times higher than the response in ground motion 2. The axial forces in the deck were about 65% higher in ground motion 1. The variances of shear forces and bending moments in most members were higher in ground motion 1. The increase in response ranged from 16% to 400%. For some members the shear forces and bending moments were higher in ground motion 2.

The results of the CSCB response to the out-of-plane ground motion are shown in Tables 4-18 to 4-20. The responses of the arch members to three correlation cases are higher in ground motion 2. The members experienced an increase in end force response ranging from 5% to 87%. The response of the deck members was not uniform. For some members ground motion 1 generated the highest response, while for others it was ground motion 2.

Table 4-15 In-plane CSCB Responses to the General Case: Ratio of Ground Motion 1 to Ground Motion 2 Responses

Elements	Shear Force Fx	Axial Force Fz	Bending moment My
	$\sigma^2_{F_x}(G_1)/\sigma^2_{F_x}(G_2)$	$\sigma^2_{F_z}(G_1)/\sigma^2_{F_z}(G_2)$	$\sigma^2_{M_y}(G_1)/\sigma^2_{M_y}(G_2)$
Bracing Elements			
1		1.14	
2		1.12	
Deck Elements			
1	1.04	1.76	1.04
2	4.96	1.73	0.73
3	1.22	1.70	2.25
4	0.82	1.66	1.11
5	1.85	1.62	0.85
6	1.16	1.61	0.93
7	1.73	1.61	1.71
8	0.81	1.58	1.69
9	1.51	1.55	0.69
10	3.82	1.53	1.12
11	1.12	1.51	-
Arch Elements			
20	0.95	6.05	0.95
21	4.52	6.10	0.70
22	1.55	6.16	2.16
23	0.87	6.20	1.07
24	2.03	6.23	0.85
25	1.17	6.10	0.94
26	1.92	5.94	1.55
27	0.87	5.94	1.68
28	1.95	5.93	0.67
29	3.61	5.90	0.98
30	0.98	5.86	-

Table 4-16 In-plane CSCB Responses to the Wave Propogation Case: Ratio of Ground Motion 1 to Ground Motion 2 Responses

Elements	Shear Force Fx	Axial Force Fz	Bending moment My
	$\sigma^2_{F_x}(W_1)/\sigma^2_{F_x}(W_2)$	$\sigma^2_{F_z}(W_1)/\sigma^2_{F_z}(W_2)$	$\sigma^2_{M_y}(W_1)/\sigma^2_{M_y}(W_2)$
Bracing Elements			
1		1.12	
2		1.10	
Deck Elements			
1	1.11	1.75	1.11
2	5.36	1.72	0.73
3	1.32	1.68	2.54
4	0.85	1.64	1.14
5	2.08	1.60	0.89
6	1.11	1.60	0.96
7	1.94	1.60	1.84
8	0.82	1.56	1.86
9	1.67	1.53	0.69
10	4.14	1.51	1.20
11	1.20	1.49	-
Arch Elements			
20	1.01	6.35	1.01
21	4.98	6.41	0.70
22	1.71	6.46	2.43
23	0.92	6.51	1.09
24	2.29	6.54	0.89
25	1.12	6.41	0.97
26	2.15	6.25	1.64
27	0.90	6.26	1.85
28	2.20	6.24	0.66
29	3.95	6.22	1.03
30	1.03	6.19	-

Table 4-17 In-plane CSCB Responses to the Fully Correlated Case: Ratio of Ground Motion 1 to Ground Motion 2 Responses

Elements	Shear Force Fx $\sigma^2_{F_x}(H_1)/\sigma^2_{F_x}(H_2)$	Axial Force Fz $\sigma^2_{F_z}(H_1)/\sigma^2_{F_z}(H_2)$	Bending moment My $\sigma^2_{M_y}(H_1)/\sigma^2_{M_y}(H_2)$
Bracing Elements			
1		1.42	
2		1.40	
Deck Elements			
1	1.55	1.72	1.55
2	1.40	1.70	1.39
3	1.52	1.67	1.11
4	1.76	1.64	1.30
5	1.35	1.61	1.38
6	1.37	1.60	1.36
7	1.40	1.58	1.28
8	1.70	1.55	1.10
9	1.50	1.53	1.43
10	1.34	1.52	1.51
11	1.51	1.50	-
Arch Elements			
20	1.54	2.83	1.54
21	1.65	2.64	1.41
22	1.47	2.31	1.10
23	1.83	1.93	1.30
24	1.37	1.57	1.35
25	1.35	1.53	1.34
26	1.38	4.61	1.29
27	1.79	6.89	1.09
28	1.46	6.95	1.44
29	1.61	6.83	1.52
30	1.52	6.53	-

Table 4-18 Out-of-plane CSCB Responses to the General Case: Ratio of Ground Motion 1 to Ground Motion 2 Responses

Elements	Fy	Mx	Mz	Mw
	$\frac{\sigma^2(G)_{F_y 1}}{\sigma^2(G)_{F_y 2}}$	$\frac{\sigma^2(G)_{M_x 1}}{\sigma^2(G)_{M_x 2}}$	$\frac{\sigma^2(G)_{M_z 1}}{\sigma^2(G)_{M_z 2}}$	$\frac{\sigma^2(G)_{M_w 1}}{\sigma^2(G)_{M_w 2}}$
Deck Elements				
1	1.35	1.26	1.00	1.18
2	1.29	0.97	0.79	1.12
3	0.89	2.08	1.21	1.11
4	0.65	1.81	1.10	1.22
5	1.01	1.07	0.73	0.98
6	1.43	0.40	0.79	0.94
7	1.06	1.09	1.01	1.45
8	0.78	2.64	0.95	1.13
9	1.16	2.29	0.71	1.13
10	1.27	1.00	0.81	1.20
11	1.04	1.25	1.20	-
Arch Elements				
20	1.03	1.06	1.03	
21	1.05	0.79	1.20	
22	1.55	1.20	1.20	
23	1.59	1.23	1.06	
24	1.17	1.20	1.33	
25	1.71	0.85	1.66	
26	1.07	1.23	1.86	
27	1.69	1.18	1.66	
28	1.85	1.23	1.08	
29	1.08	0.79	1.20	
30	1.14	0.96	1.21	

Table 4-19 Out-of-plane CSCB Responses to the Wave Propogation Case: Ratio of Ground Motion 1 to Ground Motion 2 Responses

Elements	Fy	Mx	Mz	Mw
	$\frac{\sigma^2(W_{F_y1})}{\sigma^2(W_{F_y2})}$	$\frac{\sigma^2(W_{M_x1})}{\sigma^2(W_{M_x2})}$	$\frac{\sigma^2(W_{M_z1})}{\sigma^2(W_{M_z2})}$	$\frac{\sigma^2(W_{M_w1})}{\sigma^2(W_{M_w2})}$
Deck Elements				
1	1.26	1.32	0.83	-
2	1.00	1.28	0.67	1.32
3	0.71	2.08	0.98	1.22
4	0.71	2.10	1.13	1.25
5	0.86	1.12	0.85	1.32
6	1.43	1.11	0.62	1.03
7	0.97	1.15	0.69	1.10
8	0.57	1.66	1.17	1.26
9	1.07	1.61	1.19	1.34
10	1.37	1.34	0.79	1.09
11	1.16	1.24	0.69	1.30
Arch Elements				
20	1.26	1.14	1.24	
21	1.28	1.24	1.29	
22	1.67	1.27	1.18	
23	1.64	1.07	1.21	
24	1.27	1.10	1.46	
25	1.87	1.24	1.59	
26	1.36	1.10	1.38	
27	1.32	1.05	1.34	
28	1.51	1.22	1.25	
29	1.35	1.31	1.04	
30	1.23	1.00	1.27	

Table 4-20 Out-of-plane CSCB Responses to the Fully Correlated Case: Ratio of Ground Motion 1 to Ground Motion 2 Responses

Elements	Fy	Mx	Mz	Mw
	$\frac{\sigma^2_{F_y}(H_1)}{\sigma^2_{F_y}(H_2)}$	$\frac{\sigma^2_{M_x}(H_1)}{\sigma^2_{M_x}(H_2)}$	$\frac{\sigma^2_{M_z}(H_1)}{\sigma^2_{M_z}(H_2)}$	$\frac{\sigma^2_{M_w}(H_1)}{\sigma^2_{M_w}(H_2)}$
Deck Elements				
1	1.19	1.21	0.85	-
2	0.94	1.27	0.65	1.22
3	0.78	1.68	1.19	1.20
4	0.84	2.87	1.03	1.16
5	1.03	1.15	0.81	1.39
6	1.35	1.15	0.60	1.07
7	0.79	1.09	0.66	1.03
8	0.59	2.46	1.26	1.34
9	0.92	1.93	1.21	1.08
10	1.40	1.18	0.66	1.16
11	1.24	1.18	0.59	1.19
Arch Elements				
20	1.26	1.14	1.18	
21	1.24	1.26	1.18	
22	1.54	1.13	1.13	
23	1.85	1.02	1.13	
24	1.18	1.06	1.50	
25	1.07	0.99	1.93	
26	1.10	1.00	2.17	
27	1.99	1.00	1.46	
28	1.60	1.18	1.03	
29	1.17	1.16	1.13	
30	1.21	1.14	1.19	

Table 4-21 In-plane NRGB Responses to the General Case: Ratio of Ground Motion 1 to Ground Motion 2 Responses

Elements	Shear Force Fx	Axial Force Fz	Bending moment My
	$\sigma^2_{F_x}(G_1)/\sigma^2_{F_x}(G_2)$	$\sigma^2_{F_z}(G_1)/\sigma^2_{F_z}(G_2)$	$\sigma^2_{M_y}(G_1)/\sigma^2_{M_y}(G_2)$
Bracing Elements			
1		0.91	
2		1.02	
Deck Elements			
1	0.49	1.61	0.49
2	0.62	1.61	0.49
3	0.50	1.61	0.69
4	0.80	0.75	0.46
5	0.74	0.75	0.57
6	0.51	0.75	0.53
7	0.63	0.48	0.46
8	0.63	0.48	0.53
9	0.51	0.80	0.58
10	0.77	0.80	0.46
Arch Elements			
34	0.45	0.46	0.45
35	0.67	0.45	0.52
36	0.43	0.45	0.56
37	0.52	0.45	0.43
38	0.51	0.45	0.51
39	0.45	0.45	0.59
40	0.89	0.45	0.46
41	0.78	0.45	0.58
42	0.45	0.45	0.51

Table 4-22 In-plane NRGB Responses to the Wave Propogation Case: Ratio of Ground Motion 1 to Ground Motion 2 Responses

Elements	Shear Force Fx	Axial Force Fz	Bending moment My
	$\sigma^2_{F_x}(W_1)/\sigma^2_{F_x}(W_2)$	$\sigma^2_{F_z}(W_1)/\sigma^2_{F_z}(W_2)$	$\sigma^2_{M_y}(W_1)/\sigma^2_{M_y}(W_2)$
Bracing Elements			
1		0.84	
2		0.92	
Deck Elements			
1	0.53	1.79	0.93
2	0.65	1.79	0.52
3	0.55	1.79	0.74
4	0.84	0.70	0.50
5	0.75	0.70	0.57
6	0.54	0.70	0.56
7	0.62	0.52	0.50
8	0.62	0.52	0.53
9	0.54	0.75	0.59
10	0.77	0.75	0.50
Arch Elements			
34	0.48	0.49	0.48
35	0.69	0.49	0.53
36	0.46	0.48	0.59
37	0.54	0.48	0.47
38	0.53	0.48	0.50
39	0.48	0.48	0.59
40	0.77	0.48	0.49
41	0.73	0.48	0.54
42	0.48	0.48	0.51

Table 4-23 In-plane NRGB Responses to the Fully Corrleated Case: Ratio of Ground Motion 1 to Ground Motion 2 Responses

Elements	Shear Force Fx $\sigma^2_{F_x}(H_1)/\sigma^2_{F_x}(H_2)$	Axial Force Fz $\sigma^2_{F_z}(H_1)/\sigma^2_{F_z}(H_2)$	Bending moment My $\sigma^2_{M_y}(H_1)/\sigma^2_{M_y}(H_2)$
Bracing Elements			
1		1.15	
2		1.15	
Deck Elements			
1	1.61	1.49	1.61
2	1.00	1.49	0.82
3	1.89	1.49	1.53
4	2.07	0.77	1.83
5	2.28	0.77	1.09
6	1.87	0.77	0.92
Arch Elements			
34	0.81	2.48	0.81
35	0.89	2.28	0.65
36	0.93	2.00	0.76
37	0.93	2.00	0.76
38	0.78	1.50	0.72
39	1.57	1.32	0.74
40	0.74	1.23	-

Table 4-24 Out-of-plane NRGB Responses to the General Case: Ratio of Ground Motion 1 to Ground Motion 2 Responses

Elements	Fy	Mx	Mz	Mw
	$\frac{\sigma^2(G)_{F_y 1}}{\sigma^2(G)_{F_y 2}}$	$\frac{\sigma^2(G)_{M_x 1}}{\sigma^2(G)_{M_x 2}}$	$\frac{\sigma^2(G)_{M_z 1}}{\sigma^2(G)_{M_z 2}}$	$\frac{\sigma^2(G)_{M_w 1}}{\sigma^2(G)_{M_w 2}}$
Deck Elements				
1	0.66	0.85	0.66	0.83
2	1.01	0.87	0.86	0.99
3	0.65	0.89	0.92	1.22
4	0.81	1.42	0.96	1.44
5	0.98	2.30	0.78	1.83
6	0.83	1.92	1.03	2.70
7	1.32	2.42	1.18	3.61
8	1.79	2.31	1.05	2.13
9	0.94	2.08	0.81	2.02
10	0.85	2.37	1.27	1.77
11	0.78	1.45	0.84	1.12
12	0.75	1.10	0.80	1.11
13	0.84	0.84	0.79	0.81
14	0.72	0.82	-	-
Arch Elements				
34	0.82	0.78	1.19	
35	0.74	0.75	0.66	
36	1.76	0.70	0.61	
37	1.51	0.86	0.70	
38	0.87	1.19	0.93	
39	1.34	0.75	1.19	
40	0.97	0.75	1.45	
41	1.13	0.75	1.21	
42	1.47	0.78	1.12	
43	0.86	1.06	0.77	
44	1.56	0.92	0.65	
45	1.99	0.83	0.69	
46	0.84	0.79	1.30	
47	0.91	0.78	0.89	

Table 4-25 Out-of-plane NRGB Responses to the Wave Propogation Case: Ratio of Ground Motion 1 to Ground Motion 2 Responses

Elements	Fy	Mx	Mz	Mw
	$\frac{\sigma^2(W)_{F_y 1}}{\sigma^2(W)_{F_y 2}}$	$\frac{\sigma^2(W)_{M_x 1}}{\sigma^2(W)_{M_x 2}}$	$\frac{\sigma^2(W)_{M_z 1}}{\sigma^2(W)_{M_z 2}}$	$\frac{\sigma^2(W)_{M_w 1}}{\sigma^2(W)_{M_w 2}}$
Deck Elements				
1	0.66	0.86	0.66	0.84
2	1.07	0.88	0.88	1.02
3	0.67	0.89	0.91	1.19
4	0.81	1.45	0.98	1.47
5	0.97	2.27	0.76	1.75
6	0.85	1.89	1.04	2.78
7	1.46	2.62	1.29	3.62
8	2.08	2.43	1.13	2.12
9	0.90	2.09	0.83	1.95
10	0.85	2.27	1.17	1.79
11	0.84	1.46	0.77	1.15
12	0.76	1.14	0.83	1.16
13	0.87	0.84	0.82	0.80
Arch Elements				
34	0.83	0.78	1.19	
35	0.75	0.75	0.68	
36	1.78	0.72	0.62	
37	1.51	0.87	0.72	
38	0.87	1.21	0.95	
39	1.36	0.74	1.26	
40	0.89	0.76	1.71	
41	1.08	0.73	1.35	
42	1.45	0.75	1.21	
43	0.85	1.08	0.73	
44	1.65	0.96	0.65	
45	1.99	0.77	0.69	
46	0.84	0.79	1.30	
47	0.91	0.80	0.89	

Table 4-26 Out-of-plane NRGB Responses to the Fully Correlated Case: Ratio of Ground Motion 1 to Ground Motion 2 Responses

Elements	Fy	Mx	Mz	Mw
	$\frac{\sigma^2_{F_y}(H_1)}{\sigma^2_{F_y}(H_2)}$	$\frac{\sigma^2_{M_x}(H_1)}{\sigma^2_{M_x}(H_2)}$	$\frac{\sigma^2_{M_z}(H_1)}{\sigma^2_{M_z}(H_2)}$	$\frac{\sigma^2_{M_w}(H_1)}{\sigma^2_{M_w}(H_2)}$
Deck Elements				
1	0.65	0.89	0.65	0.88
2	0.80	0.90	0.78	0.79
3	0.53	0.88	0.94	1.94
4	0.97	1.16	1.54	1.15
5	1.04	2.34	0.77	2.19
6	0.69	1.78	0.92	2.72
7	1.17	2.83	1.01	1.97
8	1.16	2.75	0.93	2.88
9	0.69	1.78	0.73	2.07
Arch Elements				
34	0.82	0.80	1.16	
35	0.74	0.80	0.66	
36	1.51	0.61	0.58	
37	1.89	0.72	0.64	
38	1.06	1.35	0.77	
39	1.40	0.79	0.92	
40	4.45	1.23	0.95	

Table 4-27: CSCB and NRGB In-Plane and Out-Of-Plane Frequencies of The First Twelve Modes

CSCB in-plane		CSCB out-of-plane	
ω(rad/sec)	f(Hz)	ω(rad/sec)	f(Hz)
2.71	0.43	2.30	0.36
5.27	0.84	3.74	0.59
9.73	1.55	5.54	0.88
9.93	1.58	8.87	1.41
14.6	2.33	9.31	1.48
15.3	2.44	10.03	1.60
21.8	3.47	15.72	2.50
28.9	4.60	19.64	3.13
29.9	4.76	23.80	3.78
36.8	5.80	24.54	3.91
44.5	7.08	31.62	5.03
50.9	8.10	34.41	5.47
NRGB in-plane		**NRGB out-of-plane**	
1.50	0.24	0.92	0.15
3.14	0.50	1.80	0.29
4.38	0.70	2.62	0.42
5.21	0.82	3.32	0.53
5.57	0.88	3.98	0.63
5.97	0.95	4.74	0.75
7.30	1.16	5.69	0.90
8.37	1.33	6.84	1.09
10.11	1.61	7.12	1.13
10.95	1.74	7.43	1.18
12.38	1.97	7.62	1.21
12.69	2.02	8.67	1.38

The comparison of the NRGB In-plane responses to the three correlation cases of ground motions 1 and 2 are shown in Tables 4-21 to 4-23. The tables clearly show that the highest responses of the bridge occurs due to the general and wave propogation cases of support excitations in ground motion 2. For the fully correlated case, the highest response occured in ground motion 1.

The out-of-plane response of the NRGB to the three correlation cases with ground motions 1 and 2 are shown in Tables 4-24 to 4-26. The responses of the arch members show that the highest responses occured due to ground motion 2. For the deck members the response in general was the highest in ground motion 1 with some members for which the highest response occured due to ground motion 2.

The in-plane response of the NRGB and CSCB for ground motions 1 and 2 are determined by their frequency content. The natural frequencies of the first twelve modes of the CSCB and NRGB in-plane and out-of-plane models are shown in Table 4-27. If we compare the first 12 natural frequencies of the in-plane model of the CSCB with the normalized autospectrum of ground acceleration (Figures 3-3), it can be seen that the area enclosed between the autospectrum and the frequency range from 0 to 40 H_z is much larger in ground motion 1 than in ground motion 2. Consequentely, ground motion 1 will contribute to a higher in-plane response of the CSCB.

For the NRGB, the first 12 natural frequencies ranging from 0.24 to 2.12 H_z. Those frequencies are very close to each other. Also, one can see that the corresponding values of the normalized autospectrum are higher for ground motion 2 than for ground motion 1 (Figure 3-3). Thus, a higher response of the NRGB will result due to ground motion 2. The

same conclusions can be made for the out-of-plane response of the CSCB and NRGB.

The in-plane displacement response of the CSCB and NRGB (Figures 4-5, Through 4-9, and Figures 4-11 through 4-15) indicate that larger displacements resulted from ground motion 2. As mentioned in Chapter 3 ; the variance of ground displacement is higher in ground motion 2. Thus, the responses of element end forces is governed by the frequency content of the ground motion, and the displacement response is governed by the displacement of the ground motion.

The out-of-plane displacement responses are shown in Figures 4-16, through 4-25. The figures show that the displacements resulting from ground motion 2 were higher at the ends of both bridges. The reason for this behavior could be due to the fact that the lateral stiffnesses of the bridges are not as high as the in-plane stiffnesses. Thus, the ground motion displacements will be effective at both ends of the two bridges, but at the middle of the bridges the frequency content of the ground motion will play a bigger role.

4.3.6 THE CSCB RESPONSE DUE TO TWO SUPPORT MOTION VERSUS FOUR SUPPORT MOTION

In this section, additional support motions were considered at the north and south supports of the approaching span of the CSCB as shown on Figure 4-26. This was done to study the effect of the additional support motion on the CSCB in-plane and out-of-plane responses.

Tables 4-28 and 4-29 show the normalized values of in-plane responses of the CSCB due to the three correlation cases of ground motions 1 and 2, respectively, when four support excitations are considered. Comparing Tables 4-7 and 4-8 with 4-28 and 4-29. We can see that the general

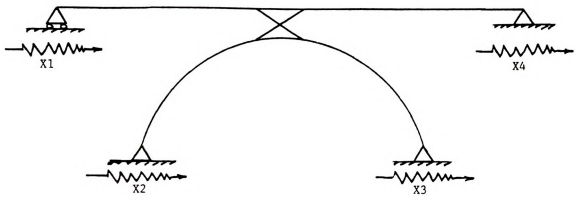

a) Ground Motion Applied to Four Supports

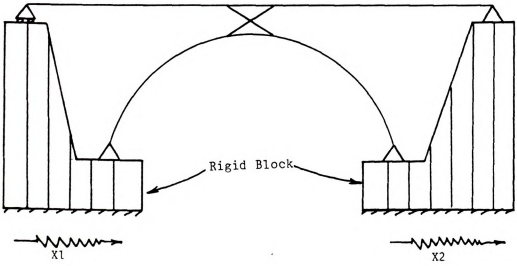

b) Ground Motion Applied to Two Supports

Figure 4-26: Two support Motion Vs. Four Support Motion

behavior did not change, except that the normalized values of axial forces resulting from fully correlated ground motion were higher when the ground motion was applied to four supports.

Tables 4-30 and 4-31 show the normalized values of the out-of-plane response of the CSCB due to the three correlation cases for ground motions 1 and 2, respectively. The general behavior is not different from the case with two support motion. In some members the normalized values were higher for the 4 support excitation.

Tables 4-32 and 4-33 compare the responses of the CSCB when two and four support motions are considered for the general correlation case of ground motions 1 and 2, respectively. The tables show that except for the increase in the deck axial forces by 7% and 9% and a decrease in bracing axial forces by 10% and 18%, ground motions 1 and 2, respectively. The responses for two and four support motions are within 2-3% from each other.

4.3.7 THE EFFECT OF INCREASING THE BRIDGE STIFFNESS ON THE RESPONSE COMPONENTS

As mentioned earlier, the total variance of the responses consists of three components; the variance of the dynamic component, the variance of the static component and the covariance of static and dynamic components. In Tables 4-1 through 4-6, it can be seen that at a given stiffness of a structure, the dynamic component are dominant, and the contribution of static and static-dynamic components is minor.

In this part of the study, the influence of the structural stiffness is examined. For this purpose, the stiffness of the CSCB members were increased, and the relative contribution of each component was monitored. The stiffness was increased by multiplying each member

Table 4-28 Normalized In-plane CSCB Responses to Four Support Motion-Ground Motion 1

Elements	Shear force Fx		Axial force Fz		Moment My	
	$\frac{\sigma^2_{F_x}(w)}{\sigma^2_{F_x}(G)}$	$\frac{\sigma^2_{F_x}(H)}{\sigma^2_{F_x}(G)}$	$\frac{\sigma^2_{F_z}(w)}{\sigma^2_{F_z}(G)}$	$\frac{\sigma^2_{F_z}(H)}{\sigma^2_{F_z}(G)}$	$\frac{\sigma^2_{M_y}(w)}{\sigma^2_{M_y}(G)}$	$\frac{\sigma^2_{M_y}(H)}{\sigma^2_{M_y}(G)}$
Deck Elements						
1	1.01	0.15	0.94	1.34	1.01	0.15
2	1.14	0.08	0.94	1.34	0.94	0.10
3	1.04	0.21	0.94	1.35	1.09	0.09
4	0.98	0.11	0.94	1.35	0.98	0.67
5	1.09	0.03	0.94	1.36	1.00	0.07
6	0.87	1.80	0.94	1.37	0.95	0.10
7	1.09	0.02	0.94	1.39	0.96	0.71
8	0.94	0.16	0.94	1.39	1.10	0.08
9	1.03	0.24	0.94	1.39	0.94	0.12
10	1.14	0.08	0.94	1.39	1.00	0.17
11	1.00	0.17	0.94	1.39		
Arch Elements						
20	1.00	0.14	1.16	0.01	1.00	0.14
21	1.47	0.06	1.16	0.01	0.93	0.10
22	1.07	0.22	1.16	0.00	1.08	0.09
23	0.99	0.09	1.16	0.00	0.98	0.67
24	1.10	0.03	1.16	0.00	1.00	0.08
25	0.86	1.80	1.16	0.00	0.95	0.10
26	1.10	0.03	1.16	0.00	0.94	0.74
27	0.97	0.11	1.16	0.00	1.10	0.08
28	1.06	0.25	1.16	0.00	0.93	0.12
29	1.14	0.06	1.16	0.00	0.99	0.16
30	0.99	0.16	1.16	0.01	-	-

Table 4-29 Normalized In-plane CSCB Responses to Four Support Motion Ground Motion 2

Elements	Shear force Fx		Axial force Fz		Moment My	
	$\frac{\sigma^2(w)_{F_x}}{\sigma^2(G)_{F_x}}$	$\frac{\sigma^2(H)_{F_x}}{\sigma^2(G)_{F_x}}$	$\frac{\sigma^2(w)_{F_z}}{\sigma^2(G)_{F_z}}$	$\frac{\sigma^2(H)_{F_z}}{\sigma^2(G)_{F_z}}$	$\frac{\sigma^2(w)_{M_y}}{\sigma^2(G)_{M_y}}$	$\frac{\sigma^2(H)_{M_y}}{\sigma^2(G)_{M_y}}$
Deck Elements						
1	0.45	0.10	0.96	1.36	0.95	0.10
2	1.05	0.29	0.96	1.34	0.94	0.05
3	0.96	0.17	0.96	1.37	0.96	0.18
4	0.95	0.05	0.96	1.37	0.97	0.58
5	0.97	0.04	0.95	1.36	0.96	0.04
6	0.94	1.48	0.96	1.41	0.91	0.06
7	0.97	0.02	0.96	1.45	0.89	0.95
8	0.92	0.07	0.96	1.44	1.00	0.12
9	0.93	0.24	0.96	1.44	0.94	0.05
10	1.06	0.23	0.96	1.44	0.93	0.13
11	0.93	0.13	0.96	1.43		
Arch Elements						
20	0.95	0.09	1.10	0.03	0.95	0.09
21	1.03	0.16	1.10	0.02	0.94	0.05
22	0.97	0.24	1.10	0.02	0.96	0.19
23	0.95	0.04	1.10	0.01	0.97	0.56
24	0.97	0.05	1.10	0.01	0.96	0.05
25	0.94	1.51	1.10	0.00	0.91	0.07
26	0.98	0.04	1.10	0.00	0.88	0.88
27	0.93	0.05	1.10	0.00	1.00	0.13
28	0.93	0.33	1.10	0.00	0.94	0.05
29	1.05	0.13	1.10	0.00	0.93	0.10
30	0.93	0.10	1.10	0.00	-	-

Table 4-30 Normalized Out-of-plane CSCB Responses to Four Support Motion-Ground Motion 1

Elements	Fy		Mx		Mz		Mw	
	$\frac{\sigma^2(W)}{\sigma^2(G)}_{F_y}$	$\frac{\sigma^2(H)}{\sigma^2(G)}_{F_y}$	$\frac{\sigma^2(W)}{\sigma^2(G)}_{M_x}$	$\frac{\sigma^2(H)}{\sigma^2(G)}_{M_x}$	$\frac{\sigma^2(W)}{\sigma^2(G)}_{M_z}$	$\frac{\sigma^2(H)}{\sigma^2(G)}_{M_z}$	$\frac{\sigma^2(W)}{\sigma^2(G)}_{M_w}$	$\frac{\sigma^2(H)}{\sigma^2(G)}_{M_w}$
Deck Elements								
1	0.86	1.60	1.04	1.02	0.96	1.59	-	-
2	0.90	1.98	1.01	0.70	0.91	0.51	1.04	0.92
3	0.97	1.72	1.03	0.96	0.82	0.91	1.02	0.94
4	0.92	1.13	0.98	1.42	0.83	1.51	1.01	0.84
5	0.80	1.70	0.93	1.17	0.92	1.83	0.96	1.13
6	1.04	0.78	0.96	0.14	1.04	1.58	0.91	1.16
7	0.99	1.07	1.01	0.83	1.04	1.45	1.02	0.71
8	0.90	1.81	0.89	1.72	1.05	0.72	0.98	1.00
9	1.06	1.14	0.96	1.05	1.00	0.63	1.05	0.78
10	1.07	0.82	1.04	0.59	0.88	0.83	0.99	0.95
11	1.01	0.79	1.07	1.00	0.87	1.38	1.07	0.86
Arch Elements								
20	1.01	0.77	1.05	0.95	1.03	0.82		
21	1.02	0.78	1.03	0.46	1.05	0.97		
22	1.02	0.93	1.06	0.98	1.04	1.11		
23	1.04	1.28	1.03	1.33	1.00	0.85		
24	1.02	0.84	1.00	1.22	0.99	1.01		
25	0.98	0.12	0.92	0.28	1.03	1.64		
26	1.06	0.71	1.03	1.17	0.96	1.74		
27	0.96	1.46	1.05	1.23	0.96	1.04		
28	0.99	0.96	1.06	0.90	1.04	0.77		
29	1.05	0.69	1.06	0.35	1.01	1.14		
30	1.01	0.75	1.02	0.98	1.07	0.91		

Table 4-31 Normalized Out-of-plane Responses to Four Support Motion -Ground Motion 2

Elements	Fy		Mx		Mz		Mw	
	$\frac{\sigma^2_{F_y}(W)}{\sigma^2_{F_y}(G)}$	$\frac{\sigma^2_{F_y}(H)}{\sigma^2_{F_y}(G)}$	$\frac{\sigma^2_{M_x}(W)}{\sigma^2_{M_x}(G)}$	$\frac{\sigma^2_{M_x}(H)}{\sigma^2_{M_x}(G)}$	$\frac{\sigma^2_{M_z}(W)}{\sigma^2_{M_z}(G)}$	$\frac{\sigma^2_{M_z}(H)}{\sigma^2_{M_z}(G)}$	$\frac{\sigma^2_{M_w}(W)}{\sigma^2_{M_w}(G)}$	$\frac{\sigma^2_{M_w}(H)}{\sigma^2_{M_w}(G)}$
Deck Elements								
1	0.90	1.70	1.01	1.10	0.97	1.64	-	-
2	0.92	2.26	1.00	0.72	0.99	0.58	1.01	0.99
3	1.00	1.65	1.01	1.22	0.92	0.80	1.01	0.95
4	1.00	1.06	0.97	1.05	0.88	1.74	1.00	0.91
5	0.90	1.61	0.96	1.16	0.94	2.11	0.97	1.11
6	1.02	0.85	0.96	0.14	1.02	1.71	0.94	1.15
7	0.99	1.42	1.00	0.87	1.01	1.57	1.00	0.75
8	0.96	2.13	0.98	1.38	1.03	0.65	1.00	1.00
9	1.03	1.38	1.01	0.95	0.99	0.60	1.01	0.95
10	1.05	0.78	1.02	0.66	0.93	1.15	1.01	0.91
11	1.00	0.75	1.03	1.02	0.93	1.87	1.03	0.92
Arch Elements								
20	1.01	0.80	1.01	0.91	1.01	0.86		
21	1.01	0.83	1.01	0.46	1.01	1.05		
22	1.00	1.05	1.02	1.08	1.01	1.14		
23	1.01	1.16	1.00	1.36	1.00	0.92		
24	1.00	0.92	0.99	1.27	0.99	1.04		
25	1.00	0.23	0.95	0.36	1.00	1.43		
26	1.02	0.86	1.00	1.27	1.01	1.21		
27	1.01	1.04	1.01	1.24	1.00	1.03		
28	1.02	0.96	1.03	0.92	1.01	0.92		
29	1.02	0.78	1.03	0.39	1.02	1.08		
30	1.01	0.79	1.03	0.39	1.02	1.08		

Table 4-32: Ratio of In-plane CSCB Responses with Four Support Motion in the General Case to the Responses with Two Supports Motion-Ground Motion 1

Elements	$\frac{\sigma^2_{F_x}(G)(4\text{ supports})}{\sigma^2_{F_x}(G)(2\text{ supports})}$	$\frac{\sigma^2_{F_z}(G)(4\text{ Supports})}{\sigma^2_{F_z}(G)(2\text{ Supports})}$	$\frac{\sigma^2_{M_y}(G)(4\text{ Supports})}{\sigma^2_{M_y}(G)(2\text{ Supports})}$
Bracing Elements			
1		0.89	
2		0.87	
Deck Elements			
1	1.02	1.09	1.02
2	1.01	1.08	1.00
3	1.03	1.08	1.00
4	1.02	1.07	1.06
5	1.01	1.07	1.03
6	1.13	1.07	0.98
7	0.99	1.07	1.02
8	0.99	1.07	0.99
9	1.01	1.07	0.99
10	1.00	1.07	1.01
11	1.01	1.07	
Arch Elements			
20	1.01	0.99	1.01
21	1.01	0.99	1.00
22	1.03	0.99	0.99
23	1.02	0.99	1.06
24	1.01	0.99	1.03
25	1.12	0.99	0.98
26	0.99	1.00	1.02
27	0.99	1.00	0.99
28	1.02	1.00	0.99
29	1.00	1.00	1.00
30	1.00	1.00	-

Table 4-33: Ratio of In-plane CSCB Responses with Four Support Motion in the General Case to the Responses with Two Support Motion-Ground Motion 2

Elements	$\frac{\sigma^2_{F_x}(G)(4\text{ supports})}{\sigma^2_{F_x}(G)(2\text{ supports})}$	$\frac{\sigma^2_{F_z}(G)(4\text{ Supports})}{\sigma^2_{F_z}(G)(2\text{ Supports})}$	$\frac{\sigma^2_{M_y}(G)(4\text{ Supports})}{\sigma^2_{M_y}(G)(2\text{ Supports})}$
Bracing Elements			
1		0.83	
2		0.80	
Deck Elements			
1	1.01	1.08	1.01
2	1.01	1.08	1.00
3	1.03	1.08	1.00
4	1.02	1.08	1.07
5	1.01	1.08	1.03
6	1.09	1.09	0.98
7	0.99	1.10	1.02
8	0.99	1.09	1.00
9	1.01	1.09	0.99
10	1.00	1.09	1.00
11	1.01	1.09	-
Arch Elements			
20	1.01	0.99	1.01
21	1.01	0.99	1.00
22	1.04	0.99	0.99
23	1.01	0.99	1.07
24	1.01	0.99	1.03
25	1.09	0.99	0.98
26	0.99	0.99	1.02
27	0.99	0.99	1.00
28	1.02	0.99	0.99
29	1.00	0.99	1.00
30	1.00	0.99	0.99

stiffness by the same factor. Five members were studied and the results are shown in Figures 4-27 through 4-31. All figures indicate that at the initial bridge stiffness, the main response contribution came from the dynamic component and the other two components were very small. By increasing the stiffness, the variance of the static component starts increasing and at one point it becomes equal to the dynamic component. Beyond that point by increasing the stiffness further, the static component becomes the major contributor to the response and the dynamic component keeps decreasing until it's contribution becomes very small. The relative contribution of the covariance of static and dynamic components is different from one member to another. What was noticed is that if the member response is sensitive to static displacement, the covariance component is higher. Also, it was noticed that the static component of axial forces increases faster than the other components such as bending moments.

The figures indicate that the stiffness can be increased by a large factor before the static response becomes significant. This implies that for bridges of this type, the static response is not expected to be significant. Only bracing members responses have a noticeable static component for a moderate increase in stiffness.

4.3.8 THE EFFECT OF WAVE VELOCITY ON THE RESPONSE OF THE TWO BRIDGES

In literature the central frequency of ground motion is calculated using one of the following formulas

$$\Omega_1 = \frac{\int \omega \, S(\omega) \, d\omega}{2\pi \int S(\omega) \, d\omega} \qquad (4.1)$$

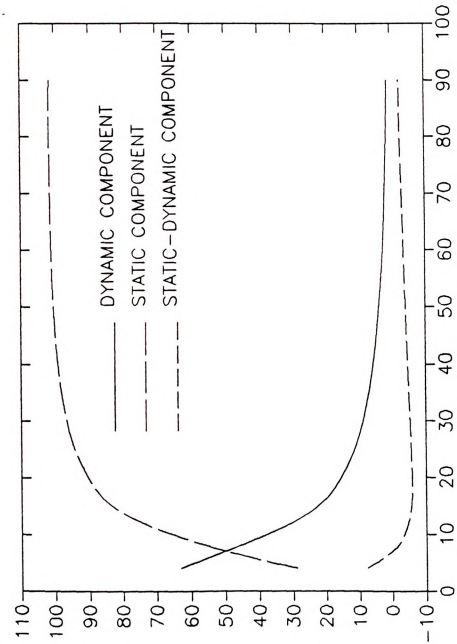

Figure 4-27: The Relative Contributions of Response Components to Axial Force in Longitudinal Bracing #1

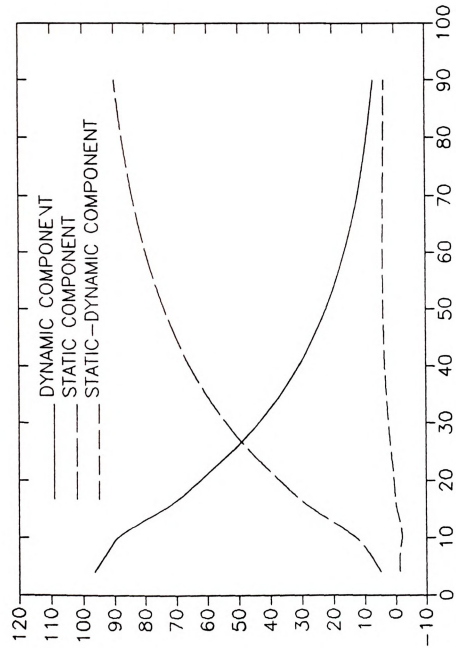

Figure 4-28: The Relative Contributions of Response Components to Bending Moment in Deck Member #3

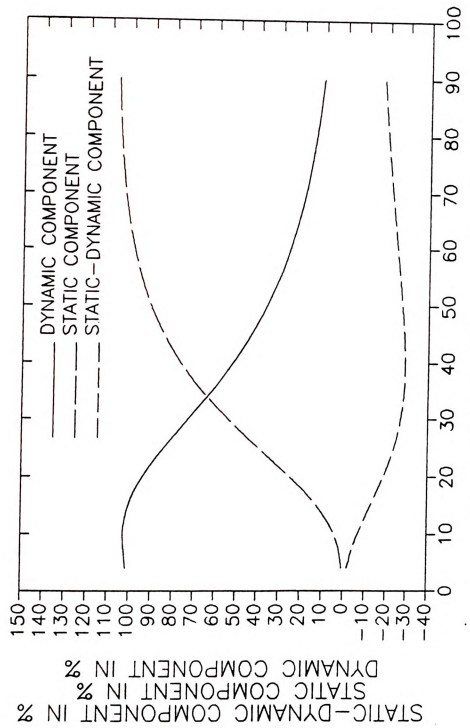

Figure 4-29: The Relative Contributions of Response Components to Axial Force in Deck Member #6

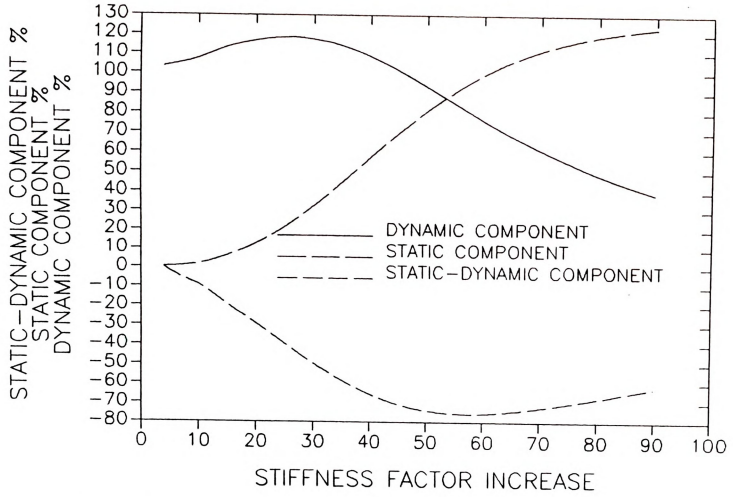

Figure 4-30: The Relative Contributions of Response Components to Forces in Arch Member #20

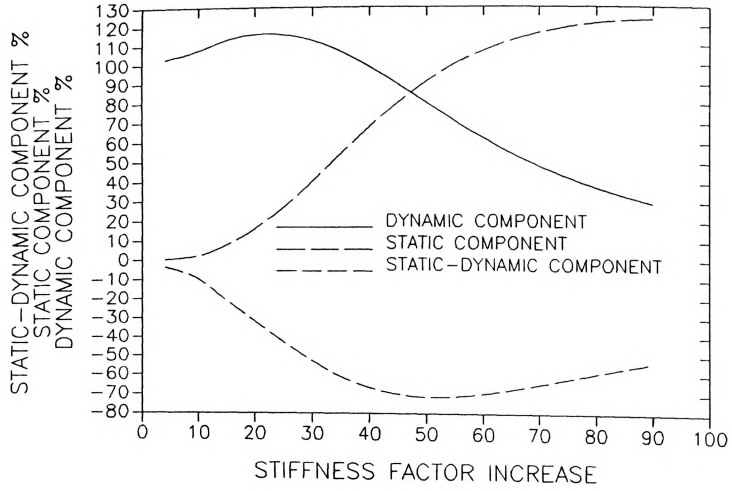

Figure 4-31: The Relative Contributions of Response Components to Axial Forces in Arch Member #24

$$\Omega_1 = \frac{1}{2\pi} \left\{ \frac{\int \omega^2 S(\omega)\, d\omega}{\int S(\omega)\, d\omega} \right\}^{0.5} \qquad (4.2)$$

where $S(\omega)$ is the spectral density function of ground motion acceleration and has the form

$$S(w) = \frac{1.0+4\beta_g^2 \left[\omega/\omega_g\right]^2}{\left(1.0-\left[\omega/\omega_g\right]^2\right)^2+ 4\beta_g^2\left[\omega/\omega_g\right]^2} \frac{\left[\omega/\omega_f\right]^4}{\left(1.0-\left[\omega/\omega_f\right]^2\right)^2+ 4\beta_f^2\left[\omega/\omega_f\right]^2}$$

Using the ground motion 1 the values of Ω_1 calculated by equations (4.1) and (4.2), are found to be 5.71 H_z and 10.77 H_z, respectively. For ground motion 2 those values are 2.25 H_z and 5.61 H_z. By choosing different wave velocity in equation (3.108) and investigating the responses of some deck and arch members, a study on the effect of seismic wave velocity was conducted.

Figure 4-32 shows the responses of axial forces and bending moments in CSCB arch members No. 20 and 26 as a function of wave velocity. The figure indicates that the bending moments and axial forces are much higher at low velocity and have a periodic behavior. Both responses tend to approach a unique level with increasing wave velocity.

Figure 4-33 shows the responses of axial forces and bending moments in CSCB deck members No. 2 and 7. The figure shows that the axial force in deck members increases with the increase of wave velocity, but the

bending moments decreases, and both responses are approaching a unique level.

Figures 4-34 and 4-35 show the axial forces and bending moments in NRGB arch members No. 34, 40 and 47 as a function of wave velocity. Both responses in all the three members show that they are decreasing with increasing the wave velocity and tend to approach a unique level.

The same conclusion can be drawn from Figure 4-36, where the bending moment responses is depicted for NRGB deck members No. 2, 7 and 12.

Figures 4-37 and 4-38 show the axil force responses in longitudinal bracing members in CSCB and NRGB, respectively.

Figure 4-37 shows that the wave velocity has no effect on the axial force responses in CSCB, while it procuces a slight increase in NRGB response.

4.3.9 NONSTATIONARY RESPONSE OF THE CSCB AND NRGB

To determine whether the CSCB and NRGB will reach their stationary response during strong ground motions of normal duration (10-15 sec), the variances of responses in both bridges were calculated at one and five seconds after the beginning of strong ground motion. The ground acceleration was assumed to start at time zero with its full stationary intensity (i.e., a Heaviside temporal modulating function was assumed). The results were compared against the stationary responses of the two bridges. The calculations were performed by replacing the frequency response function (equation 3.67) by the "time-dependent frequency response function" (equation 3.117).

Tables 4-34 and 4-35 show the response ratios of the CSCB and NRGB at one and five seconds relative to the stationary response. The tables

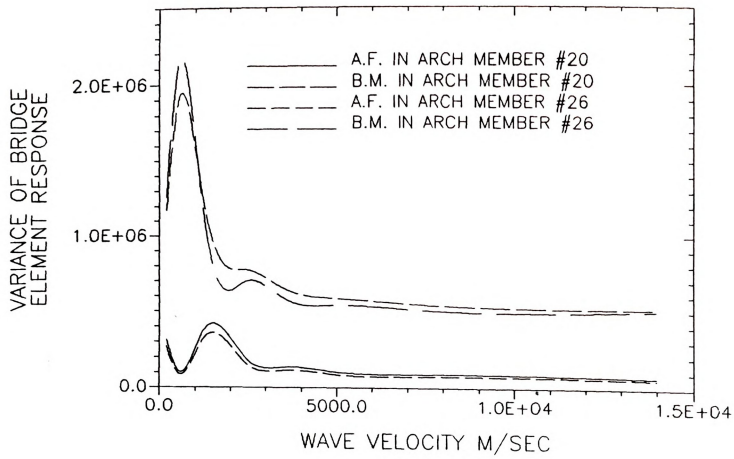

Figure 4-32: Response of the Axial Forces and Bending Moment in CSCB Arch Members No. 20 and 26

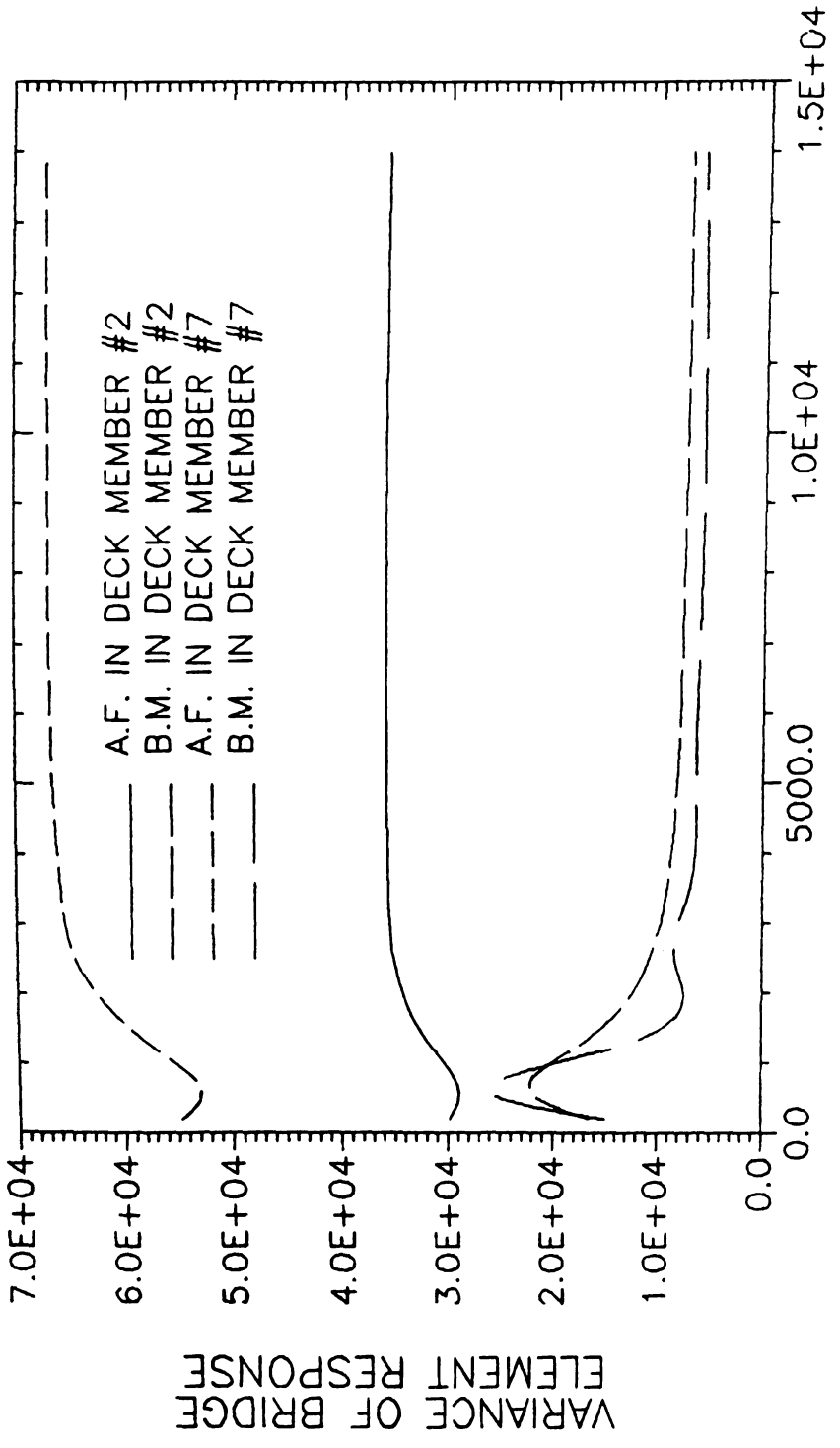

Figure 4-33: Responses of the Axial Forces and Bending Moments in CSCB Deck Members No. 2 and 7

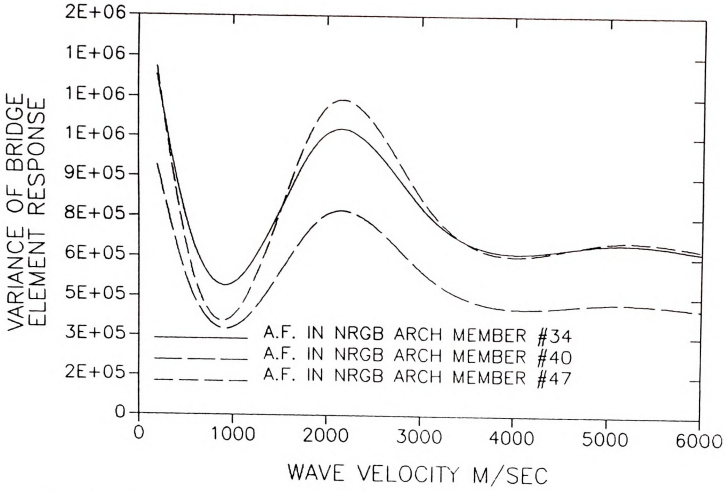

Figure 4-34: Responses of the Axial Forces in NRGB Arch Members No. 34, 40 and 47

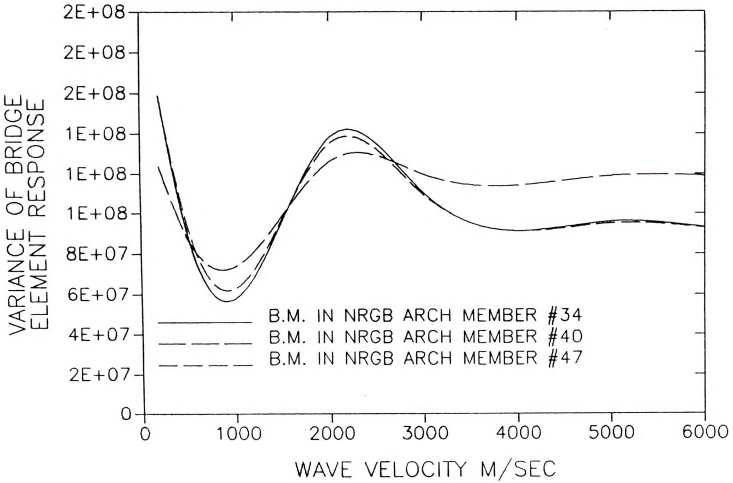

Figure 4-35: Responses of the Bending Moments in NRGB Arch Members No. 34, 40 and 47

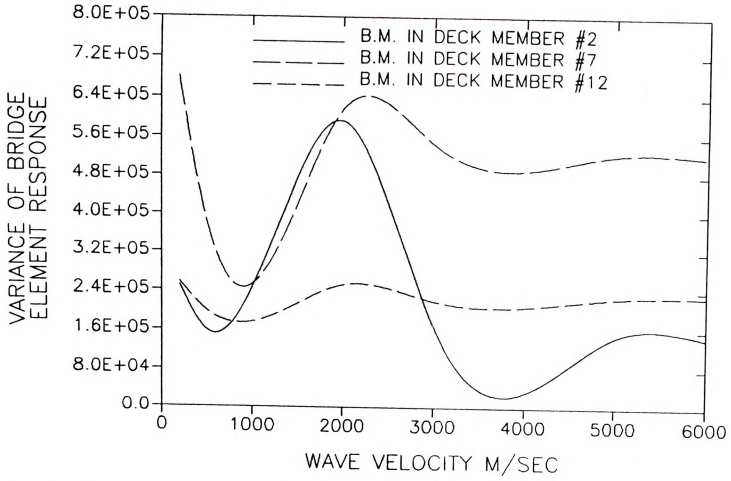

Figure 4-36: Responses of the Bending Moments in NRGB Deck Members No. 2, 7 and 12

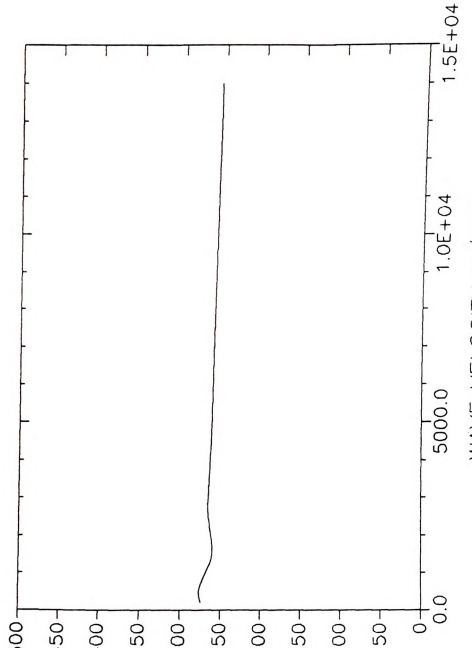

Figure 4-37: Responses of the Axial Forces in CSCB
Longitudinal Bracing

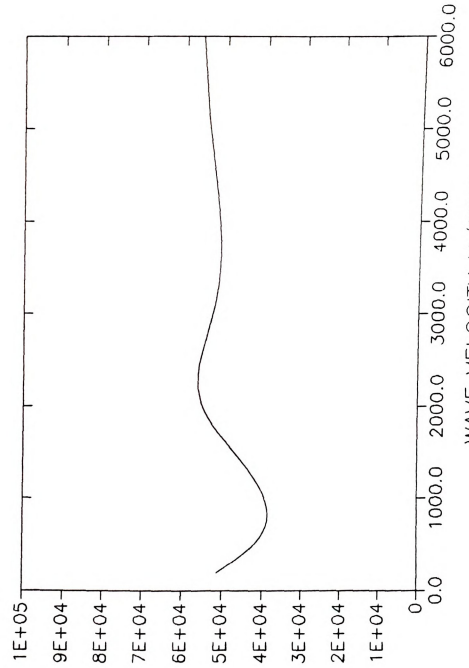

Figure 4-38: Responses of the Axial Forces in NRGB Longitudinal Bracing

indicate that the responses of the CSCB and NRGB are very close to their stationary values after about five seconds of strong shaking.

These results indicate that considering only the stationary response is reasonable for both bridges. The reason for this is that the first few modes, which have long periods and would therefore be expected to have slowly growing responses, do not contribute significantly to the overall responses. If we compare the in-plane frequencies of the CSCB and NRGB (Table 4-27) with the normalized acceleration spectra (Figure 3-4), it can be seen that the first two modes for the CSCB and the first five modes for the NRGB have frequencies lower than the dominant excitation frequencies of the ground acceleration.

4.4 COMPARISON BETWEEN DETERMINISTIC AND RANDOM VIBRATION STUDIES

The relative response between fully correlated and wave propogation excitations were obtained by Dusseau (1985) using deterministic analysis, and in this study using random vibration analysis. These are compared here.

It should be noted that there were some differences between the input excitations used in the two studies. Dusseau used scaled versions of the Caltech B1 and B2 simulated accelerogram, while in this study normalized ground acceleration 1 and 2 with the parameters given in Tables 3-1 and 3-2 were used. The frequency content of ground motion 1 is similar to that of the B1 record, and hence the comparisons are only made for these excitations.

Although the acceleration spectrum of the B1 record is similar to that of ground motion 1, there may be significant differences in the ground displacements. The filter used to attenuate low frequencies of the ground acceleration spectrum in the random vibration study

Table 4-34: Ratios of the CSCB Responses at One and Five Seconds to the Stationary Responses.

Elements	$\sigma^2_{F_x}$ (NON) / $\sigma^2_{F_x}$ (ST)		$\sigma^2_{F_z}$ (NON) / $\sigma^2_{F_z}$ (ST)		$\sigma^2_{M_y}$ (NON) / $\sigma^2_{M_y}$ (ST)	
	t=1sec	t=5sec	t=1sec	t=5sec	t=1sec	t=5sec
Bracing						
1			0.66	1.0		
2			0.66	1.0		
Deck Elements						
2	0.29	0.99	0.63	0.99	0.63	0.95
6	0.52	0.96	0.60	0.99	0.30	0.96
Arch Elements						
20	0.47	0.96	0.78	0.99	0.47	0.96
25	0.51	0.95	0.78	0.99	0.30	0.95

Table 4-35: Ratios of the NRGB Responses at One and Five Seconds to the Stationary Responses.

Elements	$\sigma^2_{F_x}$ (NON) / $\sigma^2_{F_x}$ (ST)		$\sigma^2_{F_z}$ (NON) / $\sigma^2_{F_z}$ (ST)		$\sigma^2_{M_y}$ (NON) / $\sigma^2_{M_y}$ (ST)	
	t=1sec	t=5sec	t=1sec	t=5sec	t=1sec	t=5sec
Bracing						
1			0.52	0.92		
2			0.60	0.94		
Deck Elements						
5	0.27	0.95	0.48	0.94	0.52	0.97
10	0.33	0.92	0.18	0.99	0.26	0.93
Arch Elements						
34	0.24	0.94	0.57	0.96	0.24	0.94
40	0.48	0.88	0.55	0.95	0.12	0.93

($|H_2(w)|^2$) in equation (3.111) has a significant effect on the displacement spectrum. Therefore similar acceleration spectra do not necessarily have similar displacement spectra. The ground displacement affects the pseudo-static responses but not the dynamic responses. In the bridges studied, the contribution of the static response to the total response is small (about 10 to 12% at most in the bracing elements and much smaller in the other elements), and therefore any differences in the ground displacements between the deterministic and random vibration studies is not expected to contribute significantly to the total responses (except perhaps to the bracing elements).

The apparent wave velocity along the length of the bridge also differed slightly for the results compared here: Dusseau used 1706 m/s and 853 m/s while this study used 1000 m/s. The effect of increasing velocity from 1000 m/s to 1706 m/s in the random vibration analysis was found to give similar tendencies, and therefore this difference in the velocities in not very important for the purpose of the comparisons.

To compare the results of both studies, we can only look at the response of the NRGB and CSCB under B1-B1, B1-B1', and B1-B1" loading conditions of the deterministic study, where B1-B1 represents fully correlated excitations, and B1-B1' and B1-B1" represent wave propogation cases with seismic wave velocities of 1706 m/s and 853 m/s, respectively. The results from these cases are compared to the responses of fully correlated wave propogation cases in this study. The results are discussed for bracing, deck and arch members, and also the vertical displacements.

1. Bracing: In the deterministic study (see Tables 4-9 through 4-12 in Dusseau (1985)) the axial forces in the CSCB bracing were

105.2, 97.3 and 121.8 Tons for loadings B1-B1, B1-B1', and B1-B1", respectively. Decreasing the wave velocity from 1706 m/s to 853 m/s, the axial forces increased from 97.3 Ton to 121.8 Ton. These results are compared with the ground motion 1 results of this study. From Table 4-7 (of this study) it can be seen that the difference in the bracing response to the fully correlated and wave propogation cases is negligible. The influence of wave velocity on the CSCB bracing response was minimal as shown in Figure 4-37. Since the static response contributes about 10% to the bracing response, the difference in the ground displacements between the two studies (as pointed out earlier) may be the reason for the observed differences.

2. Deck members: In the deterministic study, the stress in the deck element near the center were 15.18, 13.53 and 17.04 ksi (see Tables 4-9 through 4-12 in Dusseau (1985)). In this study, the combined normal stresses due to axial forces and bending moments were not computed. However, based on the results for varying velocity, (see Figure 4-33 in this study) the axial force decreases slightly with decreasing wave velocity, but the bending moment increases with decreasing velocity. Figure 4-33 shows that when the velocity reduces from ∞ to 1706 m/s, the bending moment does not change much but the axial force decreases. This corresponds to the decrease in stress from 15.18 to 13.53 ksi in the deterministic study. However, as the velocity decreases further to 853 m/s, the axial force reduces a little more while the bending moment increases sharply, which would give a higher combined stresses.
3. Arch members: The stresses in the arch elements at the abutment (see Tables 4-9 through 4-12 in Dusseau (1985)) were 9.78, 15.40

and 19.06 ksi for loadings B1-B1, B1-B1', and B1-B1", respectively. These results have the same behavior as in this study, but the ratios of responses between wave propogation and fully correlated excitation is larger in this study.

4. Vertical displacements also have the same tendencies in the two studies, but again the ratios between wave propogation and fully correlated excitation are larger in this study.
5. The main difference between the CSCB and NRGB responses is in the response of the bracing elements. The results in both studies confirm that the bracing axial force response is much higher in the fully correlated case of ground motion.

Some of the differences between the two studies may be due to the differences in the input ground motion acceleration and displacement models. The fact that the deterministic analysis was only one sample of the excitation process, which may produce lower or higher responses than the average, is also expected to contribute to these differences.

CHAPTER 5

SUMMARY AND CONCLUSIONS

5.1 SUMMARY

The research conducted here was to study the effect of spatial variation of earthquake induced ground motion on the response of (The New River Gorge Bridge (NRGB), and Cold Springs Canyon Bridge (CSCB)).

The equations of motion were developed using the finite element technique and the random vibration approach.

In order to perform this study, a suitable ground motion model is required. In this study a space-time ground motion model proposed by Harichandran and Vanmarcke (1986) is used. In this model the ground acceleration are assumed to constitute a homogeneous random field. The point spectral density function of the ground acceleration, is therefore assumed to be the same at all spatial locations. The correlation between the accelerations at two different points is characterized by the coherency function $\rho(\nu,f)$ and the phase due to the time delay caused by wave propogation is accounted for by an exponential function $\exp(-i\omega\nu/v)$.

In this study three cases of ground motion models were used. Case 1 is the fully correlated ground motion in which all the support points are moving identically. This assumption is not realistic for long span bridges, but it is the current practice of designing. Case 2, is the wave propogation model where only the wave travelling effect is considered with no coherency loss. Case 3, is the general case of ground motion model where the travelling wave effect as well as the correlation between the acceleration at two different points which is characterized by a coherency function are considered.

Each case of ground motion has two different sets of fitting parameters. Those cases of ground motion were applied in the horizontal direction and the responses of the two bridges were determined and analyzed.

5.1.1 MODELS OF THE CSCB AND NRGB

The models used in this study are the ones obtained by Dusseau and Wen (1985) who studied the same two bridges using the deterministic approach to analyze the response of the bridges under unequal seismic support motion. Using those models made the task of analyzing the two bridges much easier because, they transformed the two bridges from a structure with hundreds of d.o.f. to a structure with less than 100 d.o.f.

5.1.2 CSCB IN-PLANE RESPONSE

The CSCB in-plane responses were determined for the three cases of ground motion. The deck axial forces were the highest in the fully correlated case, meanwhile the bending moments and shear forces were minimum. The deck bending moment was maximum in general and wave propogation case. The most striking difference is the response of the bridge's arch to the general and wave propogation cases comparing with the response to the fully correlated case. The difference in the response between the wave propogation and the general case was about 7% in bending moments and shear forces, and about 16% in axial forces where the wave propogation response was higher than the general case response. The arch axial forces response in the wave propogation case was 4 to 6 times higher than in the fully correlated case, meanwhile the bending moment and shear forces were about 2 to 4 times higher.

The longitudinal bracing response in ground motion 1 was very close in all three cases of ground motion. In ground motion 2, the highest bracing response was in the general case followed by the wave propogation case and fully correlated case, respectively. The difference between the wave propogation and the general case was very small and both were about 25% higher than the fully correlated case response. The vertical displacement in both the general and wave propogation cases were close to each other and both were about 3 to 10 times higher than the response in the fully correlated case.

The responses of ground motion 1 comparing to ground motion 2 were much higher, and this can be explained by the frequency content of ground motion.

5.1.3 NRGB IN-PLANE RESPONSE

The deck axial forces were the highest in the fully correlated case of ground motion, where the axial forces were about 66% to 100% higher than the axial response in the general and wave propogation cases. The deck bending moments responses were the highest in the wave propogation case, where they were about 19% higher than the general case response, and about 73% to 400% higher than the fully correlated case response.

The arch responses were the highest in the wave propogation case, where the axial forces response was about 2.7 to 4.4 times higher than the response in the fully correlated case. The responses in the wave propogation and the general case of ground motion were within 20% of each other in ground motion 1, and within 12% in ground motion 2.

The response of the longitudinal bracing was the highest in the fully correlated case of ground motion. In comparison with the general case of ground motion the bracing axial forces in the fully correlated

case were about 80% to 100% higher in ground motion 1, and 44% to 78% higher in ground motion 2. The bracing axial forces in wave propogation and general cases of ground motion were within 10% to 17% in ground motion 1 ,and within 8% in ground motion 2.

The responses of ground motion 1 is about 50% less than the responses in ground motion 2. This can be explained by the frequency content of ground motions 1 and 2.

The vertical displacement was the highest in the wave propogation case at 1/3 points of the span. The displacements in the wave propogation and general cases were very close and both were in about 10 times higher than the vertical displacements in the fully correlated case of ground motion.

5.1.4 NRGB AND CSCB OUT-OF-PLANE RESPONSE

The study of the out-of-plane responses of both bridges shows that the members responded differently to different ground motion correlation. For some members the highest response was in the wave propogation case, for others it was the general or fully correlated case. Thus it was difficult to predict what is the worst case of ground motion.

For NRGB the maximum lateral displacement occured in the fully correlated case. The displacements in the wave and general cases were close the each other. The maximum lateral displacements occured at the ends of NRGB, and that was more evident in ground motion 2 where the variance of ground displacement is higher.

The lateral displacements of CSCB show that the three cases of ground motion had similar effect on the out-of-plane response.

5.1.5 RELATIVE CONTRIBUTION OF RESPONSE COMPONENTS

The variance of total response consists of three different components; the variance of dynamic component, the variance of static component and the covariance of pseudo-static and dynamic components. It was found that the dominant component is the dynamic one. The two other components could be ignored when the stiffnesses of the structure is normal.

By increasing the stiffness of the two bridges the static component starts increasing to a point where it becomes equal to the dynamic component. By increasing the stiffness more, the static component continues its increase and the dynamic component continues its decrease until it becomes negligible.

5.1.6 THE EFFECT OF SEISMIC WAVE VELOCITY

By choosing different wave velocities and calculating the responses of the two bridges, it was noticed that the responses of the two bridges were decreasing with the increase of wave velocity except, the axial forces in the deck of CSCB where they were increasing. Also, it was noticed that the wave velocity did not affect the response in the longitudinal bracing of CSCB, while increasing the velocity caused slight increase in the NRGB longitudinal bracing response. The decrease in response with increasing velocity can be related to the fact that the wave propogation effect decreases with the increase of velocity.

5.1.7 NONSTATIONARY RESPONSE OF CSCB AND NRGB

It was found that the responses of both bridges reach the stationary state response in about five seconds. Consequently, the assumption that the ground motion constitute a stationary random field is a valid one when the duration of strong ground motion is more than 5

seconds. The reason that both bridges reach the stationary response in that short period of time is due to the fact that the first modes do not contribute significantly to the response of both bridges.

5.2 CONCLUSIONS

This study of the response of NRGB and CSCB to differential support excitation illustrates that it is very important to consider the spatial variation of earthquake ground motion in the analysis of such structures. The following conclusions are made based on this study.

1. The most important component of the structural response of both bridges is the variance of the dynamic component. The variance of the static and the covariance of static and dynamic components could be ignored when the structures is not stiff. For stiff structures the variance of static componenets and the covariance of static and dynamic component must be considered in the analysis. This conclusion is true for a structure with the same end fixity conditions. For different conditions a study must be performed.
2. The most important effects of the differential support exictation is the substantial increase in arch axial forces and bending moments. The increase of the arch axial forces is much higher than the increase of bending moments. Comparing with the fully correlated case of ground motion, the wave propogation case increases the axial forces in the arch by 6 to 10 times, meanwhile the increase of bending moments was 2 to 4 times. The responses due to wave propogation and general cases of ground motion were close to

each other in most cases with a maximum difference of 20% in some cases.

3. The vertical displacements in the two bridges were high and close to each other in the wave propogation and the general case of ground motion. In the fully correlated case of ground motion the vertical displacements were very small comparing with the other two cases.
4. The lateral displacements of the two bridges were the highest in the fully correlated case of ground motion. But in all three cases of ground motion the difference in lateral displacements was not far away from each other.
5. The response of the two bridges is very dependent on the parameters of ground motion which eventually influence the frequency content of ground motion models. For example the axial forces in CSCB increased by 6 times when changing from ground motion 1 to ground motion 2, but in the NRGB the axial forces decreases by about 50% . Of course, these results are also related to the structural frequencies.
6. The seismic wave velocity has a very important effect on the response of long structures. At low wave velocity the responses of the two bridges were high and periodic, but with increasing wave velocity the responses decreased and approached a unique value.
7. Both bridges will reach the stationary values of response during a strong ground motion of five seconds or more.

5.3 RECOMMENDATIONS

The scope for future research in this area is quite wide. Some of the main points that need to be addressed are as follows:

1. Other steel deck arch bridges, and other types of long span bridges need to be studied, so that we can generalize the findings, and study the different parameters that affect the differential excitation on the structural response.
2. Perform non-linear random vibration analysis on steel deck arch bridges to better and more in depth understand the structural behavior.
3. The numerical results of the random vibration analysis is as good as the model of ground motion. So, more studies should be directed towards the modeling of ground motion on different site conditions and different ground motion intensities.

REFERENCES

1. Abdel-Ghaffar, A. M. and Rubin, L.I. (1982). "Suspension Bridge Response to Multiple Support Excitations", Journal of Engineering Mechanics, ASCE, 108(EM2).

2. Bathe, K. J., (1982). "Finite Element Procedures in Engineering Analysis", Prentice-Hall, Inc., Englewood Cliffs, New Jersey.

3. Chen, W. F. and Atsuta, T. (1977). "Theory of Beam-Columns, Volume 2: Space Behavior and Design", McGraw-Hill, New York.

4. Clough, R. W. and Penzien, J. (1975). "Dynamics of Structures", McGraw-Hill Book Company, New York.

5. Cook, D, C., (1974). "Concepts and Applications of Finite Element Analysis", John Wiley & Sons, Inc., New York, New York.

6. Dusseau, R. A. (1985). "Unequal Seismic Support Motions of Steel Deck Arch Bridges", Ph.D. Dissertation of Civil and Environmental Engineering Department, Michigan State University, East Lansing, Michigan.

7. Dusseau, R. A. and Wen, R. K. (1982). "Seismic Responses of Two Deck Arch Bridges", American Society of Civil Engineers, Meeting Preprint 82-010, Las Vages, Nevada.

8. Dusseau, R.A. and Wen, R.K. (1989). "Seismic Responses of Deck-Type Arch Bridges", Earthquake Engineering and Structural Dynamics, 18, 701-715.

9. Dusseau, R. A., (1982). "Seismic Analysis of Two Steel Deck Arch Bridges", M. S. Thesis, Department of Civil and Sanitary Engineering, Michigan State University, East Lansing, Michigan.

10. Gasparini,D,A. (1979). "Response of MDOF Systems to Nonstationary Random Excitation", Journal of Engineering Mechanics Division, ASCE, 105(EM1), 13-27.

11. Gere, J. M. and Weaver, W. (1965). "Analysis of Framed Structures", D. Van Nostrand Reinhold Company, New York, New York.

12. Harichandran, R. S., and Vanmarche, E. (1986). "Stochastic variation of earthquake ground motion in space and time." J. Engrg. Mech., ASCE, 112(2), 154-174.

13. Harichandran, R. S. and Wang, W. (1988). "Responses of one- and two-span beam to space-time earchquake excitation." Struct. Series

Report MSU/STE-88/01, Dept. of Civ. and Envir. Engrg., Michigan State University., East Lansing, Michigan.

14. Harichandran, R.S. (1987). "Stochastic Analysis of Rigid Foundation Filtering", Earthquake Engineering and Structural Dynamics, Vol. 15, pages 889-899.

15. Hindy, A. and Novak, M. (1980). "Pipeline Response to Random Ground Motion" Journal of Engineering Mechanics, ASCE, 106(EM2).

16. Lin Y.K. (1963). "Nonstationary response of continuous structures to random loading", Journal of Acoustical Society of America, 35(2), 222-227.

17. Merritt, F. S. (1972). "Structural Steel Designer's Handbook", McGraw-Hill Book Company, New York.

18. Newmark, N. M. and Rosenblueth, E. (1971). "Fundamentals of Earthquake Engineering", Prentice-Hall, Inc., Englewook Cliffs, New Jersey.

19. Zerva, A., Ang, A. H-S. and Wen, Y.K. (1988). "Lifeline Response to Random Ground Motions", Earthquake Engineering and Structural Dynamics, 16, 361-379.